JAERI-Research
2001-006

A STUDY ON RADIATION SHIELDING AND SAFETY ANALYSIS FOR A SYNCHROTRON RADIATION BEAMLINE

March 2001

Yoshihiro ASANO

日本原子力研究所
Japan Atomic Energy Research Institute

本レポートは、日本原子力研究所が不定期に公刊している研究報告書です。
入手の問合わせは、日本原子力研究所研究情報部研究情報課（〒319-1195　茨城県那珂郡東海村）あて、お申し越し下さい。なお、このほかに財団法人原子力弘済会資料センター（〒319-1195　茨城県那珂郡東海村日本原子力研究所内）で複写による実費頒布を行っております。

This report is issued irregularly.
Inquiries about availability of the reports should be addressed to Research Information Division, Department of Intellectual Resources, Japan Atomic Energy Research Institute, Tokai-mura, Naka-gun, Ibaraki-ken 〒319-1195, Japan.

編集兼発行　日本原子力研究所

JAERI－Research 2001－006

A Study on Radiation Shielding and Safety Analysis for a Synchrotron Radiation Beamline

Yoshihiro ASANO

Synchrotron Radiation Research Center
Kansai Research Establishment
Japan Atomic Energy Research Institute
Mikazuki-cho, Sayou-gun, Hyogo-ken

(Received January 23, 2001)

Methods of shielding design and safety analysis are presented for a beamline of synchrotron radiation. This paper consists of the shielding and safety study of synchrotron radiation with extremely intense and low energy photons below several hundreds keV, and the study for the behavior of remarkable high energy photons up to 8 GeV, which can creep into beamlines.

A new shielding design code, STAC8 was developed to estimate the leakage dose outside the beamline hutch (an enclosure of the beam, optical elements or experimental instruments) easily and quickly with satisfactory accuracy. The code can calculate consistently from sources of synchrotron radiation to dose equivalent outside hutches with considering the build up effect and polarization effect. Validity of the code was verified by comparing its calculations with those of Monte Carlo simulations and measurement results of the doses inside the hutch of the BL14C of Photon Factory in the High Energy Accelerator Research Organization (KEK), showing good agreements.

The shielding design calculations using STAC8 were carried out to apply to the practical beamlines with the considering polarization effect and clarified the characteristics of the typical

beamlines of the third generation synchrotron radiation facility, SPring-8. In addition, the shielding calculations were compared with the measurements outside the shield wall of the bending magnet beamline of SPring-8, and showed fairly good agreement. The new shielding problems, which have usually been neglected in shielding designs for existing synchrotron radiation facilities, are clarified through the analyses of the beamline shielding of SPring-8. The synchrotron radiation from the SPring-8 has such extremely high intensity involving high energy photons that the scattered synchrotron radiation from the concrete floor of the hutch, the groundshine, causes a seriously high dose. The method of effective shielding is presented.

For the estimation of the gas bremsstrahlung, which is generated by the interaction of residual gas molecules with stored electrons and invades the beamline, a new recommendation is proposed in order to simulate with sufficient accuracy. The measurement results of the gas bremsstrahlung by using a new type scintillator, PWO, are presented in relation to the characteristics of the stored electron beam that is a high and low betatron function beam. The gas bremsstrahlung was measured as a function of the aperture size of the slits, showing the apparent dependence on the conditions of the stored electron beam, as well as the beam current and the vacuum pressure. The measurements of the dependency of the aperture size were compared with the calculations by using the Monte Carlo code EGS4, and showed a fairly good agreement. The total power of the gas bremsstrahlung was estimated as 25.8±0.8 nW /10^{-8}Pa/mA and the corresponding equivalent dose rates for a scoring radius of 0.023 cm were calculated to be 15.8 nSv/s/10^{-8}Pa/mA for a high betatron function beamline, and 9.22 nSv/s/10^{-8}Pa/mA for a low betatron function beamline. Calculations were also made to obtain 25.9 nSV/s/10^{-8}Pa/mA neglecting the stored beam conditions at 40 m from the center of the straight section of SPring-8.

In addition to the gas bremsstrahlung, the photoneutron induced by the gas bremsstrahlung is presented by using two different photoneutron production cross sections, the difference of which comes from whether or not neglecting the quasi-deutron and photo-pion production process. The measurement results of photoneutrons generated by the interactions of the gas bremsstrahlung with lead and copper targets are presented by using high sensitive Bonner type helium-3 counters with polyethylene moderators to estimate the neutron spectrum. The measurements were performed outside

the optics hutch to reduce the effects of synchrotron radiation. The measurement data of the effective dose due to photoneutrons were compared with the calculations and previous data, and showed reasonable agreement.

Using the present methods of gas bremsstrahlung and associated photoneutron analyses, the shielding calculation of the beamline of a laser electron photon at SPring-8, which can generate polarized photons of a few GeV with high intensity, is presented in a design with two separated beamline hutches. In addition to the shielding of the beamlines of synchrotron radiation, an extremely high energy and high intensity laser electron photon beam brings other shielding problems. They are the issues of high intensity neutrons due to photonuclear reaction and high energy electrons, positrons due to pair creation in the upstream regions. The method of effective shielding is clarified by using a sweep magnet with lead collimators to reduce the leakage dose substantially.

Keywords: Synchrotron Radiation Beamline, Radiation Shielding, Safety Analysis, STAC8, EGS4, Groundshine, Gas Bremsstrahlung, Photoneutron, Laser Electron Photon, SPring-8

JAERI－Research 2001－006

放射光ビームラインの放射線遮蔽と安全解析に関する研究

日本原子力研究所関西研究所放射光科学研究センター

浅野　芳裕

（２００１年１月２３日受理）

第３世代放射光施設の放射光ビームラインに対する遮蔽設計手法と安全解析手法について開発研究を行った。本研究では、極端に大強度でそのほとんどのエネルギーが数１００ＫｅＶ以下の放射光に対する遮蔽安全解析の研究とビームラインに混入してくる非常にエネルギーの高い（数ＧｅＶ）放射線に対する挙動解析研究より構成される。

放射光に関する遮蔽研究においてはwigglerやundulatorなどで発生する挿入装置光源スペクトルから、光学素子等で散乱された光子による遮蔽ハッチ外での漏洩線量までを一貫して短時間に精度良く計算できる、放射光ビームライン遮蔽設計コード「ＳＴＡＣ８」を開発した。このコードは再生効果や放射光の直線偏光による散乱も考慮出来る。本コードの妥当性を検証するために、このコードとモンテカルロ計算コードEGS4との比較計算および高エネルギー加速器機構 Photon Factory　BL14C ビームラインのハッチ内線量分布の比較実験を行い、良い一致を得た。

開発したコード「ＳＴＡＣ８」を用いて第３世代大型放射光施設 SPring-8 の典型的な３種類の放射光ビームラインの遮蔽安全解析を実施することによって、直線偏光に依存するビームライン遮蔽上の特徴を明らかにした。またBending Magnet Beamline BL14B1でのハッチ外漏洩線量分布との比較を行い、開発したコードが測定値を良く再現できることを示した。第３世代大型放射光施設ではかつて無かったほどの大強度ビームが得られるに伴い、それまで意識されなかった新しい遮蔽上の問題点であるハッチ、コンクリート床面からの放射光散乱線による漏洩線量の影響（グランドシャイン）を解明するとともに、尤も有効と思われる対策を提示した。

蓄積リング内の残留ガスと蓄積電子との相互作用の結果、発生するガス制動放射線がビームラインに必然的に混入してくる。このガス制動放射線はエネルギーが蓄積電子の８GeVまで分布しており、安全評価

関西研究所：〒679-5143　　兵庫県佐用郡三日月町光都１－１－１

上重要である。このガス制動放射線を正確にシュミレーションするための計算条件を提示した。タングステン酸鉛シンチレーターを用いて、SPring-8のビームラインに混入してくるガス制動放射線を高精度で測定した。フロントエンドに設置されているスリットの開口幅とガス制動放射線の強度の関係を得るとともに、モンテカルロコードEGS4を用いたシミュレーション計算を実施することにより、蓄積電子のビーム発散角やビームサイズなどの電子ビーム蓄積状態との関係を解析した。この結果、SPring-8の標準挿入装置光源ビームラインに置けるガス制動放射線の全パワーは２５．８±０．８nW/10^{-8}Pa/mAであること、及び蓄積リングの直線部中心から４０mの地点でのガス制動放射線による線量当量は高ベータトロン関数ビームラインでは１５．８nSv/s/10^{-8}Pa/mA,(計数半径０．０２３cm)、低ベータトロン関数ビームラインでは９．２２nSv/s/10^{-8}Pa/mA、電子ビーム蓄積状態を考慮しないときには２５．９nSv/s/10^{-8}Pa/mAとなることが明らかとなった。

ガス制動放射線がビームシャッターなどの標的に入射することによって光中性子が発生する。ガス制動放射線によって発生する光中性子発生には、いままで巨大共鳴吸収領域のみ考慮されていた。今回、準重陽子発生およびπ中間子発生領域まで考慮してこの光中性子による線量を評価した。また、このガス制動放射線に付随して発生する光中性子を厚さの異なる減速材付きBonner Type円筒型高感度^{3}He検出器を用いてハッチ外の位置で計測し、スペクトルを評価した。評価したスペクトルから得られた線量とモンテカルロ計算結果と比較を行い、その妥当性を検証した。

SPring-8では蓄積電子の逆コンプトン散乱を利用することによって強度の非常に高い数GeVの偏光光子を得ることが出来る。このレーザー電子光ビームラインは空間的な制約から、ビーム輸送パイプで連結された２つの分離されたハッチ構造とする必要があり、精度の高い遮蔽設計が要求される。そこで本研究で整備されたガス制動放射線とそれに付随する光中性子の解析手法を用いて、このビームラインで問題となる高エネルギー光子と付随する光中性子に対する遮蔽解析を実施した。また鉛コリメーターとsweep magnetを組み合わせることにより、電磁シャワーで発生した高エネルギー電子を除去することが出来、より効率的に遮蔽できることを示した。

これらの研究結果から、第３世代放射光施設の放射光ビームラインにおける遮蔽設計手法が確立され、短時間に正確にハッチからの漏洩線量が評価できるようになった。本手法を用いてSPring-8の全ビームラインの安全評価を行うとともに、放射線測定テストを通じて本手法の有効性が確認された。また、第３世代放射光施設におけるガス制動放射線のビームプロファイルとその線量及び付随する光中性子の漏洩スペクトルが明らかとなった。その上、レーザー電子光ビームラインのような特徴のあるビームラインに対して有効な遮蔽手法が提示された。

This is a blank page.

Contents

目次

List of figures

List of Tables

1. Introduction

1.1 Historical review

Synchrotron radiation is the electromagnetic radiation emitted in the tangential direction of the orbit when charged particles, especially electrons or positrons, moving close to the speed of light are bent by a powerful magnetic field. Since 1947, when it was first observed in the US by using a synchrotron accelerator, synchrotron radiation has been used as a tool for study in the fields of material science, chemistry, biology and so on[1-1),1-2)]. Synchrotron radiation is a quite unique light as follows, (1) synchrotron radiation has the intensities of one to four digits in comparison with other sources ranging from ultraviolet to X-ray energy, (2) synchrotron radiation has a continuous spectrum of wide energy range from radio waves to the X-ray energy region, (3) the directionality is quite strong so that the light is almost close to parallel, (4) the main component of synchrotron radiation is linearly polarized light with an electric field vector within the plane of the electron orbit and elliptically polarized light in the direction tilted from the orbital plane, (5) synchrotron radiation is a quite short pulsed radiation defined by the orbiting characteristics of the electron repeating uniformly. In addition, (6) it is possible to stabilize the intensity fine with temporality, (7) the light is a source with very small size and quite strong directivity so that synchrotron radiation is a light source with extremely high brightness, (8) the characteristics of synchrotron radiation can be estimated theoretically and it agrees with the observed results so that it can be utilized as a primly standard illuminant, (9) There is no discharge except for photons from the source. As mentioned above, synchrotron radiation has many remarkable advantages as a powerful tool for basic and applied studies in biology, chemistry, medicine, and physics, as well as in applications to technology such as X-ray lithography, micro-mechanics, materials characterization, and trace element analysis.

The facilities of synchrotron radiation are classified into three categories by generation[1-3)]. **Table 1-1** lists the main facilities of synchrotron radiation in the world. The first generation facilities were originally built for high-energy physics research as mentioned above. In many cases, the

experiments of synchrotron radiation started in a parasitic mode from nineteen sixties such as the 1.3 GeV electron synchrotron accelerator in the Institute for Nuclear Study of Tokyo University. During the period of parasitic use, however, in spite of unfavorable conditions, the use of synchrotron radiation turned out to be completely rewarding and fruitful because of the remarkable improvement of brightness in comparison with the sources from X-ray tubes or spark discharge tubes. This novel scientific tool created new fields of science such as inner-shell spectroscopy of atoms and increased the number of researchers. As a natural consequence, the idea of having a dedicated synchrotron radiation source grew and the storage ring of INS-SOR[1-4] at Tokyo University, which was designed specially as a dedicated light source started operation in the middle of 1970s. In the 1980s, the new dedicated X-ray source of SRS in Daresbury[1-5], the Photon Factory in Tsukuba[1-6], and NSLS in Brookhaven[1-7] were built to extend the useful photon energy of synchrotron radiation up to the hard X-ray region. These facilities are the second generation facilities, which are characterized by the dedicated X-ray sources. In general, these storage rings have a large number of beamlines, primarily from bending magnets. This synchrotron radiation is almost less than 10 keV photon energy so that most of the beamlines are constructed without shielding or with shielding by empirical methods through leakage dose measurement on a case-by-case basis.

The successful experience with insertion devices, wigglers and undulators, has led to a new generation of more advanced rings. These third generation storage rings are distinguished by lower electron beam emittance and many straight sections for insertion devices. Especially, 6 to 8 GeV rings with a circumference of 800 to 1500 m designed primarily for harder X-rays, above about 2 keV. Three rings are now in operation at the European Synchrotron Radiation Facility (ESRF) of Grenoble in France[1-8], Advanced Photon Source (APS) of Argonne in the USA[1-9], and SPring-8 of Harima in Japan[1-10]. The stored electron energies of these rings are 6, 7, and 8 GeV for ESRF, APS, and SPring8, respectively, together with low emittance (several nm.radian). Because of the high energy and low emittance of the stored electrons, high energy synchrotron radiation of extremely high brilliance is available in the facilities. The small rings, with energy of 1 to 2 GeV, are now under design or operation

primarily for the spectral region of VUV and soft X-rays. The intermediate rings, with energy of 3 to 4 GeV, are also under design. These third generation rings have many straight sections for the installation of insertion devices. In addition, the very large, high-energy colliders such as PEP[1-11], PETRA[1-12], and TRISTAN[1-13] have been modified and planned to serve as sources of extremely high synchrotron radiation flux from bending magnets or insertion devices.

In the early days of synchrotron radiation experiments, the light from a synchrotron accelerator for high energy physics was utilized parasitically. And the light energy was not higher than soft x-rays so that the radiation safety for synchrotron radiation passed for unworthy issues of attention. The machines of the accelerator were only considered to be covered as a shield. After the second generation facilities, in which the storage rings instead of synchrotrons became the dominant tool, and a dedicated use of the source was established, the safety issues were not so much changed. The empirical method was generally equipped for the radiation shielding of synchrotron radiation by measuring the leakage dose at the same time. The studies were performed only for high energy gamma rays that invaded into the synchrotron radiation beam[1-14],[1-15],[1-16],[1-17]. Recently, third generation facilities have been constructed and operated, which have 6-8 GeV storage rings with a circumference of 800-1500 m and designed primarily for harder x-rays generated by insertion devices such as a wiggler and undulator with low emittance of stored electrons. Because of the high energy and very low emittance of the stored electrons, high energy synchrotron radiation of extremely high brilliance is available at these facilities compared to that of the existing facilities. Further, a combination of a long straight section, which is available for an insertion device, and the high energy of the stored electrons generates an extremely intense gas bremsstrahlung by interaction of the stored electrons with residual gas molecules in the vacuum chamber. These distinguishing features of the synchrotron radiation present rather sever radiation problems so that the empirical methods are no longer available. High accuracy should be required in the shielding and safety design for the beamlines of the facilities of third generation synchrotron radiation.

1.2 Objective of the present study

There are many investigations[1-18),(1-19)] and summaries[(1-20)] of safety shielding for electron accelerators. The shielding design of the accelerator of the third generation synchrotron radiation facility follows fundamentally the production of these scientific researches [(1-21)] . The data, however are not sufficient for the shielding design of high energy electron accelerators. To make data satisfactory and improve the accuracy, benchmark experiments have been performed and efforts are exerted constantly[(1-22)]. The electron beam loss assumption that makes the decision of the source term for shielding design, strongly depends on the type of the accelerator so that the values are employed individually for each machine under the present situation[(1-23)].

On the other hand, there are no more than a few investigations of shielding analysis for the beamline of synchrotron radiation. Moreover these investigations are unsatisfactory and insufficient for the third generation synchrotron radiation facilities. For example, the shielding design code PHOTON II[(1-24)] was developed for the synchrotron radiation beamline. This code can calculate consistently the photons from wigglers and their attenuation by filters, an isotropic scattering process by optical elements and shielding by the wall of the hutches with no buildup effect. Leakage dose calculations outside the hutches were reported in overestimation by using the PHOTON II code[(1-25)]. However, sever conditions were reported by using the code in the third generation facilities[(1-26)]. There was no code to apply to safety shielding design calculation of beamlines in a third generation facility such as SPring-8. For gas bremsstrahlung, many simulations[(1-27),(1-28)] were performed by using electro-magnetic Monte Carlo code such as EGS4[(1-29)] and FLUKA[(1-30)]. Some simulations were performed in insecure calculational conditions and there are some doubts in consideration of the angular distribution of emission as well as the intensity for the long straight section of the third generation facilities. The angular distribution, which affects the absorbed dose or dose equivalent, should be considered to strongly depend on the beam divergence and beam size of stored electrons. However there are no analyses of gas bremsstrahlung which consider the beam divergence and beam size. Measurements using lead glass were performed at lower energy of storage rings[(1-31)] compared to

the 8 GeV class facilities except for the APS of 7 GeV[1-32]. A systematic description, however, has not yet been made for the measurement data in spite of the existence of different results between the beamlines of APS. Moreover, large differences exist for intensity of gas bremsstrahlung calculated from the measurement data of the residual gas components of the storage ring. There are no more than a few calculations for the photoneutron due to gas bremsstrahlung[1-33]. The energy of the gas bremsstrahlung is distributed to the stored electron energy so that not only giant resonance neutrons but also high energy neutrons from the quasi deutron production process and pion production process are produced. However, there are no data except for the photoneutrons produced by giant resonance. Only two measurements of the photoneutron dose were reported by using an Anderson-Brawn type rem-meter with lead shield box[1-34] and BF_3 counter with a polyethylene moderator[1-35].

A safety related typical structure of the synchrotron radiation beamlines consists of a main beam shutter (MBS), a down stream shutter (DSS), a photon stop, a beam stop, an optics hutch for a white beam and an experimental hutch for a monochromatic beam, and in **Fig.1-1**, for example, shows the typical configuration of a SPring-8 beamline. A monochromator installed within the optics hutch is regarded as a scatterer of the synchrotron radiation for the shielding design purpose. The MBS is installed inside the shielding wall of the storage ring to control the synchrotron radiation beam to be transmitted into the beamline, and the DSS is to control the monochromatic synchrotron radiation beam to be transmitted into the experimental hutch. The photon stop made of lead is to prevent gas bremsstrahlung from expanding downstream of the beamline, while the beam stop, usually installed at the furthest downstream of the beamline, is to prevent the monochromatic synchrotron radiation beam from leaking out from the experimental hutch wall. The walls of both the optics and experimental hutches are designed to shield against scattered synchrotron radiation.

As mentioned above, the beamlines of synchrotron radiation are a very complicated system and many movable components such as monochromator and beam shutters are installed so that the intensity and spectrum of synchrotron radiation are varied easily and significantly. A code, therefore, is strongly required to be able to carry out the shielding design easily and quickly with satisfactory

accuracy under various experimental conditions. Further, including high energy photons, gas bremsstrahlung creeps directly into the beamline. The intense and high energy gas bremsstrahlung generates photoneutrons through interaction between photons and target materials such as photon stop. With grasping the behavior of the synchrotron radiation, the investigation of the gas bremsstrahlung and associated photoneutron is required to construct a new photon source such as a free electron laser[1-355)(1-36] and backward Compton scattering photon (laser electron photon)[1-37]. The study of the gas bremsstrahlung and photoneutron are expected to be applicable to new techniques such as utilization of a high energy gamma-ray and clean neutron source.

At the present time, many synchrotron radiation facilities are proposed with new concept design[1-38] so that the establishment of shielding and safety design methods for the beamline are quite important. The objectives of this present study are the development of safety design techniques and elucidation of the behavior of gas bremsstrahlung and associated photoneutrons in order to establish a shielding design method for synchrotron radiation beamlines. It is desired that the fruits of this study be applied to the shielding design of beamlines for the third generation facilities and special beamlines such as laser electron photon beamlines.

In this study, therefore a new shielding design code, STAC8[1-39], was developed to account for the deficiencies in the PHOTON II code and to be applicable to consistent calculations of the radiation emitted from the insertion devices, including undulators, the effect of linear polarization of photons on the scattering process, and the angular dependence of coherent and incoherent scattering. The validity of this code was verified in comparison with the EGS4 calculations, the measurements at two beamlines, one is the doses inside a hutch[1-40] and the other is the doses outside the hutch[1-41]. The high power beam of synchrotron radiation brings new shielding problems, which is the scattered synchrotron radiation by a concrete floor, or so called ground-shine. The analyses were performed and an effective shielding method against groundshine was proposed [1-42)(1-43] by using the combination of the STAC8 code and the general-purpose codes. The gas bremsstrahlung was measured precisely by using a lead tungstate scintillator, and the dependency of the conditions of a stored beam for gas

bremsstrahlung was investigated[1-44]. The depth dependence of an absorbed dose and the dependency of the scoring area for an effective dose due to gas bremsstrahlung were also investigated in related stored beam conditions. Simulation conditions of the generation of gas bremsstrahlung with high accuracy were investigated for long straight sections and new guidelines were proposed[1-45]. The photoneutron spectrum due to gas bremsstrahlung was measured outside the hutch of the SPring-8 beamline by using multi-moderated Bonner type helium-3 counters and the results were compared with the calculations. By using the fruits of this study, shielding analysis was carried out for the beamline of a laser electron photon which is new photon source with high energy using backward Compton scattering with a laser and the effective removal of the high energy electrons produced by electromagnetic showers due to high energy photons were pointed out by using the combination of a sweep magnet and collimators, reducing the shield significantly[1-46].

1.3 Constitution of Chapters and respective contents

The present paper consists of four chapters and two appendixes: Chapter 1 Introduction, Chapter 2 The shielding study of synchrotron radiation, Chapter 3 The study of high energy radiation within the beamline of synchrotron radiation, and Chapter 4 Summary and conclusions.

In Chapter 2, the new shielding design code, STAC8, is described in comparison with the PHOTON II code. STAC8 was developed on the basis of PHOTON II, however the code has many distinctive features that are to be applicable to the calculations of the radiation emitted from the insertion devices including undulators, the angular dependence of the coherent and incoherent scattering with linear polarization effect and K-fluorescence radiation. The angular dependent coherent and incoherent scattering cross sections including polarization effect are calculated within the code and the angle-integrated cross sections obtained by the code were compared with the evaluated data[1-47]. The build up effect is also introduced in the shielding calculation by using an empirical approximation formula, the Geometrical Progression (GP) method[1-48].

For verifying the validity of the STAC8 code, calculational results were compared with those

using the EGS4 code and with dose distribution data inside the hutch (an enclosure of the beam, optical elements or experimental instruments) of a BL14C beamline[1-49] at the Photon Factory of the High Energy Accelerator Research Organization(KEK).

SPring-8, one of the most advanced facilities of synchrotron radiation, generates synchrotron radiation with extremely high intensity and high energy by using insertion devices. The beamlines of SPring-8 are classified by a synchrotron radiation source into an undulator, wiggler and bending magnet beamlines for safety analysis. To clarify the characteristics of these beamlines, the shielding design calculations for synchrotron radiation are performed with STAC8, taking into consideration the linear-polarization effect, the slant length of the shield hutch wall and the build-up effect as functions of scattering angle and azimuthal angle. In addition, the shielding calculations by using the STAC8 code were carried out and compared with the measurements outside the shield wall of the practical beamline of the bending magnet of SPring-8. The calculational results of PHOTON II were also compared with the measurements.

The high power synchrotron radiation beam brings about new shielding problems, which have usually been neglected in shielding designs for the existing facilities. This is the issue of the synchrotron radiation scattered by a concrete floor of the beamline hutch, or so called groundshine. In the groundshine calculations, three geometric configurations were considered; one with a lead rectangular plate installed along the base of the inside of the hutch wall, one with the same plate outside of the hutch wall and one with the bottom part of the hutch wall embedded in the concrete floor.

In Chapter 3, the simulation conditions and measurement results of gas bremsstrahlung by using PWO scintillator are discussed. The simulation of gas bremsstrahlung, which generates the interaction of stored electrons with residual gas within the storage ring, were carried out to investigate the conditions of the simulation to get sufficient accuracy of the photon intensity and the angular distribution. The dependency of the spectrum and angular distribution on the number of interactions, lower cut-off energy for electron transport, AE and residual gas pressure are discussed in comparison with the results of the simulation under the previous recommendations.[1-17], and the condition of the

simulation for the beamline of the third generation facilities was also investigated to propose a new recommendation. Gas bremsstrahlung was measured for the insertion device beamlines of SPring-8 by using a new type of scintillator PWO ($PbWO_4$) and the energy resolution of the PWO was investigated by using gas bremsstrahlung photons. The measurements were made for the two beamlines, BL11XU (high betatron function beamline) and BL46XU (low betatron function beamline), in relation to the characteristics of the stored electron beam. The gas bremsstrahlung was measured as a function of the aperture size of the slits, and the dependence on the conditions of the stored electron beam, as well as the beam current and the vacuum pressure were investigated. The aperture size dependency of gas bremsstrahlung was compared with the calculations by using the Monte Carlo code EGS4 under the new condition of simulation. The dependency of the scoring area for an effective dose and the depth dose distribution due to gas bremsstrahlung were also investigated.

The calculations and the measurement results of the photoneutron due to gas bremsstrahlung are discussed. The associated photoneutron due to gas bremsstrahlung was calculated by using two different methods. One of the methods employs the Lorenzian fitted neutron production cross section[1-50], neglecting neutron production by the quasi-deuteron and photo-pion reactions of photons above 40MeV. The other method is the production cross section generated by using the MCPHOTO code[1-51] and the PICA code[1-52], taking into account the giant resonance, quasi-deuteron and photo-pion reaction processes. Photoneutron spectra due to the interactions of thick targets of lead and copper with gas bremsstrahlung were measured outside the hutch of the insertion device beamline of SPring-8, BL11XU, by using high sensitive multi-moderated Bonner type helium-3 counters. The measurement data were unfolded by using the SAND II code[1-53] and converted to the spectra and doses. The doses were discussed in comparison with the measurements at APS of a 7 GeV storage ring by using an Anderson-Braun type rem-meter with a lead shield box, the calculated results without considering high energy neutrons reported by SLAC[1-33].

The shielding design calculations for the beamline of a laser electron photon are discussed on the basis of the results of the investigations of the gas bremsstrahlung and associated

photoneutron. The shielding design of the beamline of a laser electron photon at SPring-8, which can generate polarized photons of a few GeV with high intensity, was performed and constructed with two separated beamline hutches (enclosures of beam, laser and optical elements or experimental instruments). These two hutches must be designed in tandem and connected with each other by using beam transport pipe, because of the restrictions on space. A local shield, which has special structure, must be installed, accordingly. In addition to the shielding of the synchrotron radiation beamlines, the extremely high energy and high intensity beam of laser electron photons brings other shielding problems. They are the issues of high intensity neutrons due to photonuclear reaction and high energy electrons, positrons in the upstream regions. The reduction of the leakage photoneutron dose by using the shield of beam dump, and effectiveness of a combination of sweep magnet and collimators were investigated.

In chapter 4, the results of the present study are summarized.

Table 1-1 List of the main synchrotron radiation facilities in the world.

Site	Name	Electron Energy(GeV)	Date (operation)	Web site
Japan (Harima)	SPring-8	8	1997	www.spring8.or.jp
	NewSUBARU	1.5	1999	www.lastil.himeji-tech.ac.jp
(Tukuba)	Photon Factory	2.5	1982	pfwww.kek.jp
	AR	7	1986	
	NIJI-II, -IV	0.6	1991	www.etl.go.jp
	TERAS	0.8	1980	
	INS-SOR	0.38	closed	
	TRISTAN	6-30	proposed	
(Hiroshima)	Hi-SOR	0.7	1999	
(Okazaki)	UVSOR	0.6	1983	www.ims.ac.jp
(Kusatsu)	RitsSR	0.575	1996	www.ritsumei.ac.jp
Korea (Pohang)	PLS	2.5	1994	pal.postesh.ac.kr
Chaina (Beijing)	BLS	5.5	proposed	
Taiwan (Hsinchu)	SRRC	1.3	1994	www.srrc.gov.tw
Thailand(Nakhon)	SUT		proposed	nsrc.sut.ac.th
Denmark(Aarhus)	ISA	0.6		www-isa.au.dk
France(Grenoble)	ESRF	6.0	1994	www.esrf.fr
(Orsay)	DCI	1.85		www.lure.u-psud.fr
	Super ACO	0.8		
Germany(Berlin)	BESSY	0.8	1982	www.bessy.de
(Hamburg)	DORIS(DESY)	3.7-5.2	1974	www.hasylab.desy.de
(Dortmund)	DELTA	1.5	2000	praim.physics.uni-dortmont.de
	DELTA II	7-13	under construction	
(Bonn)	ELSA	3.5	1988	www.elsa.physik.uni-bon.de
Italy (Trieste)	ELETTRA	2.0	1993	www.elettra.triestte.it
(Frascati)	ADONE(INF)	1.5	1978	
Russia (Novosibirsk)	VEPP-3	2.2	1977	ssrc.inp.nsk.su
	VEPP-4M	6.0	1992	
(Moscow)	Sibir-1	0.45	1983	
	Sibir-2	2.5		

Table 1-1 List of the main synchrotron radiation facilities in the world (continued)

Site	Name	Electron Energy(GeV)	Year (operation)	Web site
Sweden(Lund)	MAX-I	0.55	1985	www.maxlab.lu.se
Switzerland(Villigen)	SLS(PSI)	2.4	under construction	www1.psi.ch
UK(Daresbury)	SRS	2.0	1980	srs.dl.ac.uk
Canada(Saskatoon)	CLS	3.0	under design	cls.usask.ca
Brazil8Campinas)	LNLS		proposed	www.lnls.br
USA(Argonne)	APS	7.0	1996	epics.aps.anl.gov
(Ithaca)	CHESS	5.0	1979	www.chess.cornell.edu
(Baton Rouge)	CAMD	1.2-1.5		www.camd.lsu.edu
(Berkeley)	ALS(LBL)	1.5		www-als.lbl.gov
(Gaithersburg)	SURF-II,III	0.3	1976	physics.nist.gov
(Upton)	NSLS	2.6		www.nsls.bnl.gov
(Stanford)	SSRL(SPEAR)	4.0	1974	www2.slac.Stanford.edu
	PEP			
	PETRA			

The facilities with under line are third generation synchrotron radiation facilities

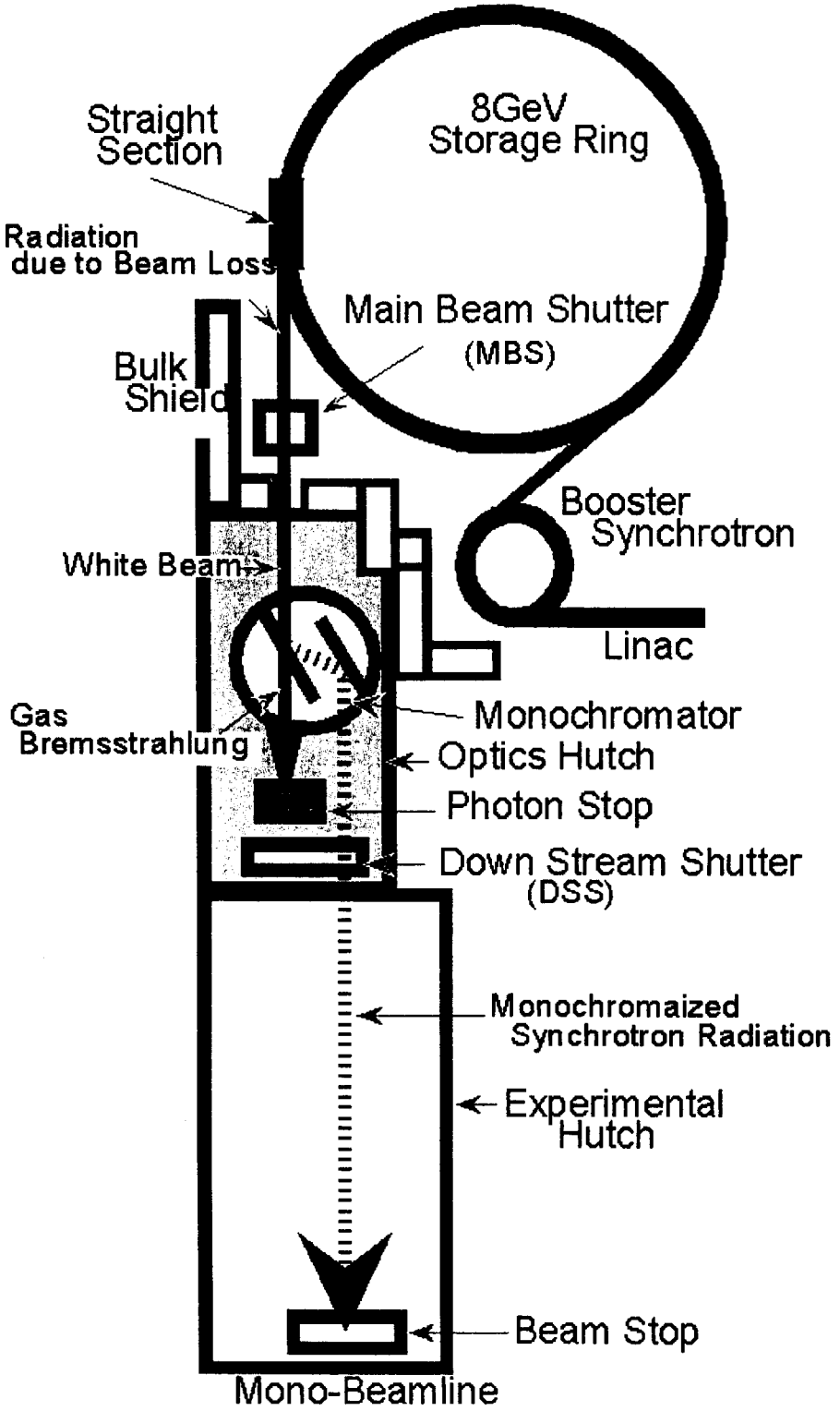

Fig.1-1 Illustration of the typical insertion device beamline of the SPring-8.

This is a blank page.

2. The shielding study of synchrotron radiation

2.1 Introduction

A synchrotron radiation beam has an extremely high power density and high brilliance with polarization. Distinctive problems on the shielding calculation of synchrotron radiation are therefore anticipated. In addition, most of the photon energy is less than 100keV. Synchrotron radiation is introduced to an experimental floor by a beamline through various filters, and the length of the beamline is more than 10m. Moreover, the spectrum and intensity of synchrotron radiation strongly depend on the type of synchrotron radiation source device such as wiggler, undulator or bending magnet.

In the third generation facilities of synchrotron radiation such as ESRF[2-1], APS[2-2] and SPring-8[2-3], many insertion device beamlines are equipped, and shielding analysis is one of the most important things for the safety of the beamlines. The photons scattered by components such as optical elements lead to a serious increase of the dose level around the beamline. Therefore high accuracy should be required in the shielding design for the beamlines.

General purpose radiation transport code, especially Monte Carlo code, is difficult to adapt to beamline shielding calculation because of the necessity of strong attenuation. The method of point kernel and single-scatter calculation will be useful for shielding design calculation of beamlines. From the viewpoint of convenience, code is desired that can calculate consistently from synchrotron radiation sources to dose equivalent outside hutches.

For shielding design calculations of beamlines of synchrotron radiation facilities, the PHOTON II[2-4] code was developed and was actually applied to the design calculation for the beamlines of ESRF[2-5]. But the PHOTON II code underestimated doses outside the shield wall of the hutches in some cases[2-6]. The PHOTON II code has been validly created for calculations of attenuation by filters, the isotropic scattering process by the optical elements and the shielding with the walls of the hutches ignoring the buildup effect of the synchrotron radiation emitted from a wiggler or a bending magnet. However, the polarization effect is

actually dominant in synchrotron radiation and the code does not simulate the scattering process. Furthermore, with the considerably high energy X-rays as generated in the third generation synchrotron radiation facilities, the dose outside the shield wall strongly depends on the scattering angle. On the basis of the PHOTON II code, a new shielding design code STAC8[2-7] has been developed in order to fulfill the above requirements and to be applicable to the calculations of the radiation emitted from the insertion devices including undulators, the effect of linear polarization of photons on the scattering process, and the angular dependence of the coherent and incoherent scattering. The buildup factors have also been introduced in the shielding calculation.

For verifying the validity of the STAC8 code, calculational results were compared with those using a Monte Carlo code EGS4[2-8] and with dose distribution data[2-9] inside the hutch at the beamline 14C of the Photon Factory of the High Energy Accelerator Organization (KEK)[2-10),(2-11)].

The emitted synchrotron radiation is transmitted to an experimental hall in a beamline through the bulk shielding wall of the storage ring. Because of high energy and very low emittance of the stored electrons, high energy synchrotron radiation of extremely high brilliance (photon intensity per unit source area per unit solid angle per second) is available at the third generation synchrotron radiation facilities such as SPring-8 compared to that of the existing synchrotron radiation facilities. These distinguishing features of synchrotron radiation present rather severe radiation problems on the shielding design for the SPring-8 beamlines. The shielding calculations using the STAC8 code were carried out in order to clarify the characteristics of the practical beamlines of a third generation synchrotron radiation facility. The four typical beamlines, which are one beamline of a bending magnet, one wiggler beamline, and two undulator beamlines, were selected in this chapter and the dose distributions outside the sidewalls and roofs of the hutches were calculated considering the linear polarization effects, the slant length of the shield hutch wall and the build-up effect as functions of scattering angle and azimuthal angle[2-12]. In addition, the shielding calculations using the STAC8 code were carried out and compared with the dose

measurements outside the shield walls of the bending magnet beamline of SPring-8[2-13]. The calculational results of PHOTON II were also compared with the measurements and the STAC8 to make clear the distinctive features of the codes.

Because of the beam power of the synchrotron radiation of the third generation facilities being so high, scattered synchrotron radiation by the concrete floor, so called groundshine, causes a seriously high leakage dose so that special consideration for the shielding design of the beamline hutch is required[2-14]. Using the STAC8 code and the combination with the codes for general purpose, the groundshine can be estimated easily and analyses were performed for three geometric configurations to prevent the leakage dose increasing outside the hutches. The three geometric configurations employed are, one with a lead rectangular plate installed along the base of the inside of the hutch wall, one with the same plate outside of the hutch wall, and one with the bottom part of the hutch wall embedded in the concrete floor.

2.2 Development of shielding design code for a synchrotron radiation beamline, STAC8

On the basis of PHOTON II, the STAC8 code was developed and designed for beamline shielding of synchrotron radiation. Therefore the distinctive features of synchrotron radiation were taken into the framing of the code. Specially, synchrotron radiation is quite a narrow beam with strong directivity so that the scattering area of a scatterer (target) within the beamline can be restricted. The point kernel and single-scatter methods are quite useful because of the above reasons and the necessity of strong attenuations of photon. **Figure 2-1** shows a flow diagram of the STAC8 code. In contrast with the PHOTON II code, the main distinctive features of the code are (1) addition of an angle-integrated undulator source calculation, (2) taking into account angular dependent coherent and incoherent scattering cross sections with the polarization effect and (3) introducing buildup factors for shielding calculations and dose conversion factors for dose equivalent calculations.

The code starts its calculation with determining the synchrotron radiation spectrum

from undulator, wiggler or bending magnet. Secondly, calculations are made for photon attenuation and heat load in several filters and optical elements and finally doses outside the shield wall of hutch roof, side and back of hutch are obtained taking into account the angular dependent scattering cross section with polarization effect and K-fluorescence radiation as illustrated in **Fig.2-2**. More detailed descriptions about the above characteristics are given below.

2.2.1 Synchrotron radiation sources

The source of synchrotron radiation, which is produced by charged particles (specially, electrons/positrons) moving with relativistic speed in curved trajectories, can be classified into three sources. There are undulator, wiggler, and bending magnet sources.

(a) Undulator source

An undulator, which consists of periodic magnets, produces a gentle and periodic orbit of electrons. And for the electron trajectories in an undulator, the angle between the trajectory slope and the observation direction is smaller than $1/\gamma$ everywhere, where γ is the electron energy in m_0c^2, a unit of the rest mass energy of the electron. The angular width of a radiation beam from an undulator is, therefore of the order of $1/\gamma$, and depends on the electron energy of the storage ring. Since the angular width is very narrow for the high energy synchrotron radiation facility, the angle integrated flux is quite useful for shielding design calculation and heat load analysis as well as flux estimation within the central cone. An effective calculation method for angle integrated flux on some assumptions is given as follows, and based on the method, a computer code URGENT[2-15] has been written. A method similar to URGENT was employed in the STAC8 code.

On the assumption of neglecting the near field and small velocity field, the spectral and angular distribution of synchrotron radiation of the *n*-th harmonics is given by the following,

$$\frac{d^2F_n(E_\gamma,\Omega)}{dE_\gamma d\Omega}=\frac{e\gamma^2 I}{4\pi\varepsilon_0 cE_\gamma}\,|A_n(\alpha,\phi)|^2\,L(\frac{\Delta\omega}{\omega_1}) \qquad (2\text{-}1)$$

$$A_n(\alpha,\phi) = \xi\left[2\alpha\cos\phi\cdot S_0 - K_y(S_1+S_{-1}), 2\alpha\sin\phi\cdot S_0 - iK_x(S_1-S_{-1}), 0\right] \tag{2-2}$$

$$S_q = \sum_{p=-\infty}^{\infty}\exp\{-i(n+2p+q)\Phi\}J_p(Y)\cdot J_{2p+q+n}(X) \tag{2-3}$$

where J is a Bessel function and p is integer, and

$$\tan\Phi = (K_x/K_y)\tan\phi_s \tag{2-4}$$

$$X = 2\xi(K_y^2\cos^2\phi_s + K_x^2\sin^2\phi_s)^{1/2} \tag{2-5}$$

$$Y = \xi(K_y^2 - K_x^2)/4 \tag{2-6}$$

$$\xi = n/(1+K_x^2/2+K_y^2/2+\alpha^2) \tag{2-7}$$

$$\alpha = \gamma\theta_s \tag{2-8}$$

$$L = \sin^2(N\pi\frac{\Delta\omega}{\omega_1})/\sin^2(\pi\frac{\Delta\omega}{\omega_1}) \tag{2-9}$$

Usually N is a large number so that the formula (2-9) can be expressed as

$$L = N\sum_n^{\infty}\delta\left[\frac{\omega}{\omega_1}\left[1+\frac{\alpha^2}{1+K_x^2/2+K_y^2/2}\right]-n\right] \tag{2-10}$$

$$\Delta\omega = \omega - \omega_n \tag{2-11}$$

$$\omega_n = n\frac{4\pi c\gamma^2}{\lambda_u(1+K_x^2/2+K_y^2/2+\alpha^2)}, \qquad n = 1,2,3\cdots \tag{2-12}$$

and e, ε_o, and c are the elementary electric charge, dielectric constant and light velocity, respectively. I (mA) is a stored current, N is the number of periods, $E_\gamma(keV)$ is the photon energy of synchrotron radiation, ω is the frequency of photons with E_γ energy, ω_n is the frequency of the n-th harmonics, θ_s is the observation angle from the electron beam axis, and ϕ_s is the azimuthal angle from the horizontal plane. Kx and Ky are deflection parameters in the X and Y directions and these are

$$Kx, y = eB_{(x,y)0}\lambda_u/2\pi mc = 93.4\lambda_u B_{(x,y)0} \tag{2-13}$$

where $B_{(x,y)0}$ is a peak magnetic field strength in Tesla in the X, or Y direction, and λ **u** is a magnetic period in meters, and K/γ is the maximum slope of the trajectory of the electrons(deflection angle). Usually an undulator is a device of the deflection parameter,

$K \leq 1.0$. The spectrum of the angle integrated flux can be obtained by summing the formula (2-1) with harmonics number n and integrating with the angle, as follows

$$\frac{dF(E_\gamma)}{dE_\gamma} = \sum_{n=1}^{\infty} \int \frac{d^2F_n(E_\gamma,\Omega)}{dE_\gamma d\Omega} d\Omega$$

$$= 4.556\times10^{10} \cdot \frac{I(mA)}{E_\gamma(keV)} \cdot \sum_{n=1}^{\infty} \int \left|A_n(\alpha,\phi)\right|^2 L(\frac{\Delta\omega}{\omega_1}) d\Omega \qquad [photons/eV/\sec] \qquad (2\text{-}14)$$

The total power $\boldsymbol{P}$ of undulator in watts is given by

$$P = 0.633 \cdot E^2 \cdot B_0^2 \cdot \lambda_u \cdot N \cdot I \qquad (2\text{-}15)$$

where $\boldsymbol{E}$ is the electron energy in GeV, $\boldsymbol{N}$ is the number of periods and $\boldsymbol{I}$ is a stored current in mA. It is seen that the energy and angle integrated flux calculated with STAC8 agrees with the total power $\boldsymbol{P}$ by the formula (2-15).

(b) Wiggler source

As the deflection parameter $\boldsymbol{K}$ becomes larger so that the deflection angle K/ γ is much larger than γ^{-1}, a small portion of the trajectory slope can be replaced by segments of a circle. Therefore, the radiation from a large $\boldsymbol{K}$ undulator will be similar to that from a sequence of circle trajectories. In such a case, an undulator is referred to as a wiggler. The spectrum of synchrotron radiation per one millli-radian of opening angle on the orbital plane from a wiggler is expressed as follows[2-16],

$$\left[\frac{dF(E_\lambda)}{dE_\gamma}\right]_{1mrad\cdot h} = \int \frac{d^2F(E_\gamma,\psi)}{dE_\gamma d\psi} d\psi = \int \frac{3\times10^{-3} e\gamma^2 I \cdot 2N}{2\pi chE_\gamma} (\frac{\lambda_c}{\lambda})^2 \left\{1+(\gamma\psi)^2\right\}^2 \cdot \left\{J_{2/3}^2(\varsigma) + \frac{(\gamma\psi)^2}{1+(\gamma\psi)^2} J_{1/3}^2(\varsigma)\right\} d\psi$$

$$= \frac{3.46\times10^6 \gamma^2 I(mA)\cdot 2N}{E_\gamma(keV)} (\frac{\lambda_c}{\lambda})^2 \left\{1+(\gamma\psi)^2\right\}^2 \cdot \left\{J_{2/3}^2(\varsigma) + \frac{(\gamma\psi)^2}{1+(\gamma\psi)^2} J_{1/3}^2(\varsigma)\right\} d\psi$$

$$[photons/\sec/eV/mrad\cdot h] \qquad (2\text{-}16)$$

$$\lambda_c = \frac{4\pi}{3}\frac{R}{\gamma^3} = \frac{18.6}{E^2(GeV)B_0(T)} \qquad [\overset{0}{A}] \qquad (2\text{-}17)$$

$$\varsigma = \frac{\lambda_c}{2\lambda}[1+(\gamma\psi)^2]^{3/2} \tag{2-18}$$

where $\boldsymbol{h}$ is the Planck constant, λ is the wave length of photons and λ_c is the critical wave length of the wiggler, ψ is the opening angle from the orbital plane. $J_{2/3}, J_{1/3}$ are the modified Bessel functions of the second kind. $\boldsymbol{R}$ is the radius of the circle trajectory of electrons. Other symbols are the same as for the undulator source.

(c) Bending magnet source

The synchrotron radiation spectrum from a bending magnet can be expressed by the same formula as a wiggler with 2N=1, because a bending magnet has one magnetic pole.

2.2.2 Attenuation and heat load process of filters

The transmitted photon spectrum through the n-th filter of thickness, T_n(cm) are expressed as follows,

$$\Phi_n(E_\gamma)[photons/\sec/eV] = \Phi_{n-1}(E_\gamma)\cdot\exp(-\mu_n(E_\gamma)\cdot T_n) \tag{2-19}$$

$$\Phi_0(E_\gamma)[photons/\sec/eV] = \frac{dF(E_\gamma)}{dE_\gamma} \tag{2-20}$$

$$\mu_n(E_\gamma) = \tau_n(E_\gamma) + \Sigma^n_{coh}(E_\gamma) + \Sigma^n_{incoh}(E_\gamma) \qquad [cm] \tag{2-21}$$

where $\Phi_n(E_\gamma)$ is the photon beam spectrum through the n-th filter, $\mu_n(E_\gamma)$ in cm is the attenuation coefficient of the n-th filter, and $\tau_n(E_\gamma)$, $\Sigma^n_{coh}(E_\gamma)$, and $\Sigma^n_{incoh}(E_\gamma)$ are the absorption coefficient of photoelectric effect, the coherent scattering coefficient, and the incoherent scattering coefficient in cm, respectively. $\Sigma^n_{coh}(E_\gamma)$, and $\Sigma^n_{incoh}(E_\gamma)$ are presented in the next section, precisely.

Heat load within the n-th filter is expressed with considering K –shell fluorescence as follows,

$$\Delta P_n[W] = \int\left\{\int_0^{T_n}\mu^n_{en}(E_\gamma)\cdot E_\gamma\cdot\Phi_{n-1}(E_\gamma)\cdot\exp(-\mu_n(E_\gamma)\cdot x))dx\right\}dE_\gamma$$

$$= \int\frac{\mu^n_{en}(E_\gamma)}{\mu_n(E_\gamma)}\cdot E_\gamma\cdot\Phi_{n-1}(E_\gamma)\cdot(1-\exp(-\mu_n(E_\gamma)\cdot T_n))dE_\gamma$$

$$= 1.6\times10^{-16}\cdot\int \frac{\mu_{en}^{n}(E_\gamma)}{\mu_n(E_\gamma)}\cdot E_\gamma(keV)\,\Phi_{n-1}(E_\gamma)\cdot(1-\exp(-\mu_n(E_\gamma)\cdot T_n))dE_\gamma \quad (2\text{-}22)$$

$$\mu_{ea}^{n}(E_\gamma) = \tau_{ea}^{n}(E_\gamma) + \Sigma_{ea}^{n}(E_\gamma) \qquad [cm] \quad (2\text{-}23)$$

$$\tau_{ea}^{n}(E_\gamma) = \tau_n(E_\gamma) - \tau_k^{n}(E_\gamma)\cdot(w_k^{n}\ \frac{E_k^{n}}{E_\gamma}) \qquad [cm] \quad (2\text{-}24)$$

where ΔP_n in watt is the heat load within the n-th filter, $\mu_{ea}^{n}(E_\gamma)$ is the energy absorption coefficient of n-th filter, $\tau_{ea}^{n}(E_\gamma)$ is the photoelectric energy absorption coefficient of the n-th filter and $\Sigma_{ea}^{n}(E_\gamma)$ is the energy absorption coefficient due to scattering process (Compton recoil electron etc). $\tau_k^{n}(E_\gamma)$ is the energy absorption coefficient at the *K*-absorption edge of the n-th filter, w_k^{n} and E_k^{n} in keV are the K-shell fluorescent yield and the average energy of the fluorescent photons, respectively.

The evaluated data of each absorption coefficients are provided for all of the elements, and forty-eight compounds and mixtures by Hubbell[2-17] and Seltzer[2-18]. In the STAC8 code, however, the approximation methods[2-19),(2-20] are employed for convenient and these are the same as PHOTON II. The data of $\tau_n(E_\gamma)$, $\tau_{ea}^{n}(E_\gamma)$, $\Sigma_{ea}^{n}(E_\gamma)$, $\tau_k^{n}(E_\gamma)$ and w_k^{n} are provided in STAC8 for twenty-four elements, which are hydrogen, helium, beryllium, carbon, nitrogen, oxygen, aluminum, silicon, phosphorus, argon, calcium, chromium, manganese, iron, nickel, copper, germanium, krypton, molybdenum, xenon, tantalum, tungsten, and lead.

2.2.3 Scattering process

The last filter is assumed to be the scatterer in the STAC8 code and cylindrical geometry is employed for the scatterer. The scattered photon intensity considering the linear polarization effect, is expressed as follows,

$$\begin{aligned}\Phi_s(E,\theta,\phi)[photons/eV/s] &= \int_0^{T_s}\Sigma_s(E_\gamma\rightarrow E)\cdot\Phi_{n-1}(E_\gamma)\cdot\exp(-\mu_n(E_\gamma)\cdot x)dx \\ &= [\frac{\Sigma_s(E_\gamma\rightarrow E)}{\mu_n(E_\gamma)}]\cdot\Phi_{n-1}(E_\gamma)\cdot\{1-\exp(-\mu_n(E_\gamma)\cdot T_s)\}\end{aligned} \quad (2\text{-}25)$$

$$\Sigma_s(E_\gamma\rightarrow E) = \Sigma_{coh}^{n}(E_\gamma) + \Sigma_{incoh}^{n}(E_\gamma) \quad (2\text{-}26)$$

where T_s is the thickness of the scatterer and n is the last number of filters. Angular

dependent coherent and incoherent scattering cross sections, including the polarization effect of photons, are given as follows[2-21].

$$\Sigma^n_{coh}(E_\gamma) = (d\sigma / d\Omega)_{coh} \cdot \rho_n \cdot N_0 \cdot Z / A_s \tag{2-27}$$

$$\Sigma^n_{incoh}(E_\gamma) = (d\sigma / d\Omega)_{incoh} \cdot \rho_n \cdot N_0 / A_s \tag{2-28}$$

$$(d\sigma / d\Omega)_{coh} = r_0^2 \cdot F^2(q,Z) \cdot \{1 - (\sin^2\theta)(\cos^2\phi)\} \tag{2-29}$$

$$(d\sigma / d\Omega)_{incoh} = (r_0^2 / 2) \cdot S(q,Z) \cdot (E/E_\gamma)^2 \cdot \{E_\gamma / E + E/E_\gamma - 2 \cdot (\sin^2\theta) \cdot (\cos^2\phi)\} \tag{2-30}$$

where r_0 is the classical electron radius, θ is the a scattering angle, ϕ is the azimuthal angle from the electric field vector of photons, E/E_γ is the ratio of scattered to incident photon energies. ρ_n (g/cm^3), Z, and A_s (g) are the density, atomic number, and atomic weight of the scatterer, respectively. N_0 is Avogadro's constant. $F(q,Z)$ and $S(q,Z)$ are the atomic form factor and the incoherent scattering function, respectively. Here $q = \sin(\theta/2)/\lambda$, where λ is the wave length of the photons.

The atomic form factors $F(q,Z)$ given in the code are as follows:

(1) Hydrogen $Z = 1$[2-22]

$$F(q,1) = (1 + 4\pi^2 \cdot a_0^2 \cdot q^2)^{-2} \tag{2-31}$$

where a_0 is the first Bohr radius.

(2) Helium Z = 2 (Bethe-Levinger's formula) [2-23]

$$F_1(q,2) = \sin(2\gamma \cdot \tan^{-1} Q) / \{\gamma \cdot Q(1+Q^2)^\gamma\} \tag{2-32}$$

$$\gamma = (1 - (\alpha \cdot Z)^2)^{1/2} \tag{2-33}$$

$$Q = q/(2\alpha \cdot Z \cdot m_0 c) \tag{2-34}$$

where α is the fine structure constant (1/137), m_0 is the rest mass of electrons and c is the velocity of light.

(3) For the atomic number Z >2

(a) If $q \leqq 2.0$, $F(q,Z)$ is given by[2-24]

$$F_2(q,Z) = \sum_i A(Z,i) \exp(-B(Z,i) \cdot q^2) + C(Z) \tag{2-35}$$

where $A(Z,i)$, $B(Z,i)$ and $C(Z)$ are coefficients as a function of Z.

(b) If $2.0 < q < 20$, $F(q,Z)$ is obtained by interpolation between $F_1(q,Z)$ and $F_2(q,Z)$.

(c) If $q \geqq 20$, we use the formula (2-32).

A simple method for calculation of the incoherent scattering function is given by Smith et al.[2-25] as follows,

$$S(q,Z) = Z[1-(1+a_0 \cdot q^2 + b_0 \cdot q^4)\cdot(1+c_0 \cdot q^2 + d_0 \cdot q^4)^{-2}] \quad (2\text{-}36)$$

where a_0, b_0, c_0, and d_0 are constants depending on Z and tabulated in the literature of Smith. The same method was used for $S(q,Z)$ in STAC8. The angle integrated cross sections obtained with STAC8 confirmed to agree well with the estimation by Hubbell et al.[2-26],[2-27], as shown in **Fig.2-3** for Silicon and in **Fig.2-4** for lead.

The fluorescent radiation from the scatterer is introduced and the total K-shell fluorescence in the scatterer is express as follows,

$$\Phi^f(E_k^n)[photons/s] = \Phi_{n-1}(E_\gamma)\cdot\frac{\tau_k^n(E_\gamma)}{\mu_n(E_\gamma)}\cdot(\omega_k^n\frac{E_k^n}{E_\gamma})(1-\exp(-\mu_n(E_\gamma)\cdot T_n) \quad (2\text{-}37)$$

Most of the photon energy of synchrotron radiation is less than 100 keV so that the self-shielding of the scatterer is important. Therefore, self-shielding of the scatterer is introduced, and then formula (2-25) can be expressed as follows,

if $(T_n - x)\tan\theta \leqq d$, then

$$\Phi_s(E,\theta,\phi) = \int_0^{T_n} \Sigma_s(E_\gamma \rightarrow E)\cdot\Phi_{n-1}(E_\gamma)\cdot\exp(-\mu_n(E_\gamma)\cdot x) \cdot\exp(-\mu_n(E_\gamma)\cdot(T_n - x)/\cos\theta)dx \quad (2\text{-}38)$$

and if $(T_n - x)\tan\theta > d$, then

$$\Phi_s(E,\theta,\phi) = \int_0^{T_s} \Sigma_s(E_\gamma \rightarrow E)\cdot\Phi_{n-1}(E_\gamma)\cdot\exp(-\mu_n(E_\gamma)\cdot x) \cdot\exp(-\mu_n(E_\gamma)\cdot d/\sin\theta)dx \quad (2\text{-}39)$$

where d is the radius of the cylindrical scatterer. The self-shielding effect for fluorescent radiation is also introduced in the STAC8 code.

2.2.4 Dose calculation with buildup effect

The flux outside the shield wall is obtained by the formula given below,

$$\phi_x(E,\theta,\phi)=\frac{\Phi_s(E,\theta,\phi)\cdot\exp(-\mu_a(E)\cdot|\vec{r}|)}{|\vec{R}|^2}+\frac{\Phi^f(E_k^n)\cdot\exp(-\mu_a(E_k^n\cdot|\vec{r}|)}{4\pi|\vec{R}|^2} \quad (2\text{-}40)$$

$$|\vec{R}|=D/(\vec{d_0}\cdot\vec{r_0}) \quad (2\text{-}41)$$

$$|\vec{r}|=d_w/(\vec{d_0}\cdot\vec{r_0}) \quad (2\text{-}42)$$

where $\phi_x(E,\theta,\phi)$ is the photon flux at the estimation point, x, $|\vec{R}|$ and $|\vec{r}|$ are the distance from the scattering point to the estimation point x, and an effective thickness of the shield wall of material a, respectively. μ_a is the linear attenuation coefficient of material a. D and d_w are the distance from the scattering point to the shield wall and the thickness of the shield wall, respectively. $\vec{d_0}$ and $\vec{r_0}$ are the unit vectors of the perpendicular direction against the plane of the shield wall and the unit vector in the direction from the scattering point to estimation point, respectively. As shown in **Fig.2-2**, three kinds of shield walls (back, roof, and side) are provided in the STAC8 code so that $\vec{d_0}$ can be expressed as (1,0,0), or (0,1,0), or (0,0,1) in rectangular Cartesian coordinates, and $\vec{r_0}$ also expressed as ($\cos\theta$, $\sin\theta\sin\phi$, $\sin\theta\cos\phi$).

The ambient dose equivalent H*(10), directional dose equivalent H'(0.07) and H'(3.0), and absorbed dose are obtained by the formula given below, taking into account the buildup factors of shielding materials,

$$D_x=\sum_E f_x(E)\cdot B(E,\mu_a\cdot r)\cdot C(E)\cdot\phi_x(E,\theta,\phi)\Delta E \quad (2\text{-}43)$$

where D_x is the ambient dose equivalent rate, directional dose equivalent rates or absorbed dose rate at position x. $f_x(E)$ is a conversion parameter of the absorbed dose buildup factor to one of these depth doses[2-28]. $B(E,\mu_a\cdot|\vec{r}|)$ is an absorbed dose buildup factor and $C(E)$ is a dose conversion factor from flux to absorbed dose rate. The buildup factor $B(E,\mu_a\cdot|\vec{r}|)$

is calculated by using the Geometrical Progression (GP) method[2-29] for 12 common shield materials. The dose conversion factor $C(E)$ is quoted from the ICRP data book[2-30] and its interpolated data. Based on the formula (2-9), the ambient dose equivalent, directional dose equivalents and the absorbed dose due to scattered photons are calculated at any position outside the shield wall. Besides these doses, doses behind the beam shutter due to directly filtered beams are also calculated, taking into account the buildup effect there.

Figure 2-5 shows, for example, that angular dependence of the dose equivalent values outside the shield wall and the buildup effects. Here the angle is measured from the incident beam direction. The radiation source is generated from the wiggler, which has 15 poles and the peak magnetic field strength of 1.5 Tesla, magnetic period of 18 cm, and critical energy of 64.0 keV. The ring current, stored electron energy, and total power are 100 mA, 8 GeV, and 24.6 kW, respectively. In the attenuation calculation, variation of the slant length of the shield wall corresponding to the angle was taken into account. As is evident from the figure, the distribution of the ambient dose equivalent, H*(10), outside the shield wall depends strongly on the photon scattering angle, forming its peak around a scattering angle of 40 degrees to 50 degrees. The buildup effect ratios on the dose value around the peak are about 2.7 and 2.3 for a lead wall of 35 mm and 20 mm, respectively.

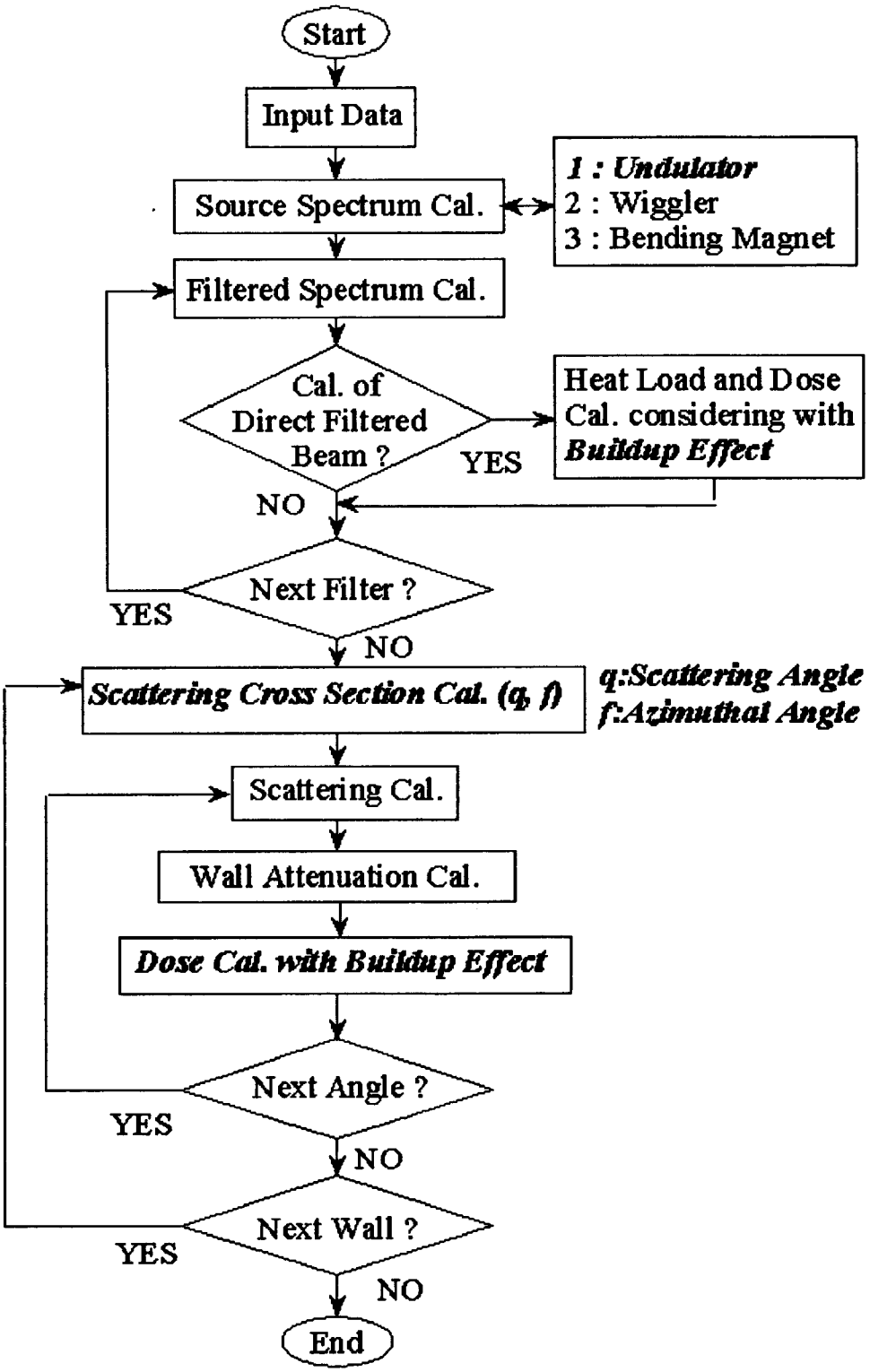

Fig.2-1 Main flow diagram of STAC8

This is a blank page.

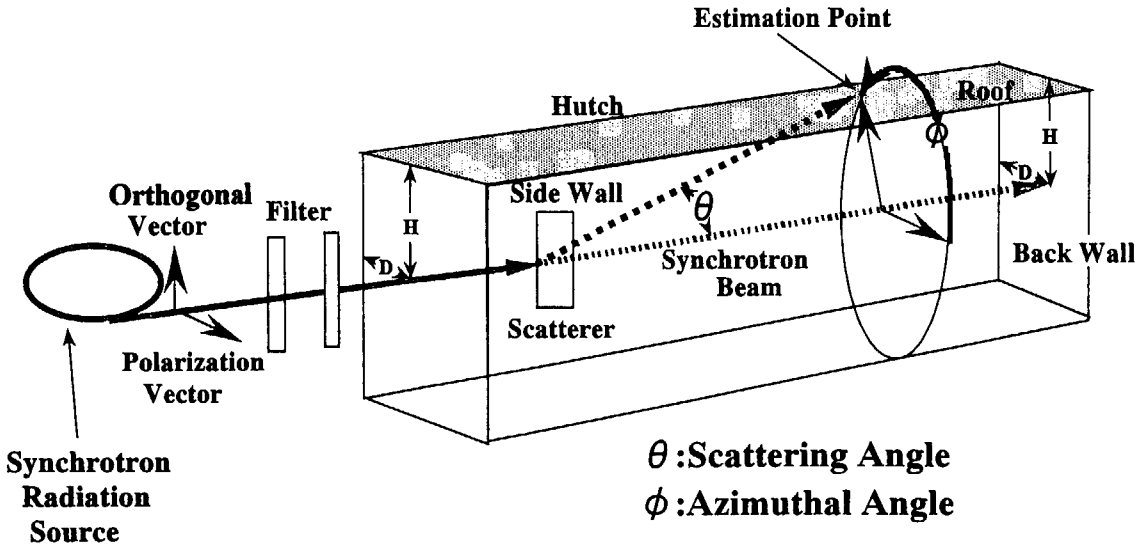

Fig. 2-2 Illustration of the process of the shielding calculation for synchrotron radiation by using STAC8. (H: Height from beam to roof, D:Distance from beam to shield wall)

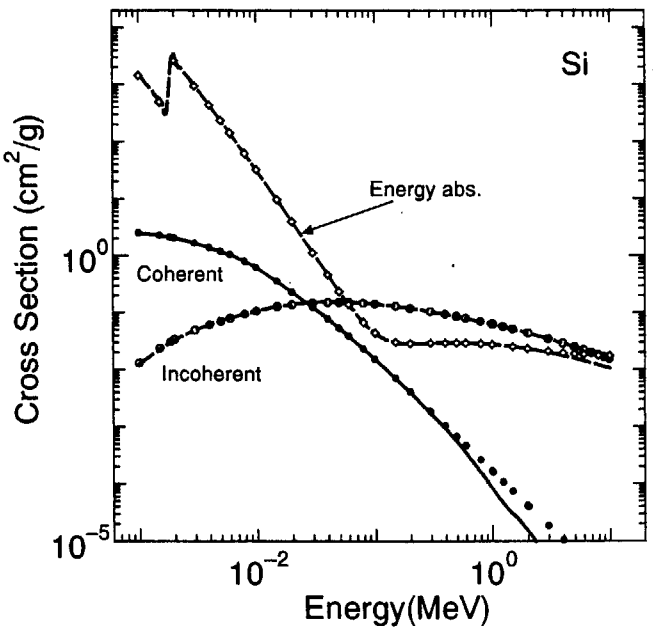

Fig.2-3 Angle-integrated scattering cross section of silicon obtained with STAC8 calculation. Solid, dot dashed, and dashed lines indicate the coherent, incoherent scattering cross sections and energy absorption coefficient by STAC8 calculations. Full circle, open circle, and open diamond indicate the evaluated data by Hubbell et al. [2-17),(2-26)].

This is a blank page.

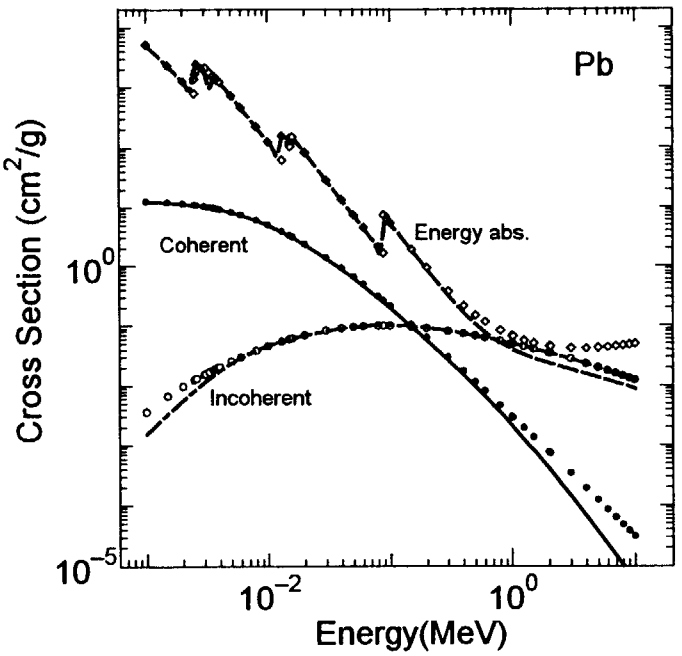

Fig.2-4 Angle-integrated scattering cross section of lead obtained with STAC8 calculation. The lines and symbols are the same as in Fig.2-3.

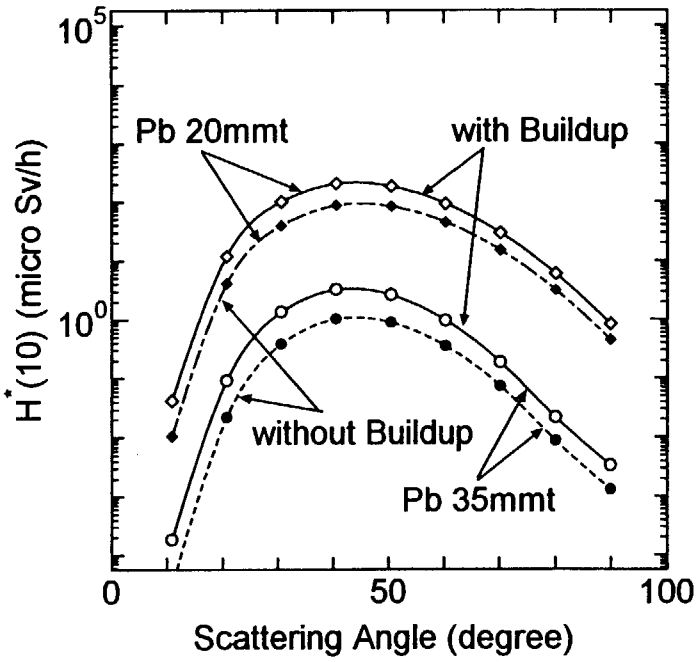

Fig.2-5 Calculated dose equivalent outside the beamline shield as a function of scattering angle for a wiggler radiation. Open circles and solid lines, full circles and dashed lines, open diamonds and solid lines, and full diamonds and dashed lines indicate the STAC8 calculations by using a lead shield wall of 35 mm thick with and without buildup effect, and 20 mm thick with and without buildup effect, respectively.

2.3 Validation Verification of STAC8

In order to verify its validity, the calculation with STAC8 was compared with the Monte Carlo calculation with an Monte Carlo electro-magnetic cascade simulation code EGS4, and with a measured dose of distribution data by using TL dosimeters inside the hutch at the beamline-14C of the Photon Factory of KEK. The actual dose outside the hutch of the bending magnet beamline of the third generation synchrotron radiation facility on the radiation measurements were also compared with the calculated results of STAC8.

2.3.1 EGS4 calculation

For the purpose of this verification, the synchrotron radiation source from a wiggler is assumed. The number of poles, critical energy, period, peak magnetic field strength and ring current are 66, 64.4 keV, 56 mm, 0.1912 Tesla and 1 mA, respectively. Some filters such as beryllium and kapton film are considered between the source and optical element by which the photons are scattered. The configuration of the problem is illustrated in **Fig.2-6**. The STAC8 calculation started with the determination of the photon source flux which was also used as input source data for the EGS4 calculation. The separation between the scattering point and shield wall is 500 mm. The shield there consists of steel and lead whose thickness are 0.01 and 1.0 mm, respectively.

The maximum and minimum energies of photons are 2.7 MeV and 30.0 keV, of which the energy range is divided into nine energy groups. 5,000,000 histories of photons are used for each energy group in the EGS4 calculation. **Table 2-1** gives the calculation results, showing that fairly good agreement was obtained between the results with STAC8 and EGS4 expect in the case of a scattering angle of 10 degrees. One of the reasons of the deviation at 10 degrees is considered as follows. The error of the calculated buildup factors will increase for a wide energy group width and its magnitude may pile up with increase of penetration, which increases with the decrease of scattering angle. And the other reason is that the geometrical progression method on the basis of normal incident photons is employed instead of the factors for obliquely incident pencil beam condition.

2.3.2 Beamline-14C of Photon Factory

The distribution of exposure due to linear polarized synchrotron radiation within experimental hutch was measured using a BL-14C beamline of the Photon Factory at the High Energy Accelerator Organization(KEK). The arrangement of experimental setup is illustrated in **Fig.2-7**. The synchrotron radiation beam from the super-conducting vertical wiggler was collimated in a size of 4.5 x 4.5 cm^2. The absolute intensity of photons was monitored with electron stored beam current, that was calibrated with a calorimeter developed for the synchrotron radiation beamline experiment[2-31]. A silicon disk of 152.4 mm in diameter was used as a scatterer and was set two ways. One way was perpendicular to the X-Z plane with an inclination of 30 degrees with respect to the X-axis (Si(X)), the other way was perpendicular to the Y-Z plane with an inclination of 60 degrees with respect to the Y-axis (Si(Y)) as indicated in **Fig. 2-7**. Another geometry is with no silicon scatterer. LiF TL dosimeters are used and setup on the concentric circles with radii of 5 cm, 10 cm, 15 cm, 20 cm, 40 cm and 50 cm on the plane at Z=22.5 cm, 72.5 cm, 122.5 cm, 172.5 cm and 222.5 cm.

The measured results of exposure on the concentric circle with radius 40.0 cm at Z=172.5 cm plane are given in **Fig.2-8**. The calculated results using the STAC8 code are also involved. The horizontal axis in the figure corresponds to the X-axis and to the azimuthal angle of 90 degrees in the positive direction and 270 degrees in the negative direction respectively. Similarly the vertical axis corresponds to the Y-axis and to 0 degrees and 180 degrees. The distance from the graph center to the data point indicates the exposure at each point in mGy per Joule of incident photons.

Asymmetric distribution on the Si(X), as shown in **Fig. 2-8**, are observed because of a shadow effect by the Silicon scatterer and its holder. On the right hand side distribution of Si(X) where no shadow effect is there, the calculations are fairly good agreement with observed distribution. The X-axis (horizontal axis) at Z=172.5 cm are shown in **Fig. 2-9**. The remarkable features of this figure are that the Si(Y) distribution is under the distribution without the Silicon scatterer and that a very low exposure rate is found near the center region of Si(X) distribution because of the shadow effect. The STAC8 calculation shows close

agreement with the Si(X) distribution in the region without shadow effect. **Figure 2-10** shows the exposure distribution along the Y-axis (vertical axis) at an azimuthal angle 0 degrees just behind the silicon scatterer at Z=1725 mm. The features that are easily noticed are that the distributions for the Si(X) and Si(Y) geometries are nearly equal at the region of larger R and that the STAC8 calculation agrees well with the exposure distribution for the Si(Y) geometry.

Table 2-1 Comparison of the calculations with STAC8 and EGS4 for the dose equivalent outside the shield.

Scattering angle (degree)	**10**	**38**	**64**	**90**
Dose (Sv/h) (by STAC8)	**0.238**	**5.76**	**15.8**	**10.9**
Dose (Sv/h) (by EGS4)	**0.112**	**5.33**	**12.9**	**8.71**
	+5.1%	**+2.5%**	**+2.5%**	**+3.0%**
	-4.7%	**-2.3%**	**-2.5%**	**-2.9%**
Ratio (STAC8/EGS4)	**2.13**	**1.08**	**1.22**	**1.25**

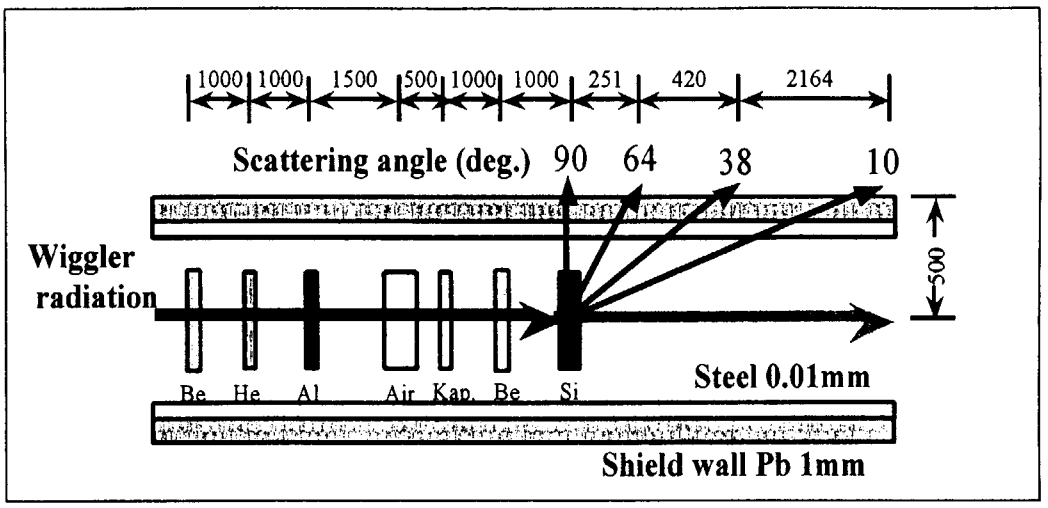

Fig.2-6 Geometrical arrangement for a benchmark problem of beamline shielding. Thickness of Be, He, Al, Air, Kapton, Be and Si are 0.009, 30, 0.015, 23.9, 0.1, 0.015 and 20mm, respectively.

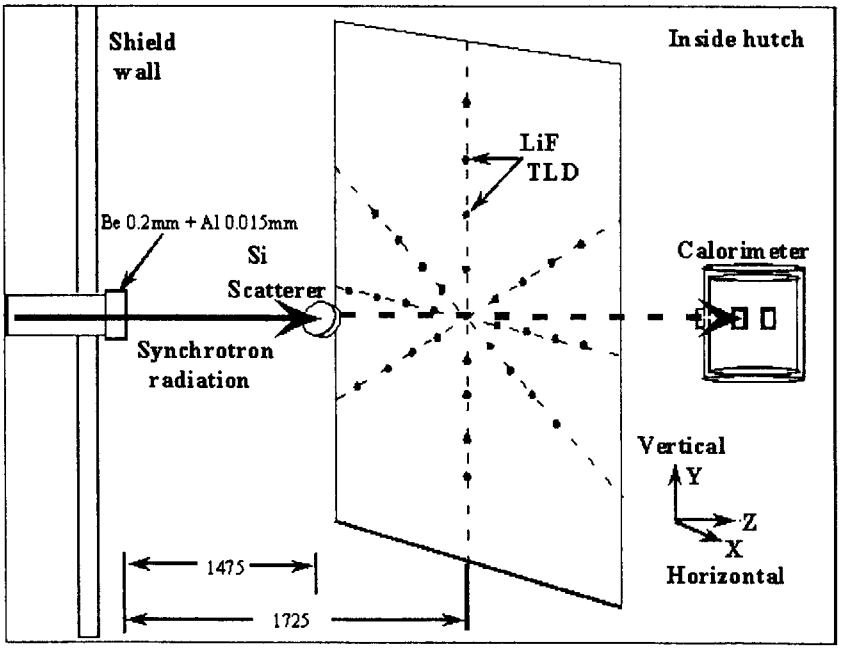

Fig.2-7 Modeled configuration for the experiment of exposure distribution within the experimental hutch of BL14C at Photon Factory of KEK

This is a blank page.

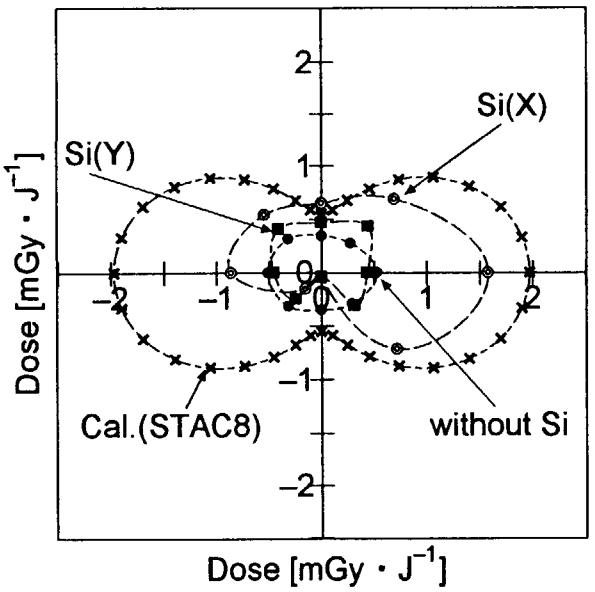

Fig.2-8 Exposure rate on the concentric circle with radius 40.0 cm at Z = 1725mm plane. The open circle and dot line indicates the measurement data with inclined silicon crystal with respect to the X-axis, Si(X), full square and dot line indicates the data with inclined silicon crystal with respect to the Y-axis, Si(Y), and the full circle and dot line indicates the data without the silicon crystal. The cross and dot line indicate the STAC8 calculation. The exposure is indicated by the distance from the graph center to the data point.

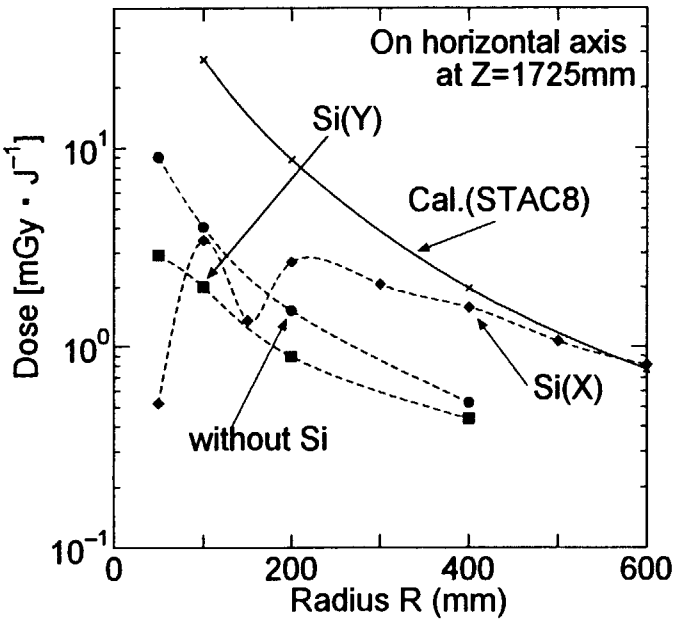

Fig.2-9 The distribution of exposure on the horizontal axis at Z=1725mm. The solid line indicates the STAC8 calculation. The full circle and dot line indicates the measurement data with inclined silicon crystal with respect to the X-axis, Si(X), full square and dot line indicates the data with inclined silicon crystal with respect to the Y-axis, Si(Y), and the full diamond indicates the data without the silicon crystal.

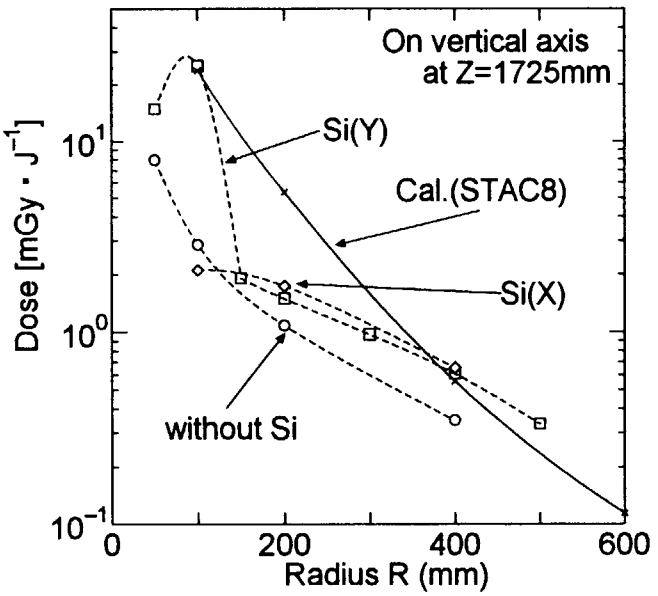

Fig.2-10 The distribution of exposure on the vertical axis at Z=1725mm. The solid line indicates the STAC8 calculation. The open circle and dot line indicates the measurement data with inclined silicon crystal with respect to the X-axis, Si(X), open square and dot line indicates the data with inclined silicon crystal with respect to the Y-axis, Si(Y), and open diamond indicates the data without the silicon crystal.

2.4 Application to the shielding design of a practical beamline

The shielding design calculations using STAC8 were carried out to apply to practical beamlines with considering polarization effect and clarifying the characteristics of the beamline of third generation synchrotron radiation facilities. In addition, the shielding calculations were compared with the measurements outside the shield wall of the bending magnet beamline. The groundshine, which demands special considerations in third generation facilities, was investigated by using the combination of STAC8 and the general-purpose codes, G33-GP2[2-32] and ITS3.0[2-33].

2.4.1 Typical beamlines of SPring-8

The beamlines of SPring-8 are classified by synchrotron radiation source into wiggler, undulator and bending magnet beamlines for safety analysis, because the energy spectra from the bending magnet, the undulator and the wiggler are quite different from each other. It is of crucial importance for the shielding design of beamlines to take into account these differences. The energy spectra of the above three types of photon sources were calculated using synchrotron radiation shielding design code STAC8 for the parameters of the typical photon sources of SPring-8[3-34] given in **Table 2-2**, including the parameters of optics hutches. The BL08W wiggler beamline is designed for Compton-scattering spectroscopy with circular polarized photons. The BL47XU and BL45XU are undulator beamlines. The former is designed for optics and imaging R&D with horizontal linear polarized photons generated by an in-vacuum type undulator, and the latter is for the research of structural biology with vertical linear polarized photons by a tandem type undulator. The BL02B1 bending magnet beamline is designed for crystal structure analysis. The calculated polar angle integrated total fluxes are given in **Fig.2-11**. Sizes and lead thickness of each optics hutch are also indicated in **Table 2-2**. The shield is fundamentally constructed with a hutch wall and local scatterer shield. The thickness of the roof is the same as the sidewall. In the calculations, a 10 mm thick copper disk was used as a scatterer in the place of an optical element such as a silicon crystal for conservative analysis. The dose distributions outside the hutches due to scattered

synchrotron radiation were calculated with considering the build-up effect and self-shielding of the scatterer. The slant length of shield wall is also considered to depend on both the azimuthal and scattering angle to introduce the polarization effect. On the other hand, in the calculations without polarization effect, the slant length of the shield wall is considered not to depend on the azimuthal angle.

The dose distributions calculated outside the optics hutch sidewall are shown in **Fig.2-12**. This figure indicates that the dose strongly depends on the scattering angle. The doses calculated by PHOTON II are 5.0×10^{-5}μGy/h-mA and 3.6×10^{-7}μGy/h-mA for the BL02B1 and the BL08W beamline, respectively. The reason that the PHOTON II obviously underestimated the dose values is thought to be caused by neglect of the build-up effect and coherent scattering. Besides, isotropic scattering is assumed with 90 degrees of scattered photon energy. **Figure 2-13** indicates the azimuthal angle dependence of the dose distributions obtained in consideration of the linear polarization effect and slant length at the side and the roof walls. The azimuthal angle is defined to be 0 degrees on the horizontal plane. These distributions were calculated at the scattering angles 40, 50 and 60 degrees to determine the maximum dose values and positions. As shown in **Figs.2-12** and **2-13**, the dose distributions strongly depend on the scattering angle and the azimuthal angle because of the anisotropic scattering process of photons and angular dependence of slant length. The dose is specially high in the scattering angle range 50 to 60 degrees and azimuthal angle range 0 to 10 degrees on the BL45XU beamline for vertical polarized photons, and 80 to 90 degrees on the BL47XU and BL02B1 beamlines for horizontal polarized photons. Besides, the figure shows that the highest dose outside the sidewall should appear on the BL45XU beamline. The local shields, therefore, will be very effective and also economical from the viewpoint of the shield weight.

2.4.2 Comparison with measured data of a bending magnet beamline of SPring-8

The shielding designs of the SPring-8 beamlines were performed by STAC8 and the construction of the BL14B1 bending beamline[2-35] was completed. This beamline is very

adequate for benchmark experiments, because the high power of the radiation can be obtained without so called local shielding and the roof of the hutch was designed to shield in severe conditions in order to reduce the weight. Thus leakage dose measurements outside the shield wall of the roof were planned to be carried out and compared with the calculations. The dose distribution around the scatterer (first mirror) was also measured to compare with the calculations.

(a) Outline of the SPring-8 BL14B1 beamline

The BL14B1 beamline was designed for experiments in various kinds of structural studies, particularly in the field of high-pressure, high-temperature science and surface-interface structural studies. This beamline can be operated in three modes with different experimental requirements. One is white X-ray experiments in the white X-ray experimental hutch. One is monochromatic X-ray experiments in the white X-ray experimental hutch, and the other is monochromatic X-ray experiments in the monochromatic X-ray experimental hutch. On the beamline, a set of two permanent filters (twin 0.25 mm of beryllium) was installed. **Figure 2-14** shows a layout of the beamline in the downstream experimental area in which an optics hutch and two experimental hutches are sited. The major optical elements are a slit, two view ports, two mirrors, a double crystal monochromator and two beam shutters. In addition, two photon stops and one beam stop were installed for radiation protection. The first mirror was installed to eliminate the higher harmonics of synchrotron radiation and to collimate the vertical component of synchrotron radiation. The second mirror is for focusing the vertical component of synchrotron radiation. The double crystal monochromator was installed to monochromize the synchrotron radiation and to focus the horizontal component of synchrotron radiation. The main beam shutter (MBS) was installed inside the shielding wall of the storage ring to control the synchrotron radiation beam to be transmitted into the beamline and the beam shutter is to control the white or monochromatic synchrotron radiation to be transmitted into the experimental hutch. The photon stop made of lead is to prevent gas bremsstrahlung[2-14] from expanding to the downstream position of the beamline, while the beam stop, usually installed at the most

downstream of the beamline, is to prevent the monochromatic synchrotron radiation beam from leaking out of the experimental hutch wall. The optical elements, which are installed in the downstream position in the optics hutch, can be moved up and down to the adequate position for the experimental purpose. Therefore the local shielding made of lead, which is normally installed for standard beamlines of SPring-8, cannot be employed. The walls of both the optics and experimental hutches are designed to shield against scattered synchrotron radiation. The thickness of the hutch wall was determined depending on the location of the hutch and the direction against the beam path.

(b) Experimental conditions

The synchrotron radiation white beam injected into the first mirror and then the doses outside the first mirror case were measured by using a TLD-100 thermo-luminescence dosimeter (Harshaw/Bicron USA). The dose distributions outside the shield wall of the roof were measured by using the white beam of synchrotron radiation with an AE133L ionization chamber made by Oyo Giken Co. Ltd. in Japan. The first mirror and the location of the TLD dosimeters are illustrated in **Fig.2-15**, including the injected condition of the synchrotron radiation beam. The dose measurements were made by the synchrotron radiation from the bending magnet and the key parameters are given in **Table 2-3**. During the measurements, the upstream optical aperture was fixed at the angular divergence of 1.0 mradian (vertical) x 1.55 mradian (horizontal) corresponding to the beam size of 35 mm (vertical) x 54 mm (horizontal) at the center of the first mirror. However, the vertical divergence of the synchrotron radiation from the bending magnet is nearly 0.063 mradian so that the vertical aperture size is extensive sufficiently and the true beam size is 4.4 mm in vertical at the center of the first mirror. The size of the first mirror made of a rhodium coated silicon body is 50 mm in thickness, 90 mm in width, and 800 mm in length. As shown in **Fig.2-15**, the white beam of synchrotron radiation is injected into the first mirror. The soft X-ray component is reflected and transmitted to the monochromator by the inclining mirror of 4 mradian, and the other component is scattered mainly by the mirror and the support made of stainless steel. The photon dose measured on the stainless steel box of the mirror was scattered from the mirror

and the support. The roof wall of the optics hutch was designed and constructed with a lead plate of 8 mm thick, sandwiched by the iron plates of 5.6 mm.

(c) Dose calculations

The dose calculations were made at two important sampling points, one was outside the roof of the optics hutch and the other was outside the mirror box. See **Fig.2-14** and **2-15**. In this calculation, a silicon rod of 540 mm in length and 2.0 mm in radius was used as the first mirror, because a cylindrical scatterer is normally employed in shielding design calculations and can only be calculated in PHOTON II and STAC8 code. The average path length in the mirror for the spread photons of the divergence of 63 μradian is 540 mm, and 2.0 mm for the scattered photons of 90 degrees in the case of the inclining mirror of 4 mradian. The incident photons would be capable of hitting the mirror support so that a scatterer made of steel, the same size as the silicon scatterer, was also considered. The distances between the scatterer and the outside of the roof and mirror box were 1900, and 185 mm, respectively.

The roof wall spans parallel to the plane expanded with the beam path and the polarization vector. The slant length is considered to depend on both the azimuthal and the scattering angle to introduce the polarization effect in the STAC8 calculation. On the other hand, in the calculations without the polarization effect, the slant length of the shield wall is considered not to depend on the azimuthal angle.

(d) Results and discussion

The spectra of radiation as emitted from the bending magnet and those attenuated by the beryllium filter, 0.5 mm in thickness, are shown in **Fig.2-16**. including the reflected photon spectrum by the inclined rhodium coated silicon body mirror of 4 mradian. The part of the synchrotron radiation photons are reflected and move into the monochromator, and the rest are scattered by the mirror. The reflected photon spectrum is calculated by using X-ray reflection theory[2-36] without considering the roughness of the rhodium surface.

Figure 2-17 shows the calculations of the dose due to scattered photons outside the mirror box. The measurement data by using TLD dosimeters are also plotted. The vertical axis indicates the cumulative absorbed dose in air during the synchrotron radiation irradiation

of 2.996 x 10^6 mA·s, and the horizontal axis indicates the distance from the center of the top plate of the mirror box. The calculations using PHOTON II are also plotted. In the calculation, two scatterer materials, silicon and steel, are considered. This figure indicates that the dose strongly depends on the sampling points of the mirror box, and the calculations by using STAC8 show good agreement with the measurements. On the other hand, the results of the PHOTON II calculations underestimated the measurements.

The calculations of the dose distribution outside the roof of the optics hutch are shown in **Fig.2-18**, including measurement results. This figure indicates that the dose strongly depends on the scattering angle and most of the measurement results are between the calculations using the silicon scatterer and the steel scatterer. Both of the dose distributions, measurement results and calculations using STAC8, are very similar and the maximum position of the distribution is well coincident with those of the measurements. The doses calculated by the PHOTON II code are also plotted in **Fig.2-18**, indicating that the PHOTON II obviously underestimated the dose values. The reason for this underestimation is thought to be caused by the neglect of the coherent scattering process and the buildup effect, however without considering the self-shielding of the scatterer in PHOTON II calculations. Besides, isotropic scattering is assumed with the ninety degree scattered photon energy.

Figure 2-19 indicates the azimuthal angle dependence of the dose distributions obtained in consideration of the linear polarization effect and slant length outside the roof of the optics hutch. The azimuthal angle is defined to be 0 degrees on the horizontal plane. These distributions were calculated at the scattering angles, 50 degrees, 55 degrees, and 60degrees, corresponding to the maximum dose values and positions. The measurement data, which correspond to doses at the positions of the scattering angles of 53.6 and 57.2 degrees, are also indicated.

As shown in **Figs.2-18** and **2-19**, the dose distributions strongly depend on the scattering angle and azimuthal angle because of the anisotropic scattering process of photons and the angular dependence of the slant length. The dose is especially high in the scattering angle of 55 to 65 degrees and azimuthal angle of 80 to 100 degrees. The STAC8 calculations

show fairly good reproducibility to the measurements results.

2.4.3 Application to the estimation of groundshine

For the shielding calculation of the beamline hutch, leakage doses outside the hutch due to scattered synchrotron radiation from the concrete floor of the hutch, so called groundshine, were considered together with the penetration component. For this purpose, the hutch wall composed of a lead plate of 10mm thick sandwiched by iron plates, 5 mm thick, was employed. In the calculations, we assumed three geometric configurations; one with a lead rectangular plate installed along the foot of the inside of the hutch wall, one with the same plate outside of the hutch wall and one with the bottom part of the hutch wall embedded in the concrete floor, shown in **Figs.2-20, 2-21**, and **2-22**. The calculations were performed with a photon shielding code G33-GP2[2-32] which allows only single scattering in the floor. Validity of the calculation was verified by comparing the G33-GP2 calculations with those using a Monte Carlo code ITS3.0[2-33]. A rectangular plate model was employed for G33-GP2 and a slab-cylinder model for ITS3.0, shown in **Fig.2-23**.

The calculational results of the doses outside the hutches due to mono-energy photons are shown in **Figs. 2-24, 2-25, 2-26, and 2-27** for each geometrical configuration of T= 1 mm, or D= 10 mm, or without additional shield on the assumption of the intensities of 1 photon per second at 2 m away from the hutch wall and 1m in height from the floor. In these cases, the effective shield can be expected for low energy photons and unexpected for high energy photons in the configuration of the lead plate installed inside the hutch. On the other hand, both energies of photons can be shielded effectively by using the lead plate outside the hutch in comparison with those of the inside lead plate. In the configuration of the bottom part of hutch wall embedded in the concrete floor, the effective shield can be expected for low energy photons and unexpected for high energy photons, moreover maximum doses appear at the nearside of the hutch wall. The same tendencies are recognized for different thickness, T, or depth, D, of the configurations.

The leakage doses due to groundshine of the SPring-8 beamlines were estimated by

using the combination of the STAC8 code calculation and the G33-GP2 calculations as indicated in the above. Photon spectra were calculated by STAC8 on the condition of synchrotron radiation perpendicularly scattered and fifty-degree scattering by copper, as shown in **Fig. 2-28**. In these cases, the synchrotron radiation sources of a typical wiggler, in-vacuum undulator and bending magnet as indicated in the former section 2.4.1 were employed. The results for the wiggler beamline are indicated in **Figs.2-29, 2-30 and 2-31** for the three different configurations. The same tendencies appeared for the undulator and the bending magnet beamlines. Seeing the calculated doses without additional shield (indicated as "Flat" in the figures), the dose rate due to groundshine will be found to be at a serious level for the 8 GeV class synchrotron radiation beamline. The G33-GP2 calculation and the ITS3.0 calculation can be compared with each other in the "Flat" case to show good agreement near outside of the hutch wall and with high level of leakage dose. In comparison with the results for the three geometrical models, the configuration with the lead plate installed along the foot of the outside of the hutch wall is found to be the most effective shielding method against the groundshine, because shielding photons after being scattered by the floor is the most effective. In this configuration, **Fig.2-30** shows that a lead plate, 2mm thick and 30 cm or more in width, is required along the foot of the hutch for reducing the dose down to the one due to penetration component at 1 m in height from the floor.

Table 2-2 Key parameters of synchrotron radiation sources and optics hutches for shielding calculation of typical beamlines of SPring-8.

Beamline	BL08W	BL47XU	BL45XU	BL02B1
Type of ID	Wiggler	Undulator (In-Vacuum)	Undulator (Tandem)	Bending Magnet
Power (W/mA)	180	110	27.5	2.25
Period length (mm)	120	32	37	39270 (Bending radius)
Number of Periods	37	140	40×2	
Magnetic field (peak) (T)	1.0	0.78	0.5	0.68
Critical energy (keV)	42.7			29.0
Polarization	circular	linear (horizontal)	linear (vertical)	(linear)
Scatterer(*1)	Cu (1cm)	Cu (1cm)	Cu (1cm)	u(1cm)
Optics Hutch size				
Distance (m) from SR beam to side wall	2.35	1.7	1.03	0.6
Distance (m) from scatterer to back wall	4.0	7.5	8.0	1.75
Lead Thickness(*2)(mm)				
Side wall	15	15	10	10
Local shield	15	5		3
(total)	30	20	10	13
Back wall	40	20	20	40
Local shield	45	30		10
(total)	85	50	20	50

(*1) Cu scatterer is assumed instead of optical elements for safety analysis.
(*2) The hutch wall is designed to be constructed with lead plate, sandwiched by iron plates, 5mm thick.

Table 2-3 The key parameters of the BL14B1 beamline of SPring-8 and experimental conditions

Light source		**Bending magnet**
Storage ring energy		**8 GeV**
Peak strength of magnetic field		**0.68 T**
Bending radius		**39.27 m**
Critical energy		**29.0 keV**
Opening angle	**Vertical**	**1.0 mradian**
	Horizontal	**1.55 mradian**
Beam size		**4.4 mm x 54 mm (V x H)**
		at the center of the first mirror
Permanent filters	**Be**	**0.25 mm x 2**
Maximum inclined angle of first mirror		**4 mradian**
Maximum stored beam current		**100 mA**
Cumulative stored current during the measurements		**2.996 x 10^6 mA·s**
Polarization vector is on the horizontal plane		

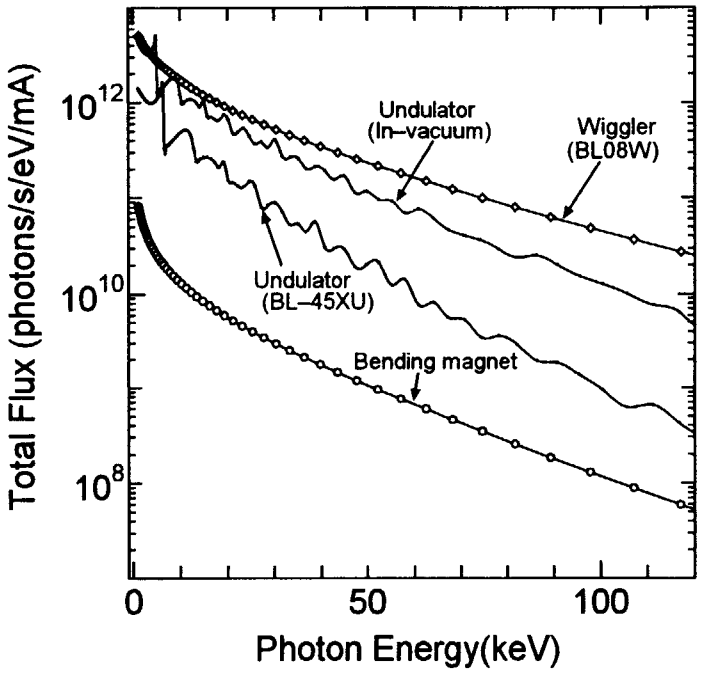

Fig.2-11 Angle-integrated synchrotron radiation spectra from the typical SPring-8 beamlines of a bending magnet, wiggler and undulator, calculated by the STAC8 code.

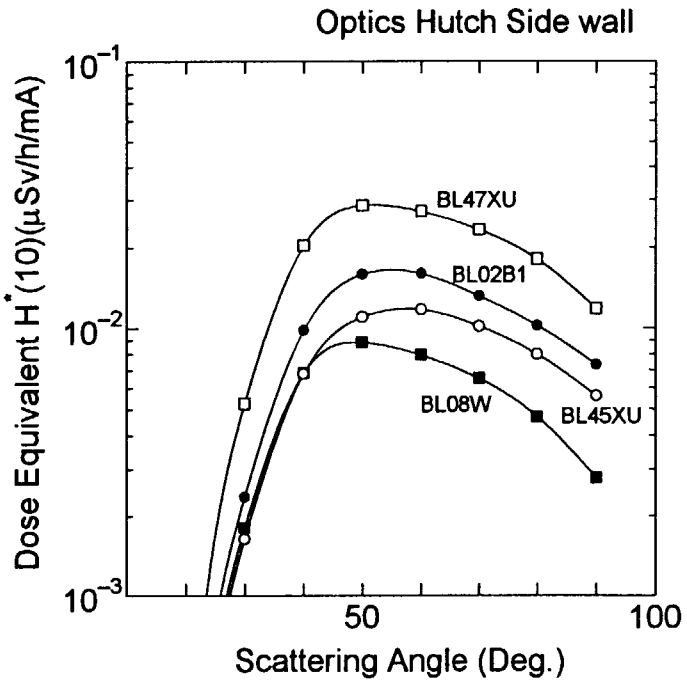

Fig.2-12 Calculated dose distributions outside the side wall of the optics hutch of the typical SPring-8 beamlines as a function of scattering angle. Full square indicates the dose outside the BL08W beamline hutch, open circle is for BL45XU, open square is for BL47XU, and full circle is for BL02B1.

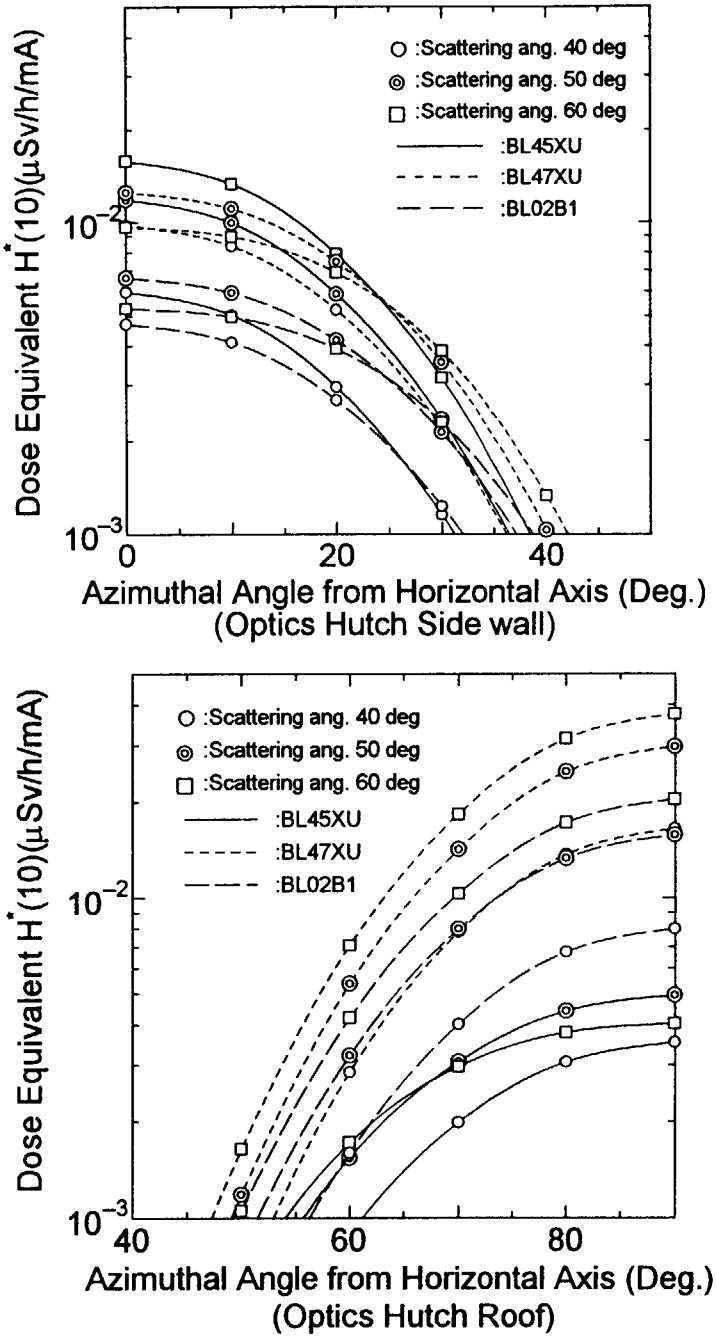

Fig.2-13 Dose distributions of the scattered photons outside the side wall (above figure) and the roof (below figure) of the optics hutches calculated in consideration of the linear polarization effect. The slant length is considered to depend on both the azimuthal and the scattering angle to introduce the polarization effect. The side walls of the BL47XU and BL02B1 beamlines stand parallel to the beam path and perpendicular to the photon polarization vector, and parallel to the photon polarization vector for the BL45XU beamline. The roof walls of the BL47XU and BL02B1 beamline are parallel to the plane expanded with the beam path and polarization vector, and perpendicular for the BL45XU beamline.

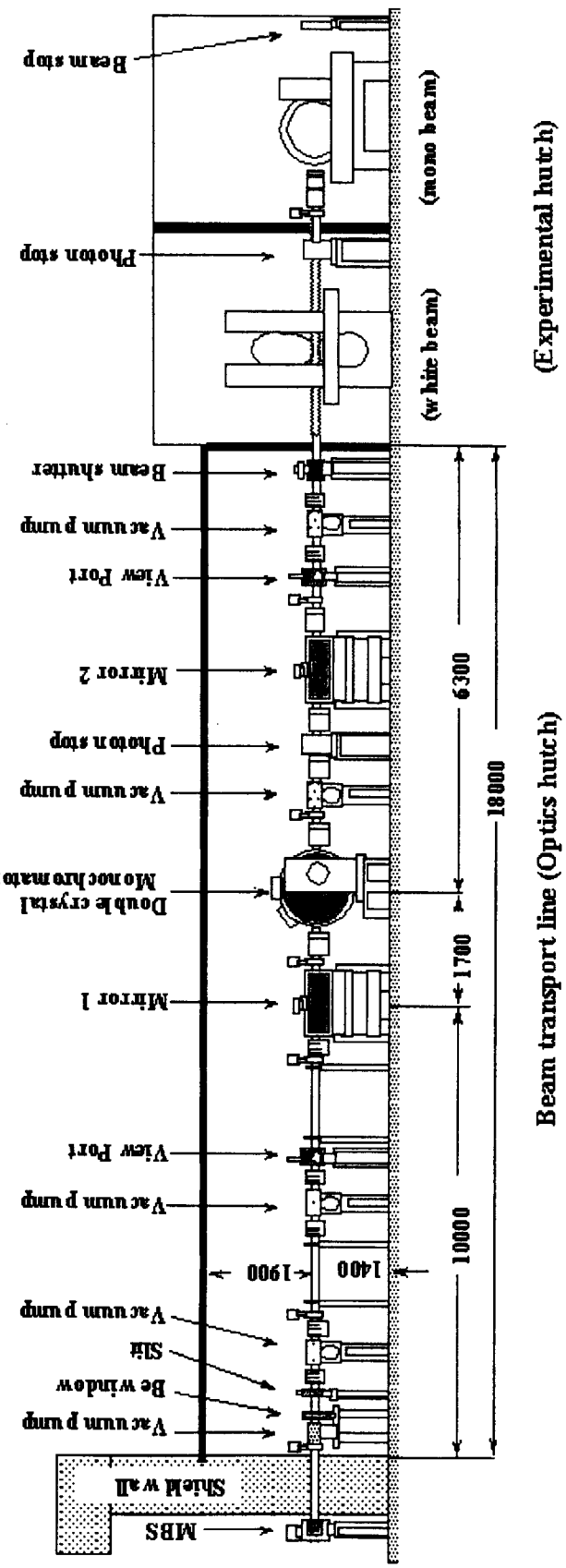

Fig.2-14 Layout of the BL14B1 bending magnet beamline of SPring-8. The synchrotron radiation beam comes from the left side of the figure. The MBS is the main beam shutter. The white and monochromatic X-ray experiments can be performed in the upstream side of the experimental hutch. Experiments using only the monochromatic X-ray beam are permitted in the downstream experimental hutch.

This is a blank page.

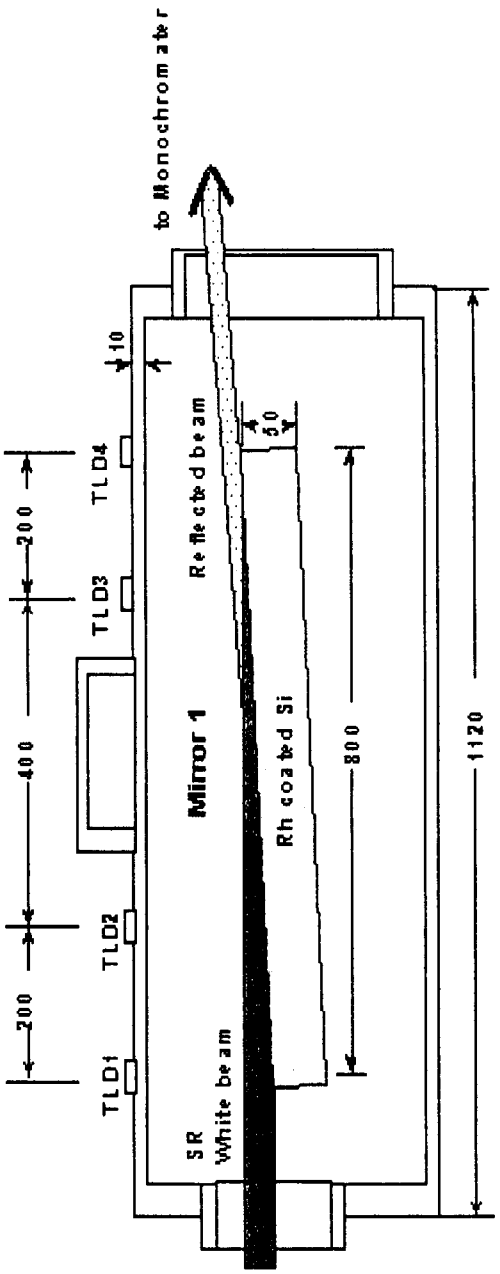

Fig.2-15 Illustration of the first mirror and the location of the four TLD dosimeters. The synchrotron radiation beam injected into the rhodium coated silicon body mirror. The soft X-ray component of synchrotron radiation is reflected and transmitted to the monochromator by the inclining mirror.

This is a blank page.

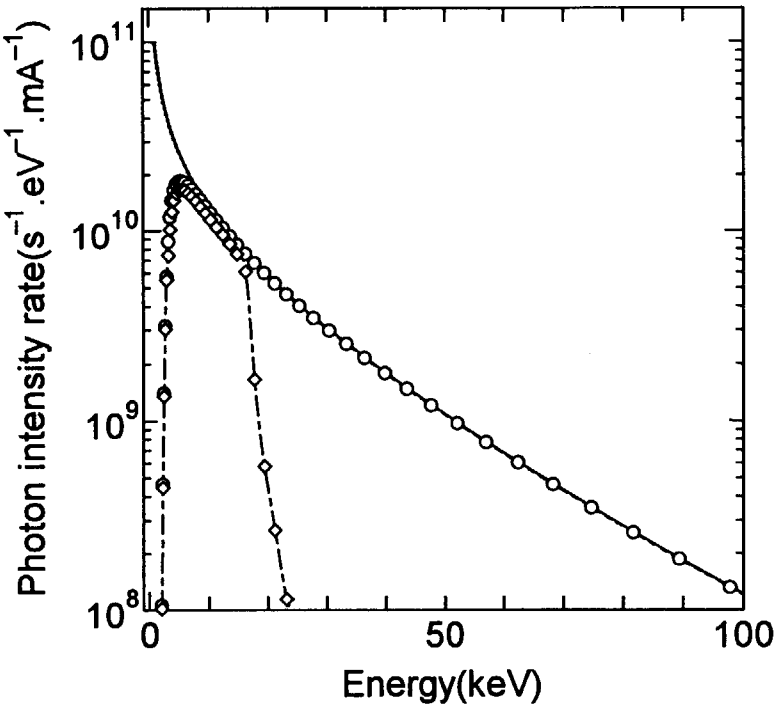

Fig. 2-16 Photon spectra of the BL14B1 beamline. The solid line indicates the synchrotron radiation source emitted from the bending magnet. The open circle and dot line indicates the attenuated spectrum by beryllium filters. The open diamond and dot-dashed line indicates the reflected spectrum by inclining the rhodium coated silicon body mirror of 4 mradian.

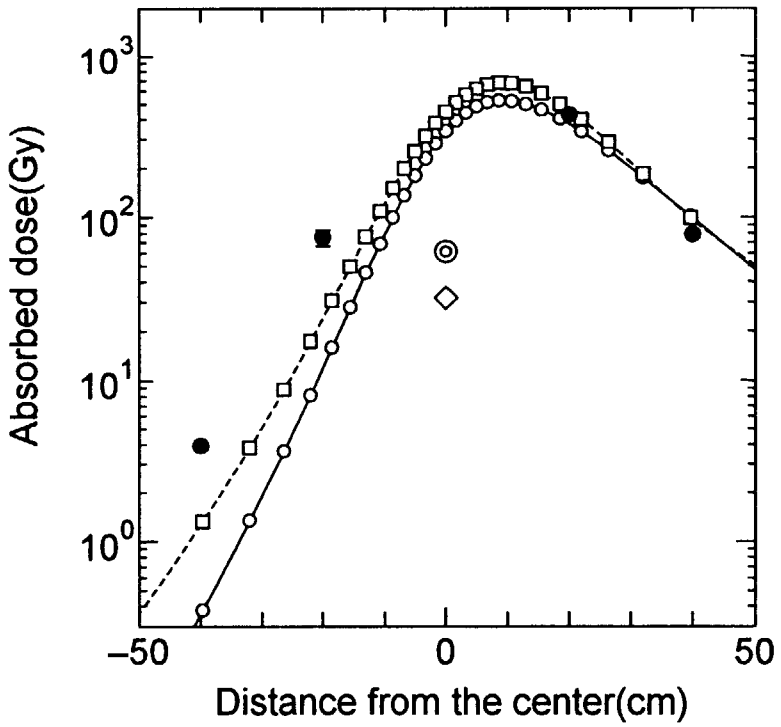

Fig. 2-17 Dose distributions of the scattered photons outside the mirror box. The horizontal axis indicates the distance from the center of the top plane of the mirror box and the vertical axis indicates the absorbed dose in air. Full circles indicate the measurement data by using the TLD dosimeters. Open circle and solid line indicates the results of the STAC8 calculation by using the silicon scatterer. Open square and dot-dashed line indicates the STAC8 calculations by using the steel scatterer. Double circle and open diamond indicate the results of the PHOTON II calculation using the silicon scatterer and the steel scatterer, respectively.

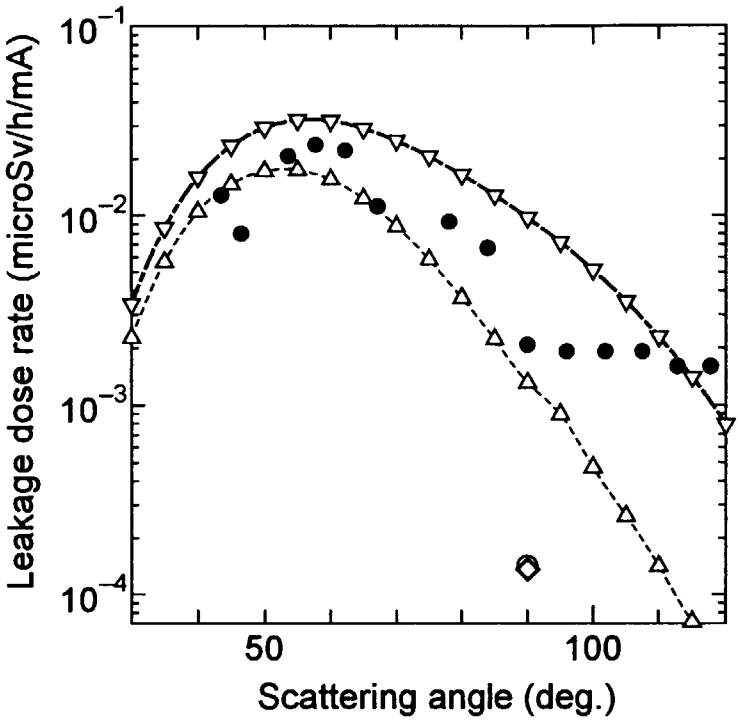

Fig.2-18 Dose distribution outside the roof of the optics hutch of the BL14B1 beamline. Full circles indicate the measurements results by using the ionization chamber. Open triangle and dot line, and inverse triangle and dot-dashed line indicate the STAC8 calculations without considering the polarization effect by using the silicon scatterer and the steel scatterer, respectively. Double circle and open diamond indicate the results of the PHOTON II calculations using the silicon and the steel scatterer, respectively.

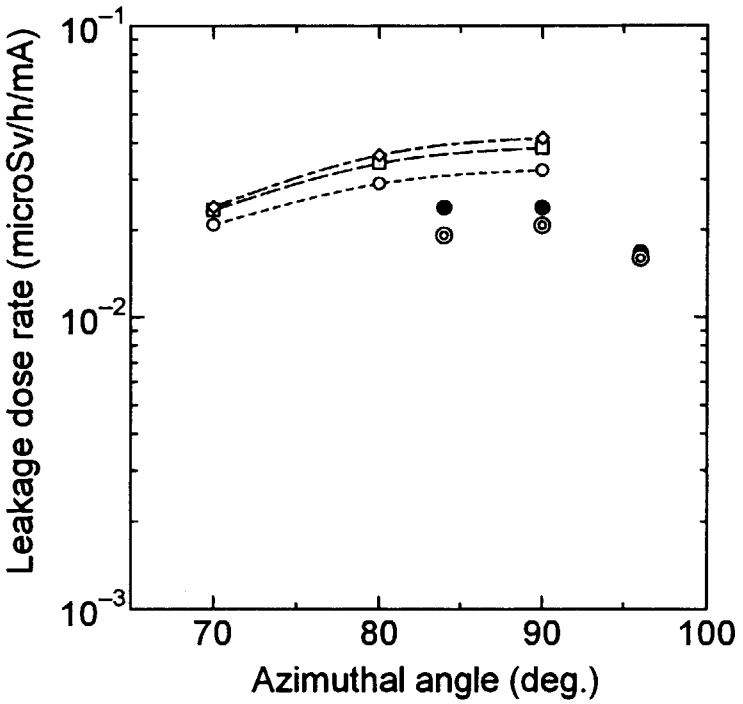

Fig.2-19 Dose distribution depending on the azimuthal angle of the scattered photons outside the roof of the optics hutch of the BL14B1 beamline calculated in consideration of the linear polarization effect. Full and double circles indicate the measurement results at the scattering angles of 57.2 and 53.6 degrees, respectively. Open circle and dot line, open diamond and dot-dashed line, and open square and dashed line indicate the STAC8 calculations by using the steel scatterer at the scattering angles of 50 degrees, 55 degrees, and 60 degrees, respectively.

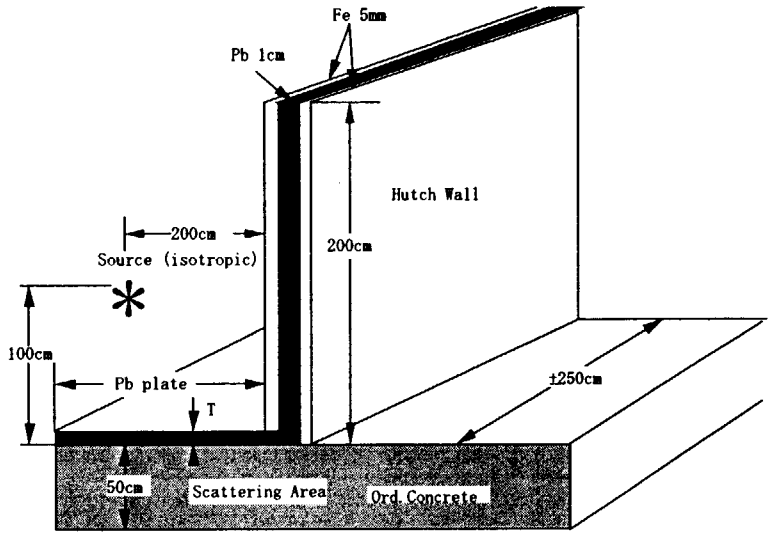

Fig.2-20 Calculational configuration of ground shine by using G33-GP2. Lead plate, T mm thick, installed along the foot of the inside of the hutch wall.

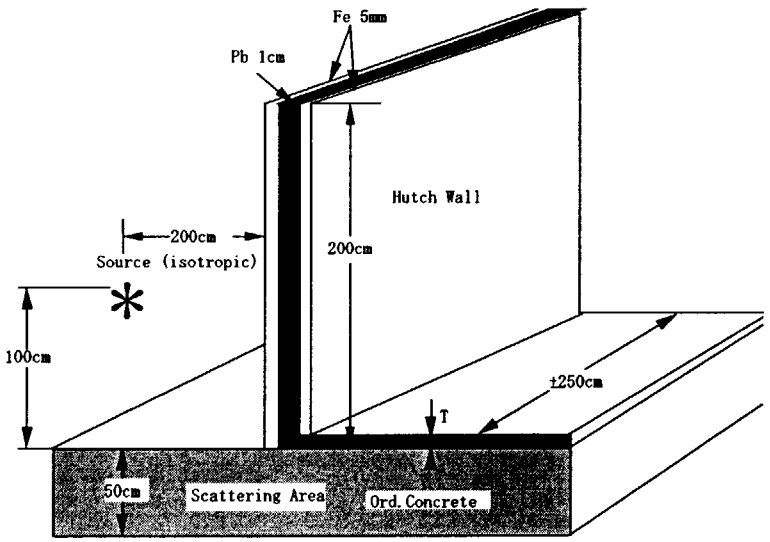

Fig.2-21 Calculational configuration of ground shine by using G33-GP2. Lead plate, T mm thick, installed along the foot of the outside of the hutch wall.

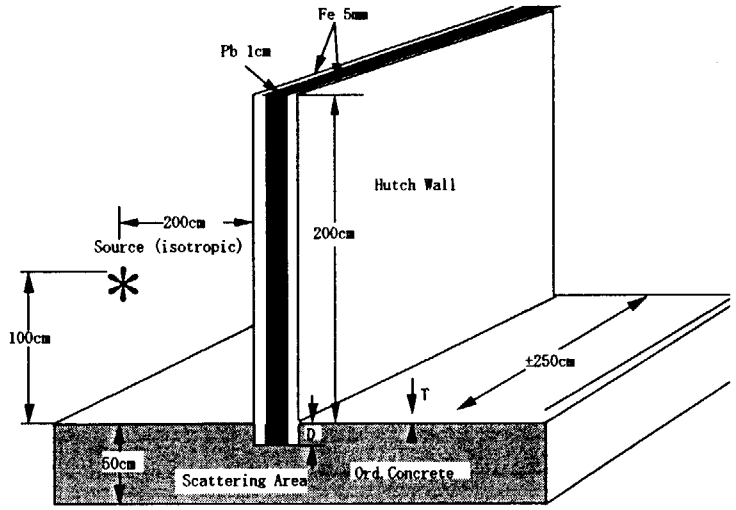

Fig.2-22 Calculational configuration of ground shine by using G33-GP2. The bottom part of hutch wall, D mm in depth, embedded in the concrete floor.

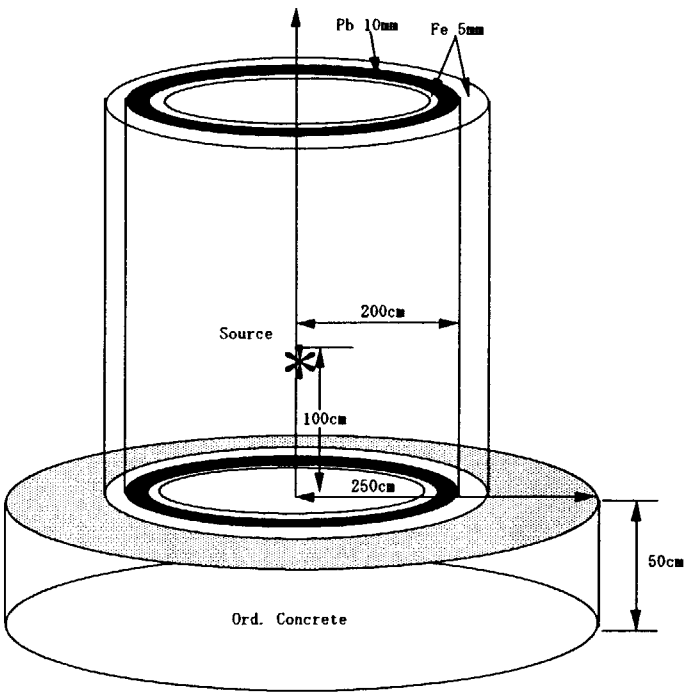

Fig.2-23 Calculational configuration of ground shine by using Monte Carlo code ITS3.0.

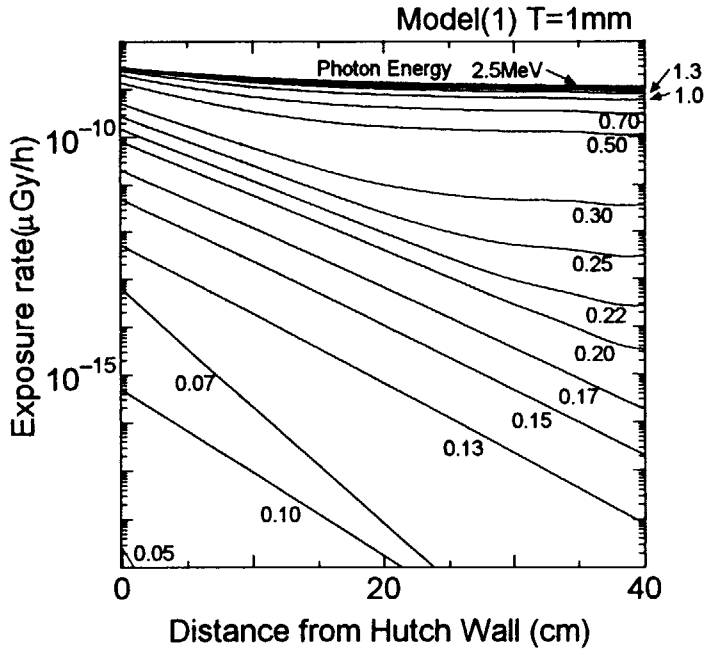

Fig. 2-24 Doses outside the hutch due to groundshine with mono-energy photons for the geometrical configuration of a 1 mm thick rectangular plate installed along the foot on the inside of the hutch wall, as shown in Fig.2-20 and T=1mm. The numbers indicate the photon energies.

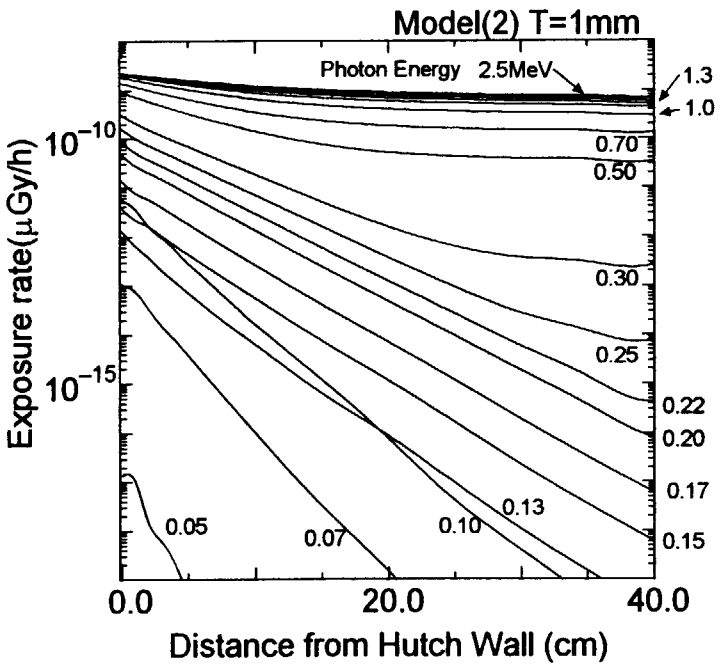

Fig. 2-25 Doses outside the hutch due to groundshine with mono-energy photons for the geometrical configuration of a 1 mm thick rectangular plate installed along the foot on the outside of the hutch wall, as shown in Fig.2-21 and T=1mm. The numbers indicate the photon energies.

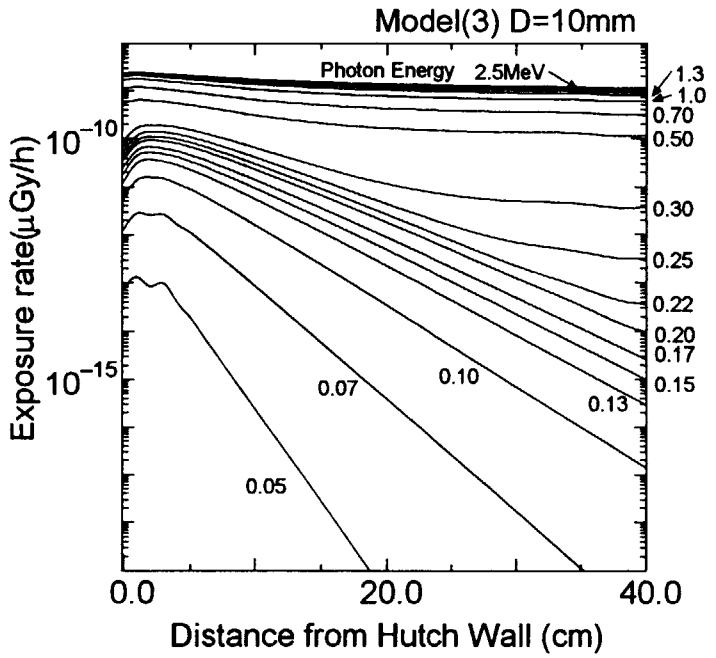

Fig.2-26 Doses outside the hutch due to groundshine with mono-energy photons for the geometrical configuration of the bottom part of a hutch wall embedded in a 10 mm deep concrete floor, as shown in Fig.2-22 and D=10 mm. The numbers indicate the photon energies.

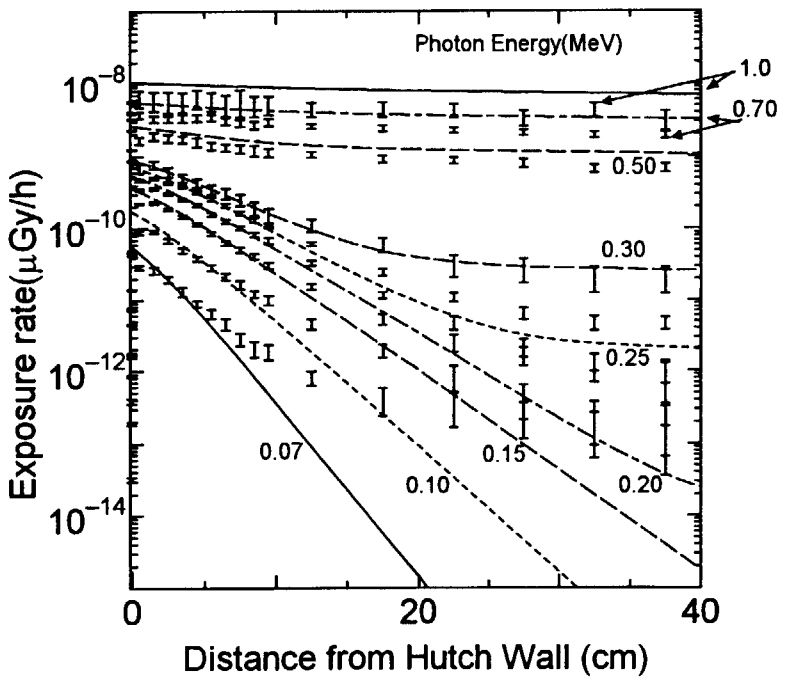

Fig. 2-27 Doses outside the hutch due to groundshine with mono-energy photons for a cylinder model, as shown in Fig.2-23. The solid, dashed, dot, and dot-dashed lines indicate the results by using G33-GP2 and the symbols of I are by using ITS 3.0. The numbers indicate the photon energies.

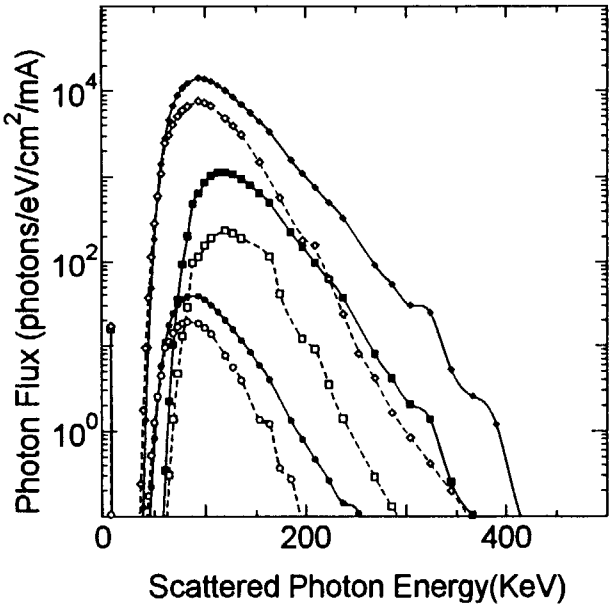

Fig.2-28 Scattered photon spectra of a synchrotron radiation beam by STAC8 calculations. Full circle with solid line indicates the scattered photon spectra with fifty degrees scattering angle due to a copper scatterer, 10 mm thick, with photon beam from a bending magnet. Open circle with dot line indicates the scattered photon spectra in a perpendicular direction scattering from the bending magnet source with a copper scatterer. Full square and solid line, and open square and dot line also indicate the scattered photon spectra from an undulator in direction of fifty and ninety degrees, respectively. Full diamond and solid line, and open diamond and dot line also indicate the scattered photon spectra from the wiggler in direction of fifty and ninety degrees, respectively

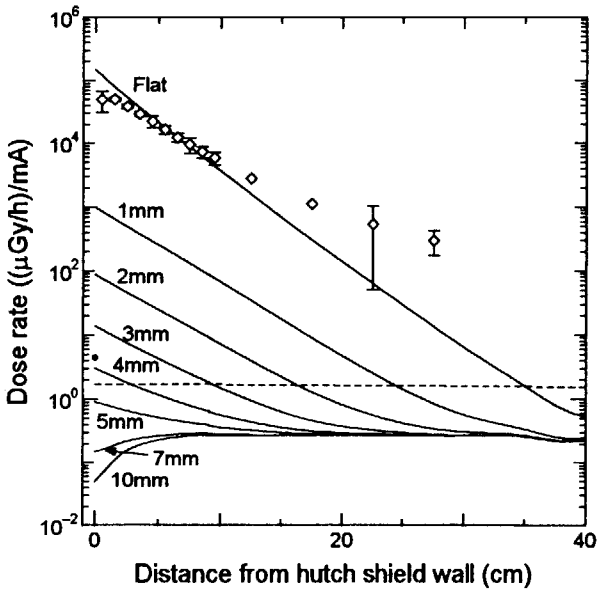

Fig. 2-29 Dose distributions due to groundshine along the outside floor of the hutch with and without a lead shield of various thickness. The lead plate is installed along the inside foot of the hutch. Photon sources are the photons scattered in the ninety degree direction by copper at 2m away from the hutch wall. Solid line: dose distribution due to groundshine; dot line: dose distribution due to penetrated photons; black circle: the dose due to direct photons at 1m in height above the floor (the same level as the source point inside the hutch).

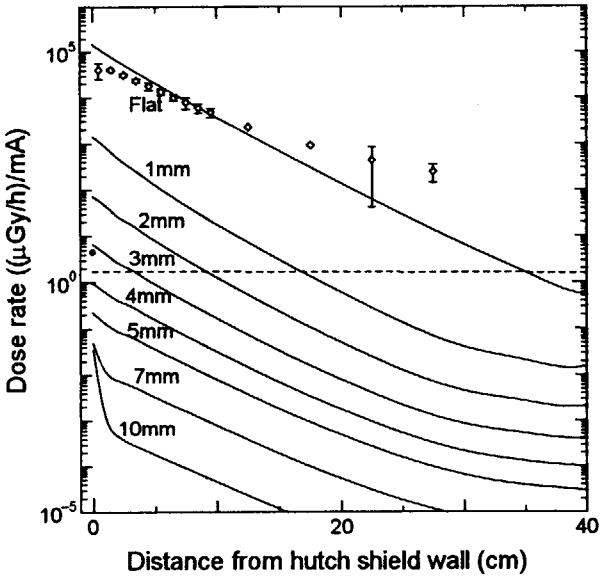

Fig. 2-30 Dose distributions due to groundshine along the outside floor of the hutch with and without a lead plate shield of various thickness installed along the outside foot of the hutch. Solid line: dose distribution due to groundshine; dot line: dose distribution due to penetrated photons; black circle: the dose due to direct photons at 1m in height above the floor (the same level as the source point inside the hutch).

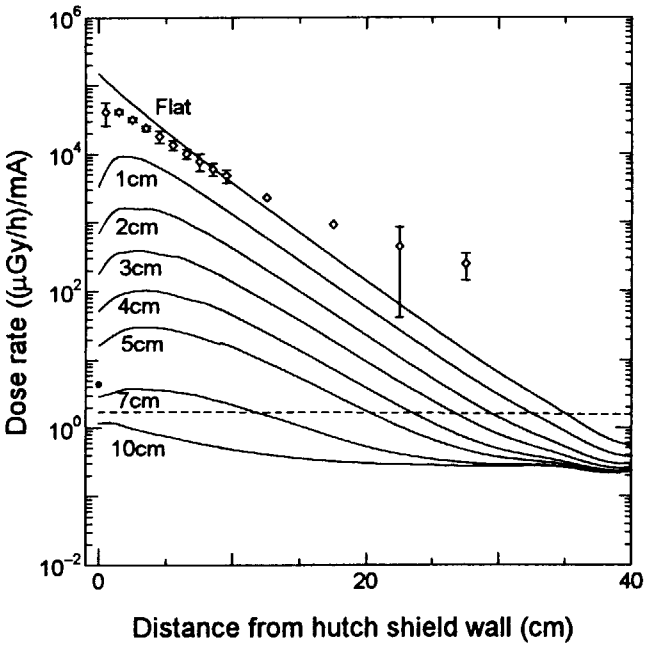

Fig. 2-31 Dose distributions due to groundshine along the outside floor of the hutch with and without a hutch wall of various depth embedded in the floor. Solid line: dose distribution due to groundshine; dot line: dose distribution due to penetrated photons; black circle: the dose due to direct photons at 1m in height above the floor (the same level of the source point inside the hutch).

2.5 Conclusions

An advanced shielding design code for synchrotron radiation beamlines, STAC8, has been developed on the basis of the PHOTON II code for the purpose of shielding design of the so-called third generation synchrotron radiation beamline. With this code, we can make a radiation source estimation from the bending magnet, wiggler and undulator, attenuation calculations of photons by the filter and beam-shutter, taking into account buildup factors, scattering calculations by various optical elements considering angular dependence of the scattering process and the polarization effect of photons, and penetration calculation through the shield wall, consistently.

In order to verify its validity, the calculations with STAC8 were compared with the calculational results using the EGS4 calculations and the measurements of the dose inside the hutch of a linear polarized wiggler beamline. The agreement of the STAC8 and the EGS4 calculations was fairly good except for the region of small scattering angles. This fact suggests that it is necessary to take into account buildup factors in the shielding calculations, while PHOTON II does not. The calculations with shield design code, STAC8, using the beamline of the wiggler, the BL14C beamline of KEK, were compared with the measurements using the TLD dosimeters. The calculations and measurements had good agreement and the dose distributions inside the hutch strongly depend on the scattering angle and azimuthal angle.

To realize the characteristics of the shielding conditions of the beamlines in third-generation facilities, the dose distributions outside the hutch due to the synchrotron radiation of the typical beamlines in SPring-8 were calculated with the STAC8 code. The results showed that the dose distribution outside the hutch strongly depends on the scattering angle and the azimuthal angle, while PHOTON II does not.

In comparison with the measurement using TLD dosimeters and the ionization chamber for the dose distribution outside the hutch of the practical beamline of the bending magnet, the results of STAC8 calculations had fairly good agreement. The position, which indicates the maximum value of calculated leakage dose using STAC8 is well coincident with

those of the measurements. This concludes that STAC8 is very reliable for shielding design calculation of the beamline hutch. On the other hand, with PHOTON II the dose of the scattered photons were underestimated.

In addition to the bulk shielding calculation for the scattered synchrotron radiation, the consideration for the groundshine is required in designing the synchrotron radiation beamlines of the third generation facilities such as SPring-8 because the distinguishing feature of the synchrotron radiation from the SPring-8 is extremely high intensity involving high energy photons. The groundshine was found to be a dominant source to determine the structure at the joint between the hutch wall and the concrete floor. The present calculation shows that adding lead plate shielding along the foot outside of the hutch wall is more effective than any other shielding structures.

Using the STAC8 code, we can obtain the leakage dose distribution due to synchrotron radiation with satisfactory accuracy and can easily find out the direction in which the maximum leakage dose value will occur so that we can make full use of so called local shielding.

3. The study of high energy radiation within the beamline of synchrotron radiation

3.1 Introduction

In addition to the synchrotron radiation as discussed in the previous chapter, other radiations can creep into beamlines. These are gas bremsstrahlung, as well as neutrons, photons, muons due to stored electron beam loss within the storage ring vacuum chamber. Including high energy photons, gas bremsstrahlung directly creeping into the beamlines can be a serious radiation source because of its extremely high intensity and high energy at the straight sections for insertion devices of the third generation synchrotron radiation facility. In addition, the intense and high energy gas bremsstrahlung generates photoneutrons through the interaction with high Z materials. The gas bremsstrahlung and associated photoneutrons can pose a serious radiation hazard for the beamline personnel. A detailed study of gas bremsstrahlung is, therefore, required especially for third generation synchrotron radiation facilities, such as ESRF[3-1], APS[3-2], and SPring-8[3-3]. The radiation due to stored electron beam loss can be estimated by using the same shielding methods for the electron accelerators, and the doses are small in comparison with that of gas bremsstrahlung during the period of the stable stored electron beam mode (see **Appendix 1**).

Many gas bremsstrahlung measurements have been made at several facilities with various methods[3-4],[3-5],[3-6],[3-7],[3-8],[3-9]. These measurements were performed at lower energies compared to the storage ring energies of the third generation facilities and quantitative evaluations have been carried out by various authors[3-10],[3-11],[3-12],[3-13]. However, it is doubted that the results of the estimations can be applied to the third generation facilities because of the long straight sections and the stored electrons with high energy. Moreover, it is not sure whether the simulation conditions based on the recommendation of Ferrari [3-13] for gas bremsstrahlung production can be applied to the third generation facilities to get sufficient accuracy of angular distribution of the

photon emission. The simulation usually assumes air at atmospheric pressure and the results obtained are linearly scaled to the typical pressure of the storage ring of 133 nPa 810-9 torr), but the scaling procedure is not necessarily always possible. Recently detailed bremsstrahlung measurements were conducted for the beamlines of the 7.0 GeV APS using a lead glass detector[3-14]. The measurements of the APS show the measured intensities are about one fifth of the estimated intensities obtained from the measured effective atomic number of the residual gas. Moreover, the total emission angle of the gas bremsstrahlung is assumed to be $1/\gamma$, where γ is the ratio of the stored electron energy to electron rest mass and the characteristics of the stored electron beam conditions such as beam divergence were ignored.

A few measurements of the photoneutrons due to gas bremsstrahlung were performed, however there are some problems in the experiments. At the 7 GeV Advanced Photon Source[3-15] storage ring, the photoneutrons were measured using an Andersson-Braun type rem-meter. However, the effect of pile up of the rem-meter due to extremely high exposure rate of synchrotron radiation was not discussed. In addition, the rem-meter was set inside a small lead shield box to reduce exposure rate so that the response of the rem-meter should be changed. Also, measurement results were compared with the estimations using Monte Carlo electromagnetic shower code EGS4[3-16] at the Stanford Synchrotron Radiation Laboratory [3-17] with a 3 GeV storage ring. As indicated in the paper, however, the errors of the measurements were about a factor of two and about 50 % for the calculations. Besides, the photons emitted from ^{226}Ra were employed in the calibration of the Geiger-Mueller counter for the measurements of gas bremsstrahlung, and radioisotope neutrons in calibration of moderated BF_3 detector for photoneutron measurements. Both measurements of the facilities were performed without considering the high energy neutrons above 20 MeV which are produced by the quasi-deuteron production and photo-pion production process.

Detailed investigation on the behavior of gas bremsstrahlung and associated

photoneutrons is required for SPring-8, which is the synchrotron radiation facility with currently the highest stored energy of 8 GeV together with the features of very low beam emittance and many long straight sections up to 40 meters. In this study, therefore the simulation conditions of gas bremsstrahlung production were investigated to apply to the third generation facilities with sufficient accuracy and the measurements of gas bremsstrahlung were performed as a function of the aperture sizes of two beamlines. The measurements were compared with the simulations, considering the stored beam conditions of sizes and beam divergences. The dose distribution due to direct gas bremsstrahlung that was investigated, strongly depends on the size of the scoring area in the Monte Carlo simulation for averaging the calculated dose and also depends on the stored beam conditions strongly.

The photoneutron production and the dose due to gas bremsstrahlung were estimated, taking into account giant resonance, quasi-deuteron and photo-pion reaction processes by preparing the photoneutron production cross sections, and the results were compared with and without considering the quasi-deuteron and photo-pion reaction processes. The measurements of photoneutrons generated by the interactions of gas bremsstrahlung with lead and copper targets are presented using high sensitive Bonner type helium-3 counters with polyethylene moderators of different thickness to estimate the neutron spectrum. The measurements were performed outside the optics hutch to reduce the effects of synchrotron radiation. The photoneutron production and transport calculations were also performed to get the initial guess spectrum for the unfolding calculation. The measurement data of the effective dose due to photoneutrons were compared with the calculations and the previous data[3-15),(3-17)].

The laser electron photon beamline of SPring-8 is an unique beamline which provides a large number of tagged and polarized photons with an energy up to 3.5 GeV to be used for investigations of quark nuclear physics[3-18),(3-19)]. Multi GeV class photons with incommensurably high intensity are generated by a method of Compton back-scattering of a short-wavelength laser light from a stored 8 GeV electron beam.

Besides, photo-neutrons are produced with seriously high intensity through interactions between the laser electron photons and beamline components like a beam dump. The beamline is required to be shielded sufficiently at the restricted narrow space, which is surrounded by the adjacent synchrotron radiation beamlines. Therefore we must make full use of the so-called local shielding to shield effectively. Actually, two hutches must be designed in tandem and connected with each other using beam transport pipe, because of the restrictions on space. The local shield, which has special structure, a combination of sweep magnet and collimators, must be installed, accordingly. Although these distinguishing features present extremely sever radiation problems for the shielding design, the shielding methods, which are based on the measurements of gas bremsstrahlung and associated photoneutrons can be applied with sufficient accuracy.

3.2 Characteristics of gas bremsstrahlung at a SPring-8 insertion device beamline

One of the distinguishing features of third generation synchrotron radiation facilities is the low emittance electron beam used to get extremely highly brilliant synchrotron radiation. SPring-8 achieved the beam emittance of 6.7 nm·radian[3-20], where two types of betatron functions, high and low, have been adopted to meet the requirement of the low emittance and to keep the ring operation stable. Two types of electron beam conditions (beam size and beam divergence distribution) were utilized to investigate direct effects upon the behavior of the gas bremsstrahlung generation.

The gas bremsstrahlung was measured as a function of the aperture size of the photon beam, by using a new type scintillation crystal, $PbWO_4$ (PWO) array. The PWO detector has good performance for measuring the high energy gas bremsstrahlung photons because of its short radiation length and fast decay time[3-21]. Because of its better performance, the PWO should provide a finer energy resolution for GeV photons than lead glass. Consequently, improved precision should be expected.

The measurements were compared with the Monte Carlo simulations using EGS4[3-16], considering the electron beam sizes and beam divergences. The dose rate due to gas bremsstrahlung should strongly depend upon the stored beam conditions. These considerations are especially necessary for dose estimation due to gas bremsstrahlung.

3.2.1 Simulation condition of gas bremsstrahlung

The simulation of gas bremsstrahlung is normally carried out with the residual gas density corresponding to atmospheric pressure because of the low interaction probability at the operating pressure (less than 133nPa) and the result is linearly scaled to the operating pressure of the storage ring. However, the scaling procedure is not necessarily always possible. Since multiple Coulomb scattering and Møller scattering are practically negligible in the storage ring, whereas these scatterings occupy most of the interactions at atmospheric pressure. In the calculation, in order to suppress Møller scattering (hard collisions of incident electrons with atomic electrons) in the extremely low-pressure air target below 133nPa (10^{-9}torr), many parameters were employed as indicated in **Table 3-1**, and Ferrari et al.[3-13] recommended to set the gas pressure as 10.13 kPa (0.1 atm) for a long straight section over 10 m and lower cut-off energy for electron transport, AE of 10 MeV, to eliminate multiple Coulomb scattering and Møller scattering in a gas bremsstrahlung production calculation. The AE is also defined as the threshold energy of Møller scattering to minimize any angular deflection. But it is not sure whether the recommendation can be applied to a third generation synchrotron radiation facility such as SPring-8. The length of straight section of SPring-8 is up to 40 m and stored electron energy is 8GeV, so verification of the recommendation is required to get sufficient accuracy of photon intensity and angular distribution of emission. Using the EGS4 code, simulations of the production of gas bremsstrahlung were performed as the functions of the number of the stored electron interaction with residual gas molecules, the residual gas pressure, and AE. The option of the true angular distribution of the emitted photons[3-22] is employed in all calculations with

double precision.

The calculated photon energy spectra and photon emission angle distributions are given in (1) **Fig.3-1** for the number of interactions, (2) **Fig.3-2** and **Fig.3-3** for several AE values ranging from 0.521 to 10 MeV under 1.0 and 0.1 atm, and (3) **Figs.3-4,** to **9** for several gas pressure values ranging from 1 to 10^{-3} atm under the straight section lengths of 1m, 19m, and 40m, respectively. The sensitivity analyses of stored electron energies and residual gas molecules are summarized in **Appendix II**.

As shown in **Fig.3-1**, the gas bremsstrahlung generated within single interactions between the electrons and 0.1205 g/cm^2 air molecules is about 60 % of that generated within multi-interactions. The gas bremsstrahlung is nearly saturated within triple or more interactions. As shown in **Figs.3-2, 3-3,** AE value dependence is apparent on the intensity of gas bremsstrahlung generation, while the energy spectrum and the emission angle distribution are independent of AE values under 0.01205 g/cm^2 (0.1 atm). **Figure 3-4** shows that the energy spectrum is independent of gas pressure under the length of a straight section of 1 m, while as shown in **Fig.3-5**, although gas pressure dependence is apparent on the emission angle distribution, its dependence becomes less for a gas pressure below 0.01205 g/cm^2 (0.1 atm). However, as shown in **Figs.3-6,3-7,3-8**, and **3-9**, gas pressure dependence is apparent on both the intensity of energy spectrum and the emission angle distribution under the lengths of a straight section of 19 m and 40 m. Moreover, the longer the straight section, the tendency of the dependence is more apparent. Calculation with sufficient accuracy is no longer expected under gas pressure of 0.1 atm with the AE value of 10 MeV for SPring-8. **Figure 10** shows the relations between the angular distributions and electron path lengths that depend on the gas pressure, indicating the ratio of the emissions within 0.1 mradian to total emissions in the vertical axis. As shown in this figure, the ratio can be on one curve. Moreover, the curve indicates that the ratio is focused to a constant value below the electron path length of 10^{-2} g/cm^2.

As mentioned in above the calculations, the simulations under the

recommendations of Ferrari et al. have some problems for the conditions of SPring-8 beamlines. The spectrum of gas bremsstrahlung is independent of the gas pressure, however the angular distribution of photon emission strongly depends on the pressure. In order to correct the defect, it is clarified that the path length of stored electrons must be set to be less than 10^{-2}g/cm^2. This means that the simulation conditions must be set to be less than 0.1 atm of air in the case of a straight section of 1 m and 0.0025 atm for 40 m. Moreover, it is clarified that the simulations of gas bremsstrahlung with sufficient accuracy can be performed under a path length of less than 10^{-2}g/cm^2 without considering the AE (lower cut off energy for electrons and threshold energy of Møller scattering to minimize any angular deflection) and the restriction of single interaction of stored electrons with residual gas molecules.

3.2.2 Measurement of gas bremsstrahlung

(1) Experiment

Lead tungstate $PbWO_4$ (PWO) scintillation crystal has recently been developed for use in high energy physics experiments. The PWO crystal has many advantages in comparison with lead glass such as a short radiation length, a higher density, better light outputs and fast decay time of scintillations. Instruments for gas bremsstrahlung measurements with the PWO crystals can, therefore, be compact in size and have high accuracy. The performance of the PWO crystal is summarized in **Table 3-2**, as well as that of lead glass.

Nine PWO crystals, the size of which are 20 mm square in cross section and 200 mm in length (21.7 radiation length), are bundled and set on the beam axis of gas bremsstrahlung so that the beam is injected into the center of the central crystal, as shown in **Fig.3-11**. A copper absorber, 8 mm thick, shields the synchrotron radiation. Each crystal was wrapped with 15 μm-thick aluminum foil and a photo-multiplier tube was attached to the end of the crystal. The PWO detector was mounted on the stage, which is movable automatically in both the horizontal and vertical directions in 20 μm

steps. **Figure 3-12** shows a schematic diagram of the data acquisition system for the PWO detector. The signals from individual photo-multiplier tubes go into ADCs through a 125 ns cable delay. The signal from the central crystal is split into two signals, one is used to generate the gate to the ADCs. Digitized data from the ADCs are stored in a buffer memory for subsequent read out by a computer. The data can be analyzed and displayed graphically during data collection at the same time.

Energy calibration was performed by using the collimated gas bremsstrahlung photon beam, 1 mm x 1 mm, to fit a function with the end-point of the bremsstrahlung spectrum. According to EGS4 simulations, 74.0 % of the energy of the incident photon is deposited in the central crystal of the detector and 17.9 % is deposited in the surrounding eight crystals. The energy leaking out from the detector is 8.1 %. The ratios of the deposited energy to the incident energy are almost constant for the incident photon energy ranging from 200 MeV to 8.0 GeV. The bremsstrahlung photons were injected into the center of each crystal, one by one, and the end-points of the ADC's outputs were calibrated to be 5.92 GeV by fitting them individually, using a functional ADC output distribution form as follows[3-24],

$$\frac{dF(N,C,\sigma_0)}{d(ADC)} = N\int_{E_{min}}^{E_{max}} \frac{1}{E_\gamma^{3/2}} \exp\left\{\frac{-(E_\gamma - ADC/C)^2}{2\sigma_0^2 E_\gamma}\right\} dE_\gamma \qquad (3-1)$$

where $E\gamma$ is the photon energy, ADC the measured ADC output value, N the normalization factor, C the energy calibration constant and σ_0 the relative energy resolution of the PWO detector. E_{min} is the minimum photon energy chosen in the fitting and is set to be 2.0 GeV. E_{max} is the maximum photon energy, 5.92 GeV. An unfolding calculation was made to obtain N, C and σ_0. After the calibration, the beam was injected into the center of the central crystal (the crystal No.5 in **Fig.3-11**) and the ADC's outputs were summed up. The end-point of the summed up data was confirmed to be 7.35 GeV which shows a good agreement with the simulation. After the confirmation, the end-point of the summed up data was regarded as 8.0 GeV.

By using the center of gravity of leakage energies to the surrounding crystals, the

photon injection point can be determined[3-25] within the central crystal and the beam profile of the incident photons can be obtained.

The PWO detector was set in the optics hutch at the typical in-vacuum type undulator beamline, as shown in **Fig. 3-13**. The beamline consists of the light source of the insertion device that is installed into the straight section of the storage ring, the front-end components within the accelerator tunnel, and the transport channel outside the shield wall including the optics and experimental hutches. The effective length of the normal straight section is 16.54 m. The front-end consists of a fixed mask, a movable X-Y slit, and a beam shutter with the heat absorber, mainly to control the photon beam. The X-Y slit, made of oxygen-free copper 50 cm in length, and tantalum, 2 cm in length, is installed to set the maximum aperture size of 8 mm × 8 mm (277 μradian × 277 μradian). The transport channel consists of optical elements such as a monochromator and a photon beam shutter. They are all enclosed in the optics hutch and experimental hutch to protect workers from radiation exposure. The PWO detector was installed on the photon beam axis upstream of the monochromator. The vacuum pressures are monitored during operation of the stored electron beam 1.5 m from each side of the center of the straight section.

The high betatron function beamline BL11XU and the low betatron function beamline BL46XU are chosen taking into account the characteristics of the stored electron beam. **Figs. 3-14 and 3-15** show the horizontal and vertical beam sizes and beam divergences of the stored electron beam at the straight sections with the arrangement of the magnets for each beamline[3-26]. The horizontal electron beam size and beam divergence strongly depend on the beam position within the straight section. In contrast, the vertical beam size and divergence are nearly stable and have small values. The average electron beam sizes and beam divergences are summarized in **Table 3-3**, together with the values at the center of the straight sections.

(2) Calculations

Based on the previous discussion of the gas pressure dependence[3-27] , air at 10^{-3} (0.1013 kPa) atmospheric pressure was employed in the interaction region to calculate angular distribution of the emission with sufficient accuracy.

Since the stored beam profile is practically of a Gaussian shape, the size and divergence of the stored electron beam are approximated by assuming the four Gaussians in the horizontal and vertical directions, independently. Dividing the 16.54 m long straight section into 17 regions, the distributions of the beam size and the beam divergence are considered for the gas bremsstrahlung generation calculations.

The bremsstrahlung beam, which is generated within the straight section, is transferred through the vacuum region into a cylindrical phantom of ICRU with four elemental tissues[3-28] located at 40 m from the center of the straight section. The tissue phantom, which is 30 cm in radius and 30 cm in length, contains fifteen small cylindrical regions on the central axis to calculate the depth dependence of the energy deposition. The size of the small regions is defined as having a 0.5 cm thickness and 0.1 cm radius. The electron /positron and photon cut-offs for the tissue phantom were employed as 40 keV and 10 keV, respectively. The effective dose rates were obtained by multiplying the photon fluence rates by photon-fluence- to-effective-dose conversion coefficients, reported by Ferrari et al.[3-29], as a function of the scoring radius of the gas bremsstrahlung photons crossing the surface. The conversion coefficients of anterior-posterior irradiation geometry and isotropic irradiation geometry are employed in the present study

(3) Results

The inside of the storage ring is irradiated by synchrotron radiation so that the storage ring vacuum pressure depends on the stored beam current. During the experiments, the dependence of the vacuum pressure versus the stored beam current was examined and the measurements were made at pressure ranging from 2.5×10^{-8} Pa

to 4.5 × 10^{-8} Pa, as shown in **Fig.3-16**. The fluctuation of the pressure was less than 1.5 % during one measurement. The energy spectrum, which was obtained by summing up all the ADC's output, is shown in **Fig.3-17**. The knee of the spectrum at 8 GeV is observed very clearly. The photons beyond 8 GeV energy are due to multiple gas bremsstrahlung events. The probability of these events at the vacuum pressure of the storage ring was estimated to be less than 1 % of the bremsstrahlung production during the gate width of 250 ns. Besides, as shown in **Fig.3-17**, the effect on the profile of the gas bremsstrahlung is negligibly small in the neighborhood of 8 Gev energy. The energy resolution of the PWO detector was obtained as $(3.0\pm0.3)\%/\sqrt{E}$ by using the formula (4-1), which is nearly three times as good as that of lead glass.

Figure 3-18 shows the measurements of the gas bremsstrahlung spectra as a function of the aperture size defined by using the X-Y slit of the beamline, BL11XU. As shown in **Fig.3-18**, the shapes of the spectra are quite similar and only the intensity depends on the aperture size. The dependence of the intensity of the aperture size and photon energy above 1 GeV is shown in **Fig.3-19**, together with the EGS4 calculations. The calculations were made considering the stored electron beam size and beam divergence distribution, and were normalized at the aperture size of 277 μradian × 277 μradian. Good agreement was obtained between the calculations and the measurements in every energy region of the gas bremsstrahlung.

To compare the behavior of the gas bremsstrahlung for the high and low betatron function beamlines, the intensity at photon energy above 2 GeV for the beamlines BL11XU and BL46XU were measured at the same aperture sizes, 34.6 μradian in the horizontal axis and 34.6 μradian in the vertical axis. As shown in **Fig.3-20**, the measured intensities at the beamline, BL46XU, were obtained to be about 36 % lower than that of the beamline, BL11XU. The figure also shows that the intensity rate of gas bremsstrahlung per unit pressure and unit current is nearly constant versus the stored beam current. The measurements and the calculations of the intensities at photon energy above 1 GeV are summarized in **Table 3-4**, where four

calculations are presented. The first one is the calculation considering the distribution of the stored beam size and divergence. The second one is the calculation for the average stored electron beam size and divergence. The third one is the calculation with the beam size and the divergence at the center of the straight sections, and the last one is the calculation neglecting the beam size and divergence. As indicated in **Table 3-4**, the calculations considering the beam size and divergence distribution agree fairly well with the measurements in both beamlines. On the other hand, the calculations neglecting the beam size and divergence disagree in both beamlines. The remaining two calculations can be explained by the differences of the intensity between the BL11XU and BL46XU beamlines.

Figure 3-21 shows the absorbed doses as a function of depth in the tissue phantom for the beamlines, BL11XU and BL46XU. In the figure, the results neglecting the beam size and divergence are also shown. Both the depth dose distributions considering the electron beam size and divergence have a tendency to saturate, while the depth doses reach a maximum at the back of the tissue phantom. The ratios of the maximum doses to the dose neglecting the beam size and divergence are obtained to be 71 % and 44 % for BL11XU and BL46XU, respectively. The effective doses of anterior-posterior irradiation geometry as a function of the radius of the surface of the photon fluence crossing are shown in **Fig.3-22** with and without considering the electron beam size and divergence at 40 m from the center of the straight sections. Three doses are almost the same over the radius of 0.5 cm. As the radius decreases the effective dose rate increases. Three doses are quite different from each other for small radii, and the ratios of the effective doses for BL11XU and BL46XU to the dose neglecting the beam size and divergence become 60 % and 30 % at the radius of 0.023 cm, respectively.

The effective doses for the isotropic irradiation geometry condition are obtained to be about 1.8 times as high as the doses for the anterior-posterior geometry in **Fig.3-22**.

(4) Discussion

The average horizontal beam divergence of the stored electrons was estimated on the basis of the distributions of the gas bremsstrahlung intensity and the results are given in **Table 3-4**. The electron beam size and the divergence can be approximated by Gaussian distributions so that the photon beam profile can be expressed by the convolution of the Gaussians of the electron beam size, divergence and the gas bremsstrahlung. The beam intensity distributions as a function of the aperture size by using the X-Y slit, therefore, can be fitted by the Gaussians. The sizes of the photon beam profile at the X-Y slit were obtained to be σ = 1.71 ±0.05 mm and σ = 1.38 ±0.04 mm for the horizontal and vertical directions of BL11XU, and σ = 2.49 ±0.10 mm for the horizontal direction of BL46XU. Here, the electron beam size is very small so it can be considered to be a point. The vertical electron beam divergence is well known to be sufficiently small compared with that of the gas bremsstrahlung. The spread of the photon beam in the vertical direction is therefore considered to be only due to gas bremsstrahlung, and the effective distance from the point source to the X-Y slit was obtained as 21.6 m using a divergence of gas bremsstrahlung of 63.9 μradian and 1.38 ±0.04 mm. The effective distance of 21.6 m is nearly equal to the distance from the outlet of the straight section to the center of the X-Y slit. By using the effective distance and the horizontal beam sizes at the X-Y slit, the horizontal divergences are obtained to be 46.5 μradian for BL11XU and 95.9 μradian for BL46XU, showing good agreement with the averaged values in **Table 3-3**.

An analytical formula for spectrum of gas bremsstrahlung is given as follows [3-30],

$$EdN/dE = 4\alpha r_e^2 Z(Z+1)(Na/A)\left[(\frac{4}{3}-\frac{4}{3}v+v^2)\ln(183Z^{-1/3})+\frac{1}{9}(1-v)\right] \qquad (3-2)$$

where E is the photon energy and dN/dE is the number of the photons within dE, α the fine structure constant (1/137), γ_e the classical electron radius (2.82×10^{-13} cm) , Na the Avogadro constant (6.02×10^{23}), A the atomic weight per unit mol, and v is E/E_0

(E_0 equal stored electron energy, 8GeV). Z, which is the effective atomic number of the residual gas components to be estimated under the assumption of monatomic molecules, is obtained by fitting the observed spectrum. The average effective Z on the assumption of monatomic molecules is 8.1±0.3 as given in **Fig. 3-23** as a function of the stored current. The effective Z at the beamline BL11XU agrees well with that at the beamline BL46XU. If the residual gas consists of hydrogen and carbon oxide, the mole fractions are about 36 % and 64 %. The present result is seen to be different from the APS data of 4.6[3-14]. The in-vacuum type undulator in SPring-8 is employed for insertion devices and rare earth permanent magnets are coated by titanium nitrate ion plating to prevent out-gassing from its porous structure. Therefore, it seems probable that the chemical composition of the residual gas differs from other devices in ultra-high vacuum conditions.

The power of the gas bremsstrahlung above the photon energy of 1 GeV was measured to be 21.5±0.5 nW/10^{-8}Pa/mA (134 ± 3 GeV/s/10^{-8}Pa/mA). The power below photon energy of 1 GeV was evaluated to be 4.3 nW/10^{-8}Pa/mA (27.0 GeV/ s/10^{-8}Pa/mA) by using the formula (4-2) with effective atomic number of 8.1. Then the total power of gas bremsstrahlung at the 16.54 m long straight section of SPring-8 was estimated to be 25.8±0.8 nW/10^{-8}Pa/mA (161± 5 GeV/s/10^{-8}Pa/mA) by summing up the measurements and calculations.

The maximum dose equivalent rates were obtained by multiplying the photon fluence rates by the maximum fluence to dose equivalent conversion factors published by Rogers [3-31]. Because of the different irradiation situations, however, this technique tends to overestimate the doses as pointed out by several authors, it is meaningful to compare these results with other reports, reference numbers (3-14) and (3-23). The maximum dose equivalent values at 40 m from the center of the straight section for a scoring area, 0.023 cm radius of BL11XU, BL46XU, and neglecting the stored beam size and divergence were obtained as 53.6 nSv/s/10^{-8}Pa/mA, 31.7 nSv/s/10^{-8}Pa/mA, and 82.5 nSv/s/10^{-8}Pa/mA, respectively. Ipe et al.[3-23] obtained the maximum dose

equivalent rate for a scoring area of 0.0013 cm^2 (radius = 0.02 cm) at 40.1 m from the center of the straight section and at stored electron energy of 7 GeV as 2.1 Sv/h/300mA/nT, neglecting the stored beam size and divergence, which is about 1.8 times as high as the present result. Since Ipe's result was derived using the residual gas composition of air and a stored electron energy of 7 GeV, the difference between the two is reasonable.

Table 3-1 List of Monte Carlo simulations and parameters for gas bremsstrahlung production.

Auther	Organization	code	maximum electron energy	target length	AE (MeV)	AP (MeV)	pressure (atm)	gas material	date	ref. No.
G.Tromba & A.Rindi	Sincrotrone Trieste	EGS4	10GeV	1m	1.0	0.01	1.0	air	1990	(3-9)
J.C.Liu	SLAC	EGS4	10GeV	1m	1.511	0.1	1.0	air	1994	(3-10)
A.Ferrari Et.al	INFN	FLUKA	1GeV	1,10m	10.0	0.01	1.0, 0.1	air	1993	(3-11)
N.E.Ipe & A.Fasso	SLAC	FLUKA	7GeV	15m	10.0	0.01	1.0, 0.1	air	1994	(3-6)

Table 3-2 Characteristics of a PWO scintillator, lead glass, and NaI(Tl) scintillator.

	PWO	Lead glass	NaI(Tl)
Composition	$PbWO_4$	PbO 51 % SiO_2 41% K_2O 7%	NaI(Tl)
Density (g/cm3)	8.2	~4.5	3.67
Radiation length (†)			
Xo (cm)	0.92	2.6	2.59
Moliére radius(‡)			
Rm (cm)	2.2	3	4.8
Light intensity (arbitrary unit)	0.3	~0.03	100
Main decay time (ns)	< 3	~20	230

(†) Radiation length, Xo means the thickness of a material with electron energy decrease due to bremsstrahlung to the average ratio of 1/e.

(‡) Moliére radius, Rm =21MeV.Xo/Ec, and about 99% of the energy is confined within 3Rm. Ec indicates the critical energy, which is the loss of energy due to bremsstrahlung equal to the ionization.

Table 3-3 The size and divergence of the stored electron beam of SPring-8 for high and low betatron function for a beam emittance of 6.7 nm·radian. The average and center are the size and divergence averaging over the straight section and at the center of the straight section, respectively.

	BL11XU (High β)		BL46XU (Low β)	
	Average	Center	Average	Center
Beam size (m)				
Horizontal	$3.6_6\times10^{-4}$	$3.8_9\times10^{-4}$	$2.6_5\times10^{-4}$	$8.4_8\times10^{-5}$
Vertical	$1.6_4\times10^{-5}$	$1.4_7\times10^{-5}$	$1.4_7\times10^{-5}$	$1.2_4\times10^{-5}$
Beam divergence (radian)				
Horizontal	$4.9_7\times10^{-5}$	$1.7_1\times10^{-5}$	$9.4_3\times10^{-5}$	$7.8_6\times10^{-5}$
Vertical	$2.0_7\times10^{-6}$	$1.3_6\times10^{-6}$	$2.5_4\times10^{-6}$	$1.6_1\times10^{-6}$

Table 3-4 The relative intensities of measured and calculated gas bremsstrahlung as a function of the aperture size of the X-Y slit. The intensities are normalized at the aperture size of 277 μradian on the horizontal axis (H) and 277 μradian on the vertical axis (V) of BL11XU. The intensities of BL11XU are for the photons of energy above 1 GeV and above 2 GeV for BL46XU.

BL11XU						BL46XU				
Aperture size(HxV) μrad.	Measure.	Calculation				Measure.	Calculation			
		emit6.68(*1)	emit av.(*2)	mini(*3)	point (*4)		emit6.68(*1)	emit.av.(*2)	mini(*3)	point(*4)
34.6 × 34.6	0.076_2	0.076_9±4.1%	0.055_4	0.083_4	0.10_6	0.044_7	0.036_8±7.4%	0.034_3	0.039_2	0.10_4
69.2 × 34.6	0.13_9	0.13_8±3.2%	0.10_7	0.15_4	0.18_3	0.081_4	0.084_1±5.0%	0.066_0	0.077_5	0.18_0
69.2 × 69.2	0.26_5	0.24_1±2.5%	0.19_2	0.26_9	0.31_5	*	0.15_1±3.8%	0.12_0	0.14_1	0.31_1
138 × 69.2	0.42_2	0.39_3±2.1%	0.34_9	0.42_7	0.44_9	*	0.27_9±3.0%	0.23_5	0.26_7	0.44_8
138 × 138	0.65_8	0.58_6±1.8%	0.52_1	0.63_0	0.66_1	*	0.43_2±2.5%	0.35_5	0.40_3	0.66_1
277 × 138	0.83_1	0.81_3±1.7%	0.79_8	0.79_6	0.79_6	*	0.72_6±2.2%	0.63_1	0.67_5	0.86_9
208 × 208	0.86_9	0.84_4±1.7%	0.80_3	0.86_2	0.87_1	*	0.69_5±2.1%	0.59_1	0.64_9	0.79_7
277 × 277	1.0	1.0±1.1%	1.0	1.0	1.0	*	0.89_8±2.0%	0.79_6	0.84_8	1.0

(*1); considering the electron beam size and divergence distribution with the emittance of 6.68nm.rad. (*2): calculation with the average beam size and divergence on the emittance of 6.68nm.rad. (*3); calculation with beam size and divergence at the emittance of 6.68 nm.rad. (*4); calculation without the beam size and divergence.

Table 3-4 The relative intensities of measured and calculated gas bremsstrahlung as a function of the aperture size of the X-Y slit. The intensities are normalized at the aperture size of 277 μradian on the horizontal axis (H) and 277 μradian on the vertical axis (V) of BL11XU. The intensities of BL11XU are for the photons of energy above 1 GeV and above 2 GeV for BL46XU. (continued)

	BL11XU						BL46XU			
Aperture size(HxV) μrad.	Measure.	Calculation				Measure.	Calculation			
		emit6.68(*1)	emit av.(*2)	mini(*3)	point (*4)		emit6.68(*1)	emit.av.(*2)	mini(*3)	point(*4)
277 × 34.6	0.31_5	0.29_9±2.3%	0.29_7	0.31_3	0.29_7	*	0.25_9±3.1%	0.23_0	0.24_7	0.29_4
34.6 × 277	0.26_8	0.23_1±2.6%	0.17_9	0.24_7	0.29_5	*	0.14_4±3.9%	0.11_7	0.13_4	0.29_2
1380 × 1380	*	1.3_9±1.5%	1.4_0	1.3_0	1.2_9	*	1.4_0±1.8%	1.3_9	1.3_0	1.2_8

(*1); considering the electron beam size and divergence distribution with the emittance of 6.68nm.rad. (*2): calculation with the average beam size and divergence on the emittance of 6.68nm.rad. (*3); calculation with beam size and divergence at the emittance of 6.68 nm.rad. (*4); calculation without the beam size and divergence.

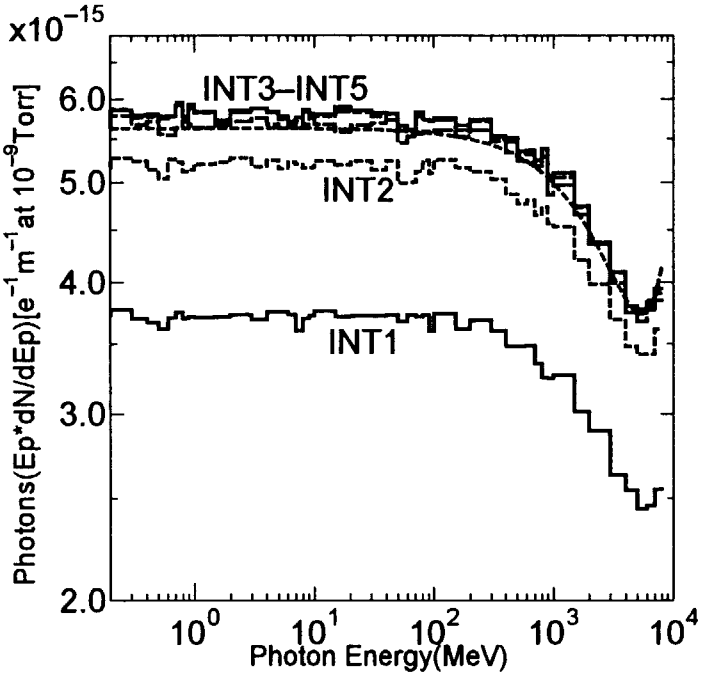

Fig.3-1 Gas bremsstrahlung spectra depending on the number of the interactions generated by EGS4 resulting from 8 GeV electron and interacting with 0.1205 g/cm^2 air. (INT1; single interactions, INT2; double interactions, INT3,4,5; triple or more interactions.)

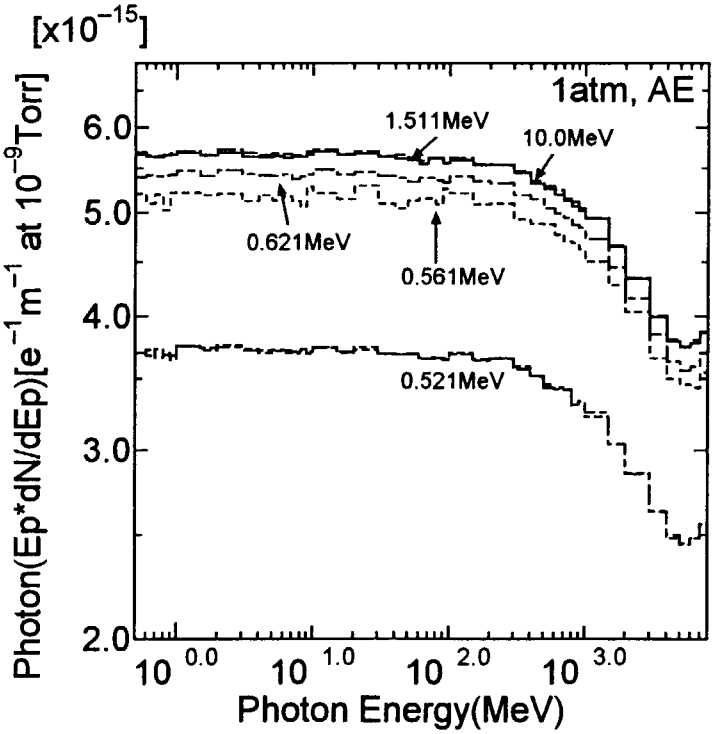

Fig.3-2 Gas bremsstrahlung spectra depending on the lower cut off energy for electrons, AE, allowing only single interaction of electrons with residual gas of 0.1205 g/cm^2 air.

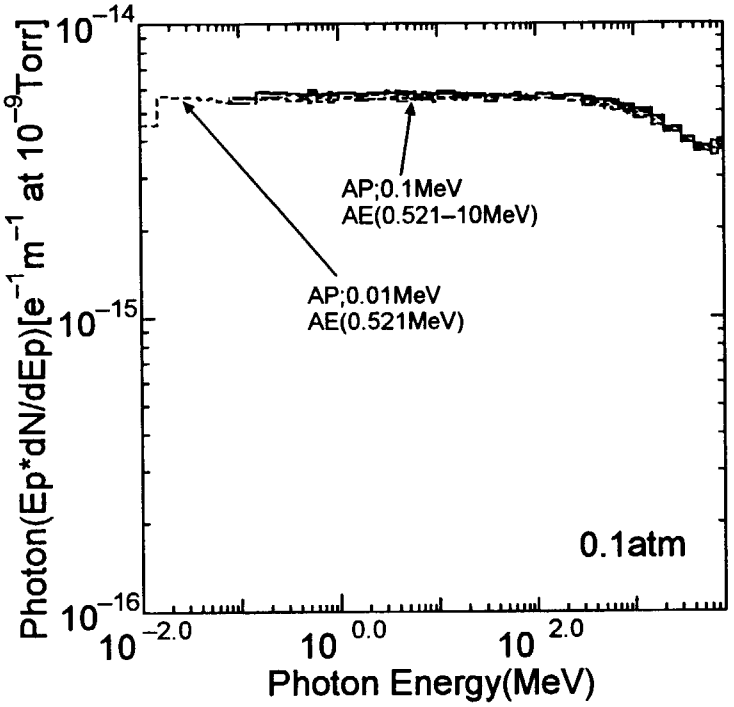

Fig.3-3 Gas bremsstrahlung spectra depending on the lower cut off energy for electrons, AE, and the lower cut off energy for photons, AP, allowing only single interaction of electrons with residual gas of 0.01205 g/cm^2 air.

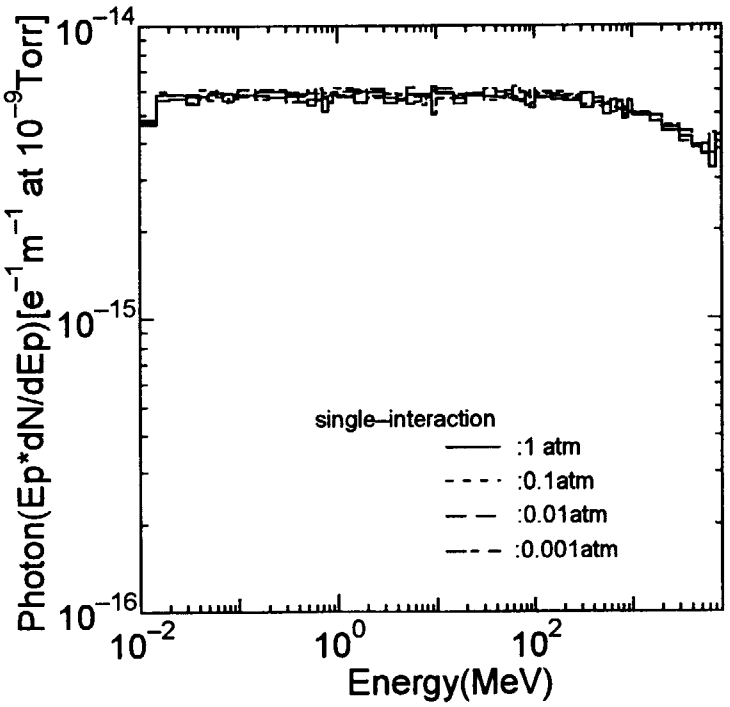

Fig.3-4 Gas bremsstrahlung spectra depending on gas pressure with the path length of 1 m and AE of 10 MeV, allowing only single interaction of electrons

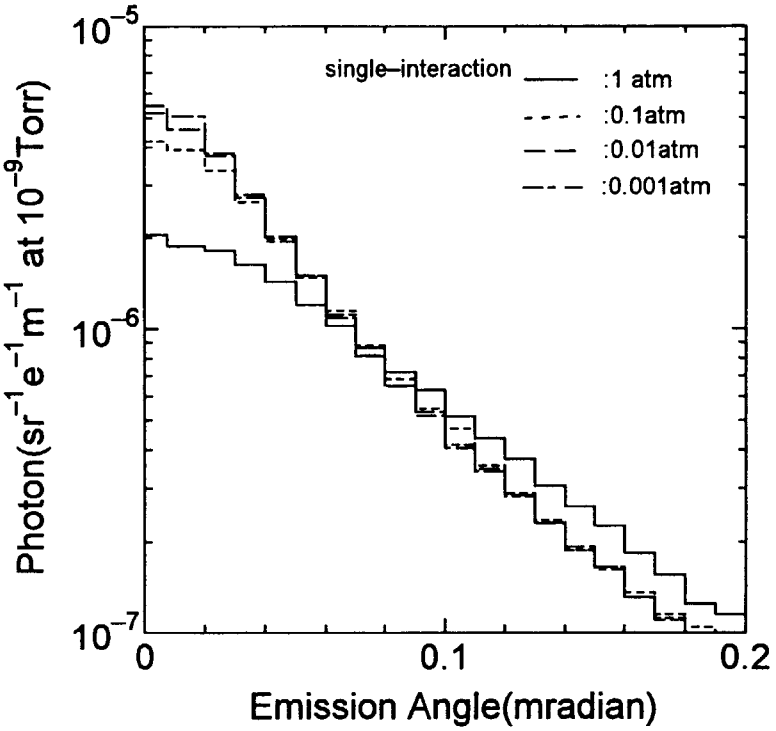

Fig.3-5 Angular distributions depending on gas pressure with the path length of 1 m and AE of 10 MeV, allowing only single interaction of electrons

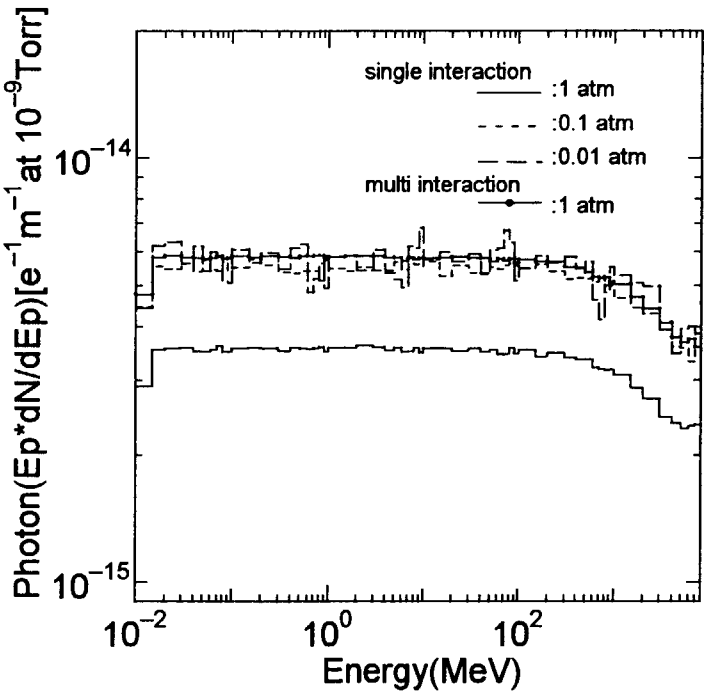

Fig.3-6 Gas bremsstrahlung spectra depending on gas pressure with the path length of 19 m and AE of 10 MeV, allowing only single interaction of electron and multi interaction.

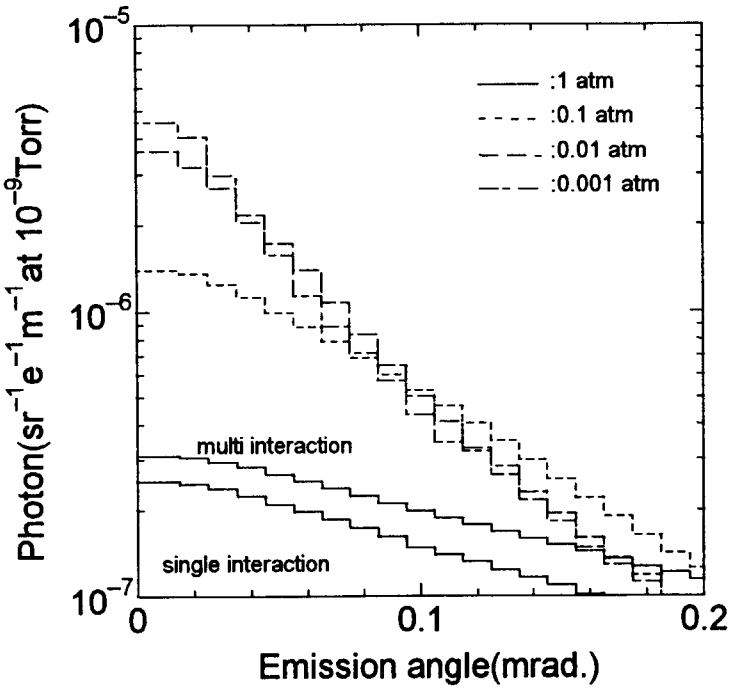

Fig.3-7 Angular distributions depending on gas pressure with a path length of 19 m and AE of 10 MeV, allowing only single interaction of electrons and multi interaction within 1 atm.

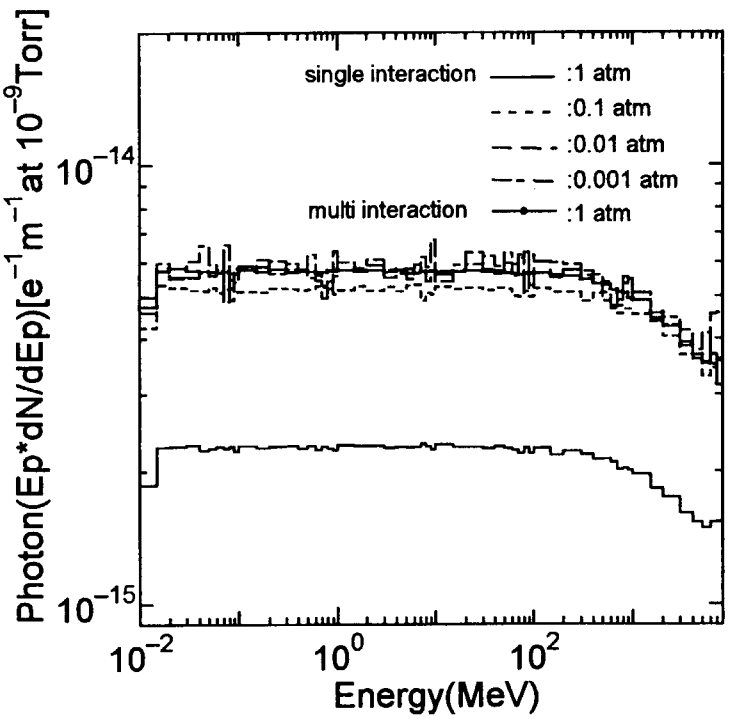

Fig.3-8 Gas bremsstrahlung spectra depending on gas pressure with a path length of 40 m and AE of 10 MeV, allowing only single interaction of electrons and multi interaction.

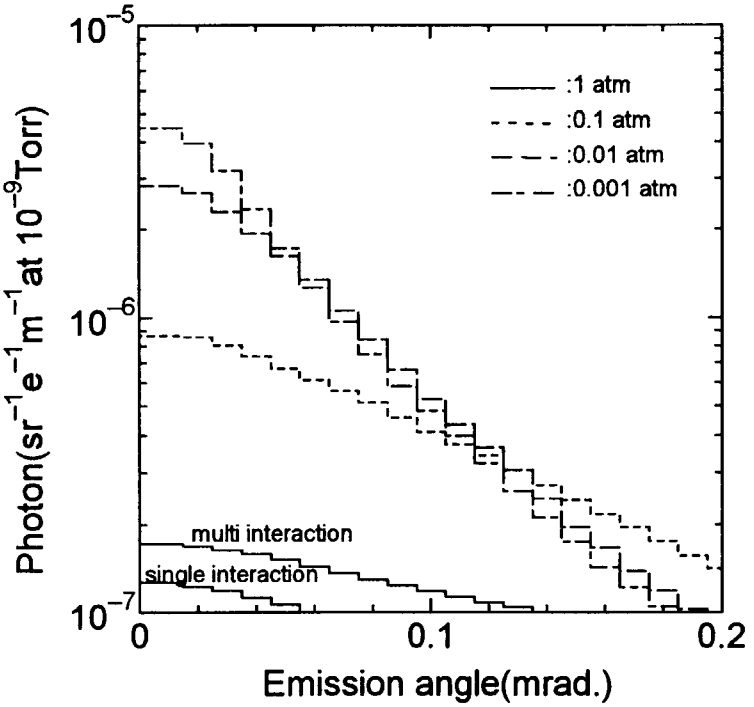

Fig.3-9 Angular distributions depending on gas pressure with a path length of 40 m and AE of 10 MeV, allowing only single interaction of electrons and multi interaction within 1 atm.

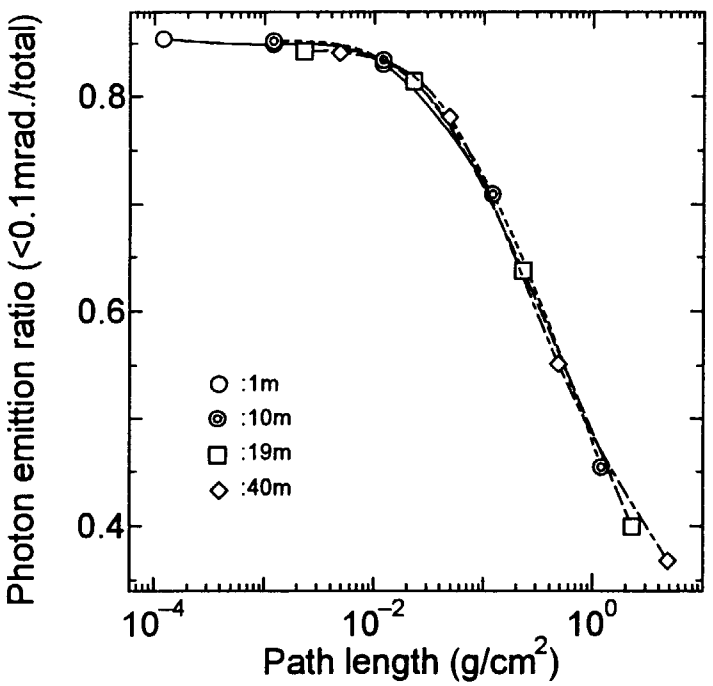

Fig.3-10 Emission angle dependence of gas bremsstrahlung on the electron path length. The vertical axis indicates the ratio of the photons within 0.1 mradian to the total photons.

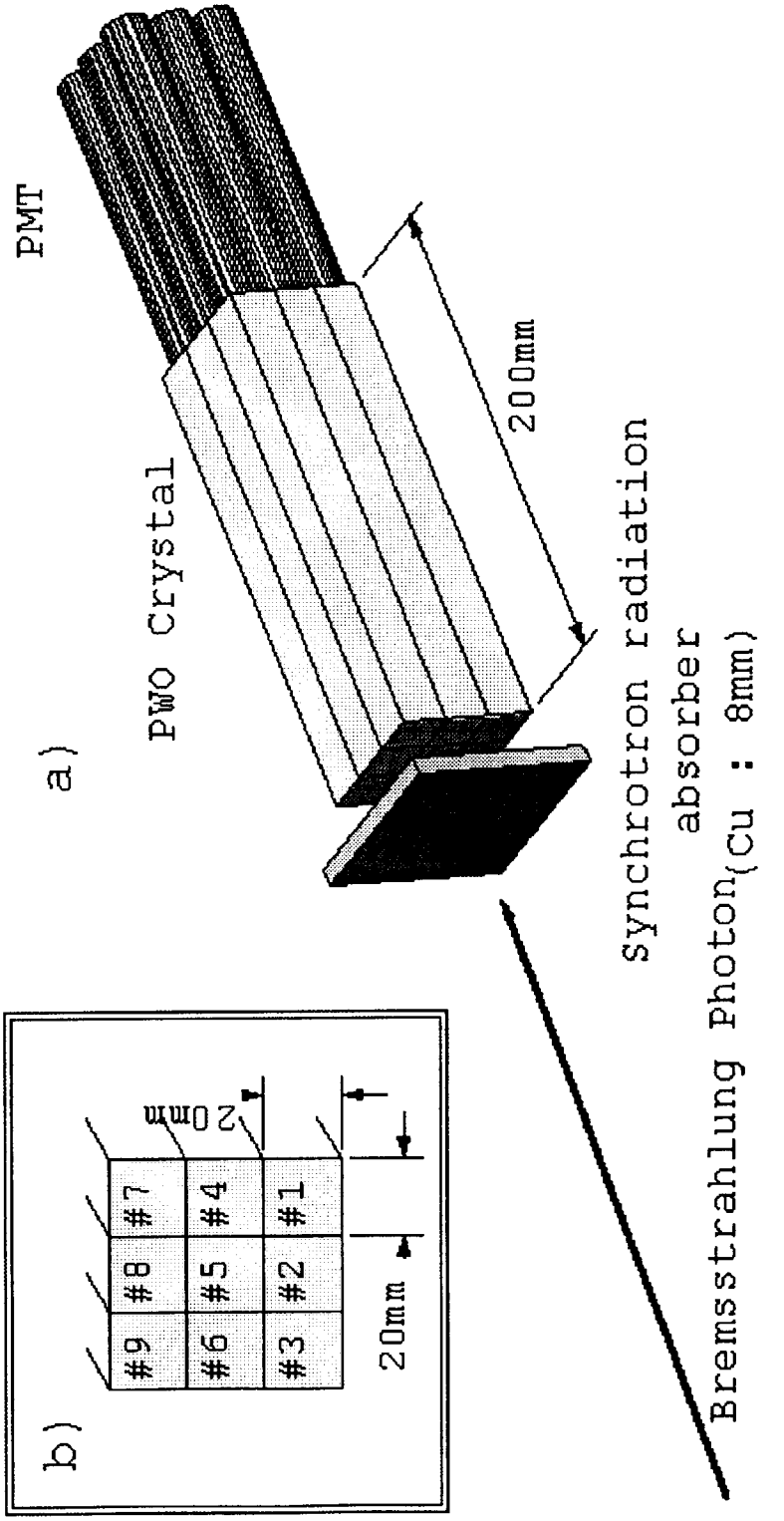

Fig.3-11 Illustration of the PWO calorimeter which consists of nine crystals. The size of the crystal is 20 mm square in width and 200 mm in length. The copper absorber is set in front of the calorimeter to protect it from the synchrotron radiation beam. (a) Bird's-eye view, (b) cutaway view of PWO calorimeter.

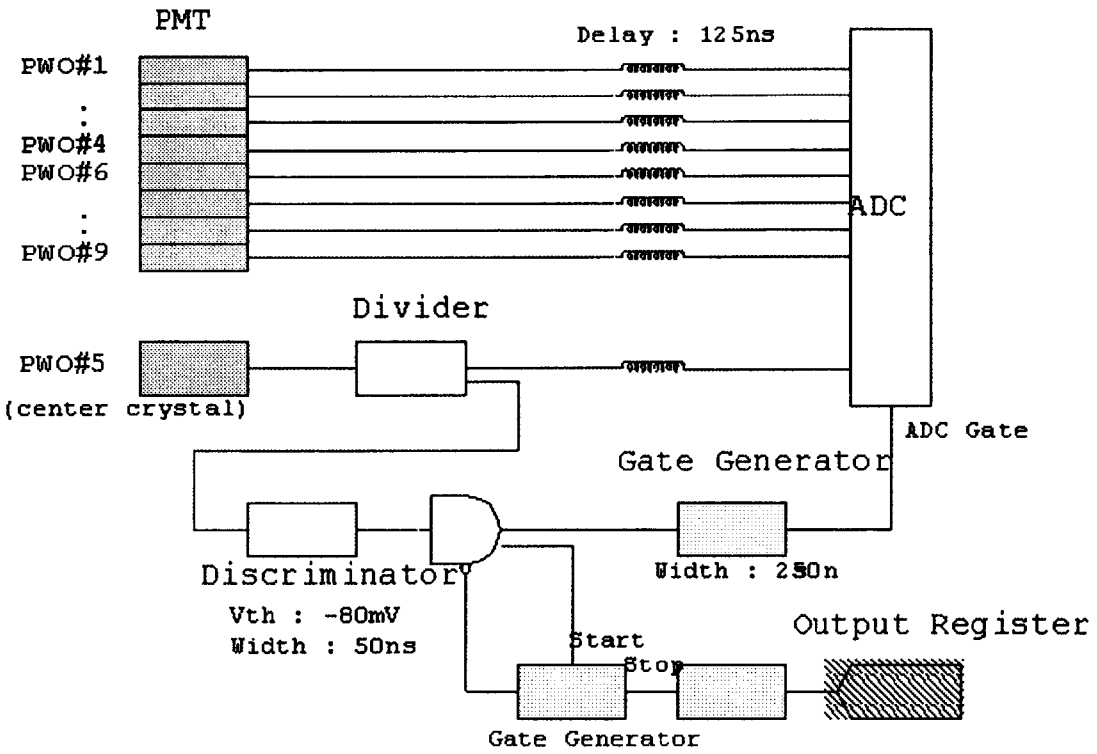

Fig.3-12 Data acquisition system of gas bremsstrahlung measurements using nine PWO scintillators.

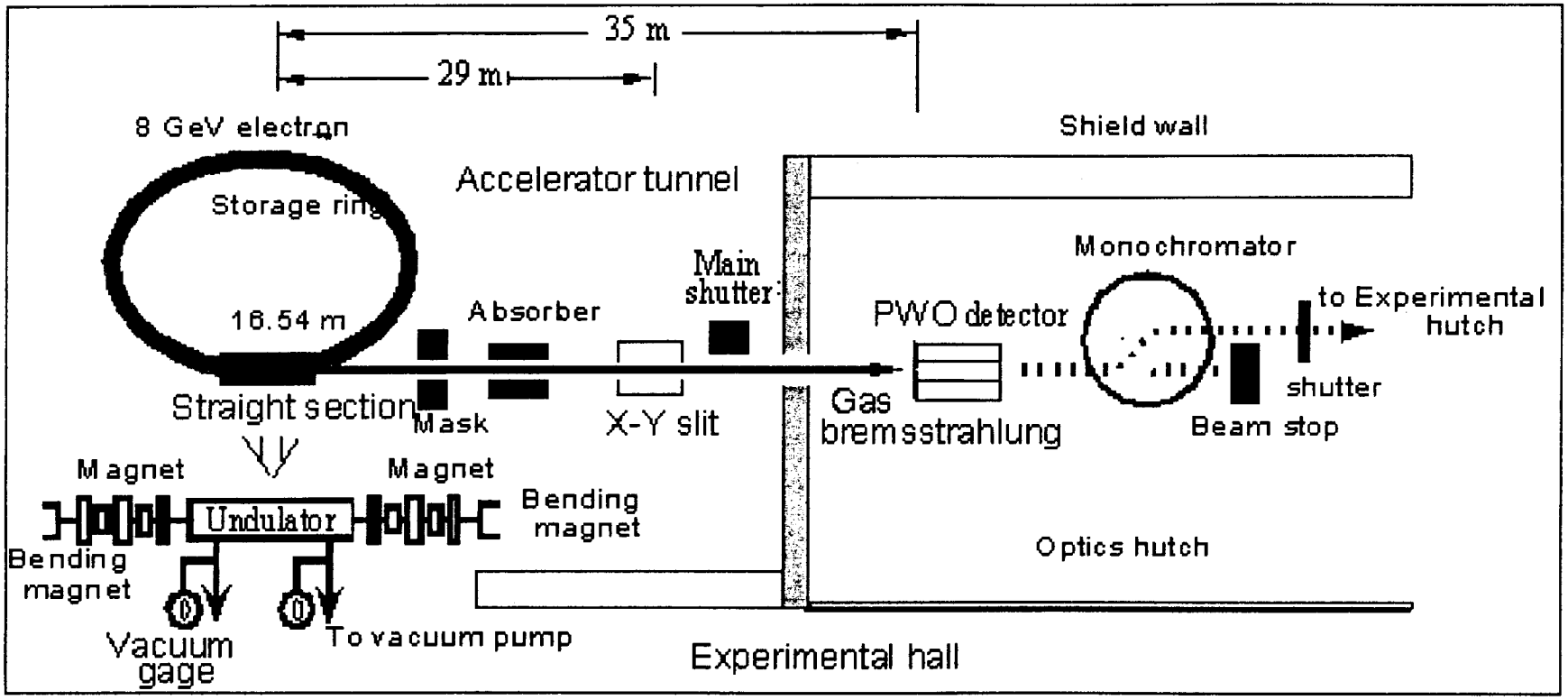

Fig.3-13 Illustration of the overall experimental set up. In a straight section, quadrupole and sextupole magnets are installed in addition to an undulator. The double ion gages and ion pumps are installed at 50 cm inside from both tips of the undulator that is 4 m in length. An X-Y slit is installed as one of the front-end components inside the shield wall of the accelerator tunnel and a monochromator is installed outside the shield wall within an optics hutch in the experimental hall. The PWO detector was located on the beam axis upstream of the monochromator.

This is a blank page.

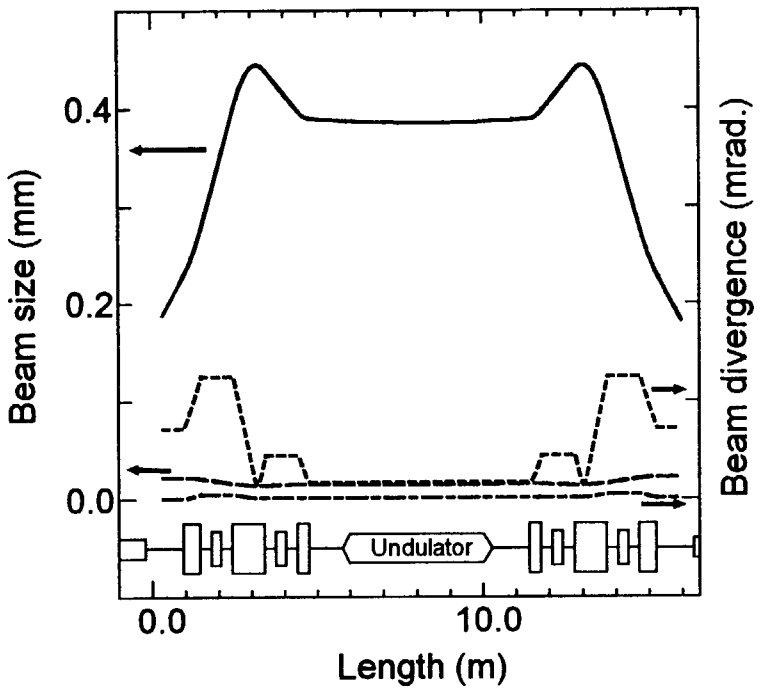

Fig.3-14 The distributions of the stored electron beam size and beam divergence for the high betatron function of BL11XU at a beam emittance of 6.8 nm.radian. The solid line indicates the horizontal beam size, dot line: the horizontal beam divergence, dashed line: the vertical beam size, dot dashed line indicates the vertical beam divergence. The geometrical arrangements of the magnets are also indicated.

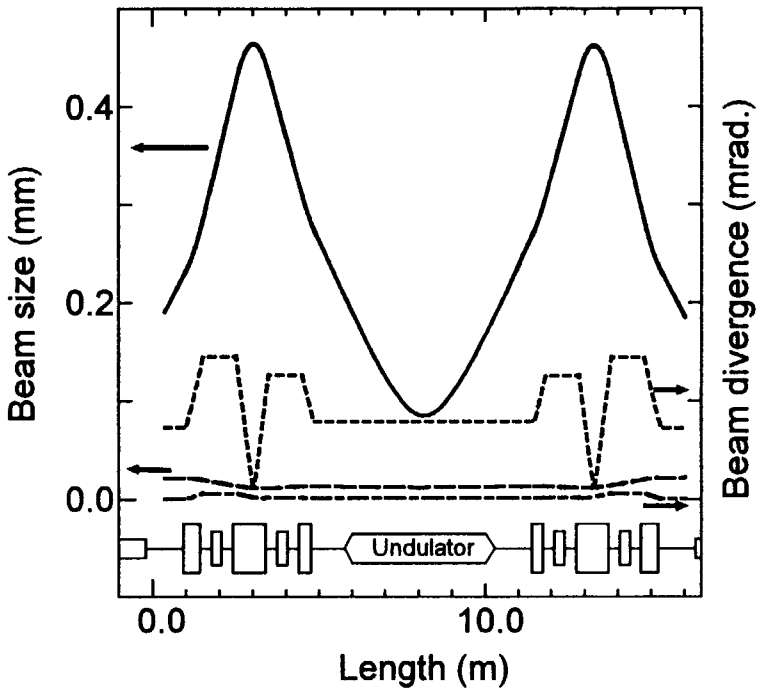

Fig.3-15 The distributions of the stored electron beam size and beam divergence for the low betatron function of BL46XU. The lines indicate the same as in Fig.4-4, and the geometrical arrangements of the magnets are also indicated.

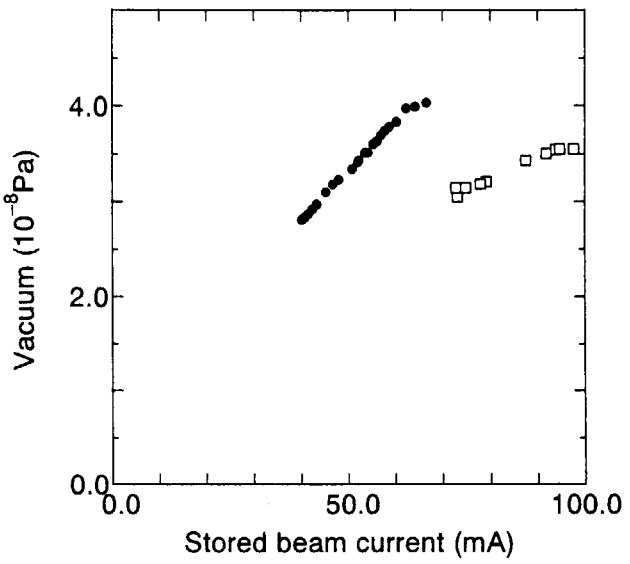

Fig.3-16 The relation between the output of vacuum ion gages and stored electron beam current. The open squares indicate the values at BL11XU and the full circles at BL46XU.

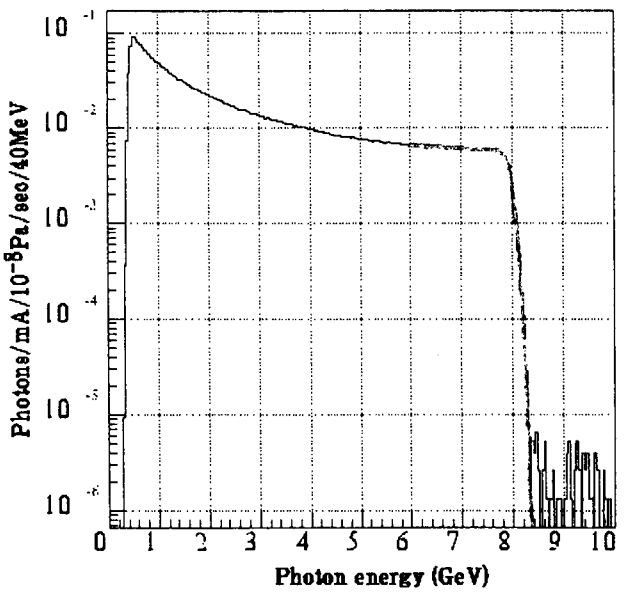

Fig.3-17 The spectrum of gas bremsstrahlung obtained by summing up the output of the nine PWO crystals. The bold red line indicates the line fitting by formula (4-1) to get the energy resolution.

This is a blank page.

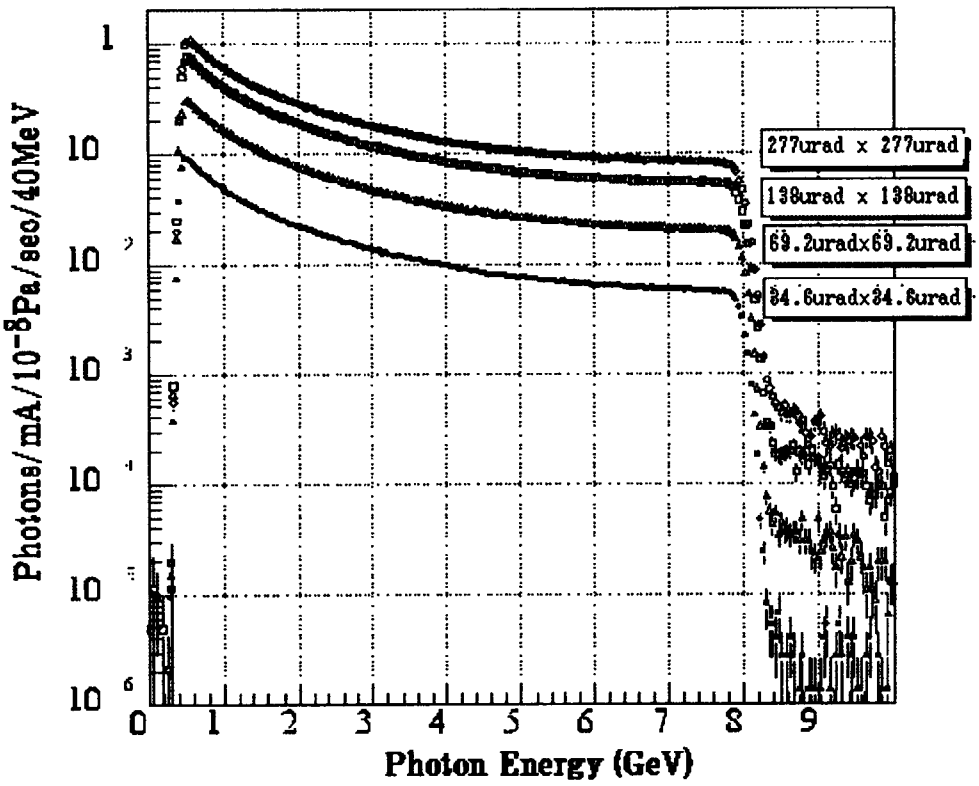

Fig.3-18 The spectra of gas bremsstrahlung for various aperture sizes of the X-Y slit at the BL11XU beamline. The full circles indicate the spectrum for the aperture size of 34.6 μradian(H) × 34.6 μradian(V), the triangles: for 69.2 μradian(H) × 69.2 μradian(V), the squares: 138 μradian(H) × 138 μradian(V), the open circles: 277 μradian(H) × 277 μradian(V).

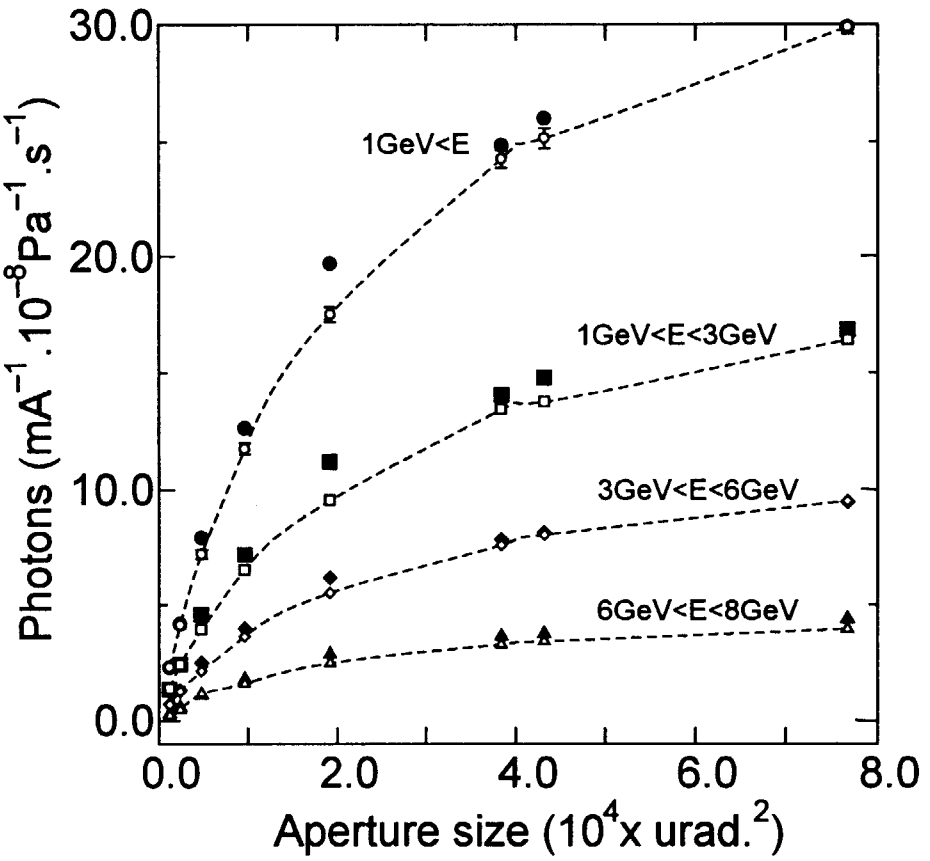

Fig.3-19 The intensity distributions of gas bremsstrahlung as a function of the aperture size of the X-Y slit and energy ranges at the BL11XU beamline. The Monte Carlo calculations are also presented. The full circles indicate the data of the measurements for the photon energy above 1 GeV and open circles indicate the calculations considering the beam size and beam divergence distributions. The full squares: the measurements ranging from 1 GeV to 3 GeV photon energy, open squares: the calculations. The full diamonds: the measurements ranging from 3 GeV to 6 GeV photon energy, open diamonds: the calculations. The full triangles: the measurements ranging from 6 GeV to 8 GeV, open triangles: the calculations.

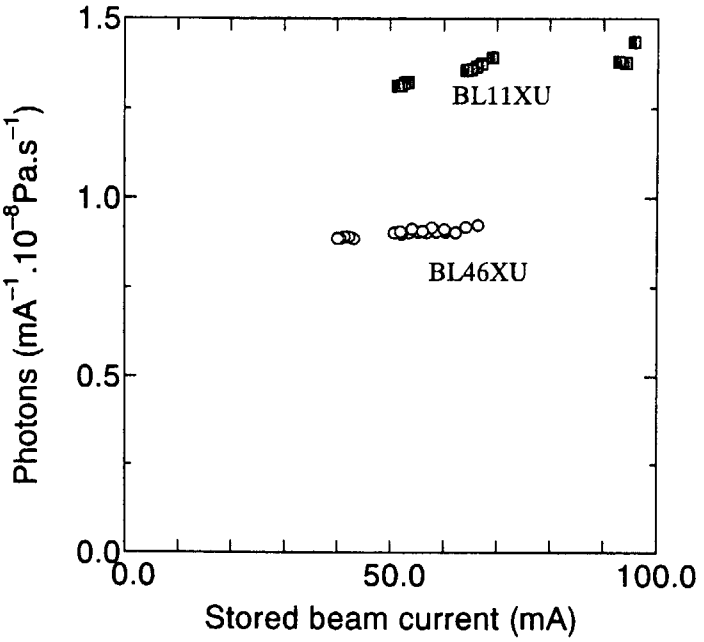

Fig.3-20 The intensities for the stored current for an aperture size of 34.6 μradian(H) × 34.6 μradian(V) at the high betatron function beamline BL11XU, and comparison with that of the same aperture size of the low betatron function beamline BL46XU. The open squares indicate the intensity of photon at BL11XU and open circles are at BL46XU.

This is a blank page.

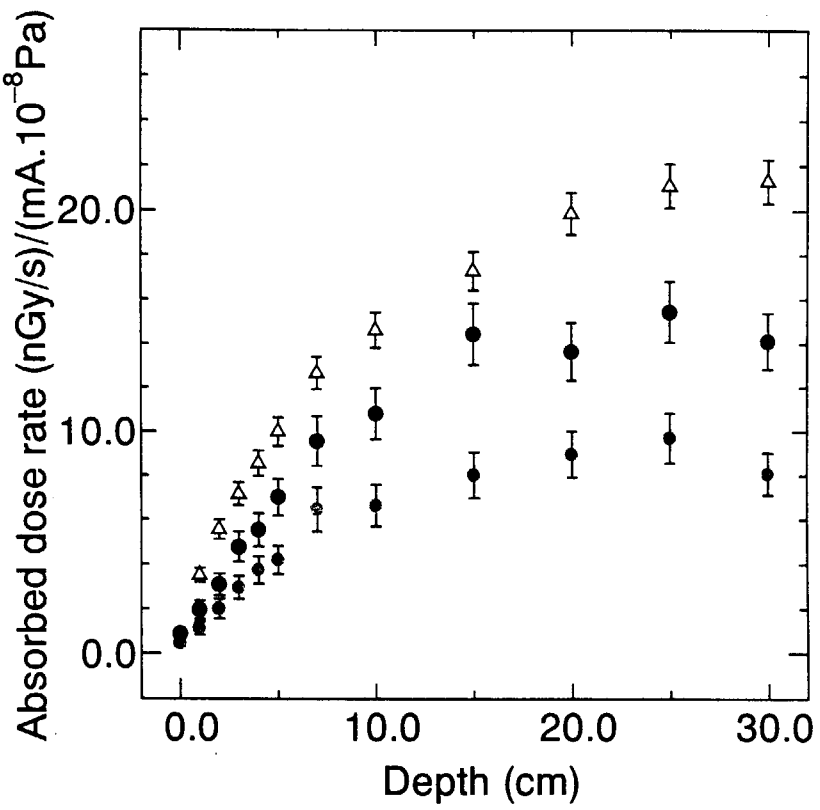

Fig.3-21 The depth distributions of absorbed dose due to gas bremsstrahlung within an ICRU tissue phantom at 40 m from the center of the straight section. The open triangles indicate the calculations neglecting the stored beam conditions. The blue circles indicate the calculations considering the beam size and beam divergence of the high betatron function beamline BL11XU and the red circles are for the low betatron function beamline BL46XU. The size of the cylindrical phantom is, 30 cm radius and 30 cm long.

This is a blank page.

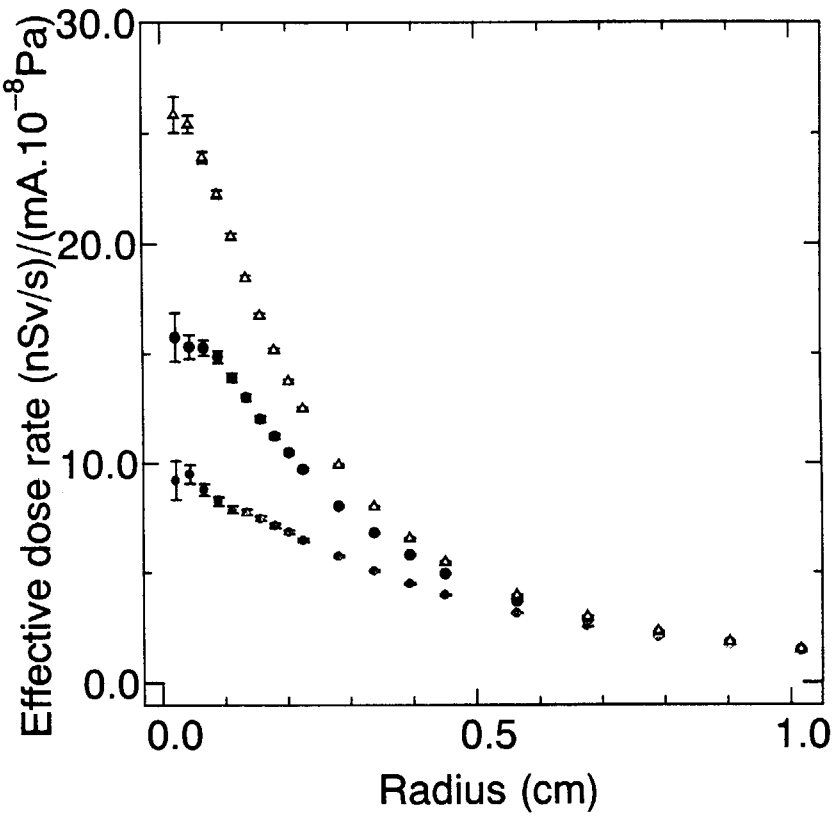

Fig.3-22 The effective dose distributions as a function of radial scoring area due to gas bremsstrahlung in anterior-posterior irradiation geometry at 40 m from the center of the straight section. The open triangles indicate the calculations neglecting the stored beam conditions. The blue circles indicate the calculations with considering the beam size and beam divergence of the high betatron function beamline, BL11XU, and the red circles are for the low betatron function beamline, BL46XU.

This is a blank page.

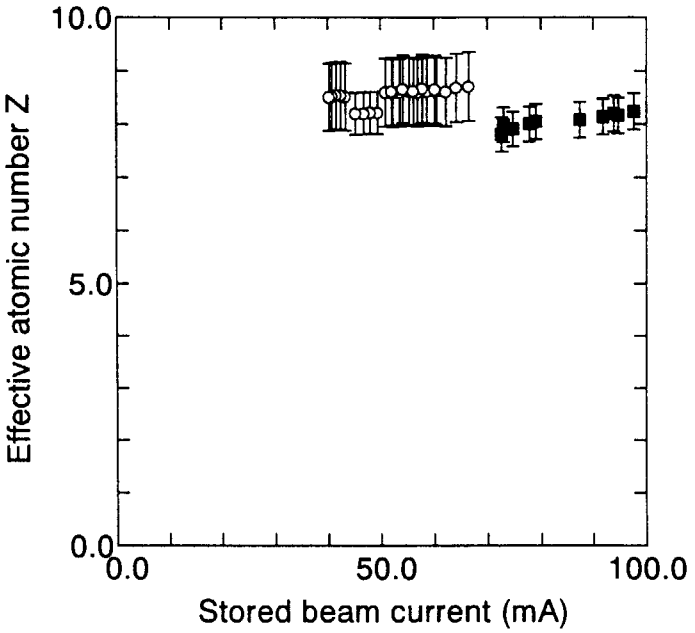

Fig.3-23 The effective atomic numbers of the residual gas components at the straight sections of the BL11XU and BL46XU beamlines. The blue squares indicate the effective atomic numbers at BL11XU, and red circles are for BL46XU

This is a blank page.

3.3 Photoneutrons due to gas bremsstrahlung

3.3.1 Photoneutron production calculation

Shielding designed to suppress gas bremsstrahlung must be enhanced because of the production of photo-neutrons. Photo-neutrons are generated by the interaction of gas bremsstrahlung with beamline components, such as a photon stop.

In order to calculate the photo-neutron spectrum, at first, a track length distribution of gas bremsstrahlung inside a lead photon stop, 30cm in length with radius of 20cm, was calculated using EGS4, as shown in **Fig.3-24**. Based on the calculated track length distribution, we obtained energy spectra of the photo-neutrons using the following two calculation methods.

The neutron spectral yield by the first method is given by,

$$N(En) = f(En) \cdot A \cdot \int dL(E\gamma)/dE\gamma \cdot \sigma(E\gamma) \cdot dE\gamma \qquad (3-3)$$

where $dL(E\gamma)/dE\gamma$ is the track length distribution of gas bremsstrahlung and $E\gamma$ the photon energy. $\sigma(E\gamma)$ is the Lorenzian fitted neutron production cross section of Dietrich and Berman[3-32] with neutron multiplicity, neglecting neutron production by the quasi-deuteron and photo-pion reactions of photons above 40MeV. $f(En)$ indicates a Maxwellian with T=0.98MeV[3-33]. A is the number of atoms per unit volume.

The neutron spectral yield by the second method is given as,

$$N(En) = A \cdot \int dL(E\gamma)/dE\gamma \cdot \sigma(E\gamma, xEn) \cdot dE\gamma \qquad (3-4)$$

where $\sigma(E\gamma, xEn)$ is the production cross section of x photo-neutrons with energy En, generated by using the MCPHOTO[3-34] code and the PICA[3-35] code, taking into account the giant resonance, quasi-deuteron and *photo-pion* reaction processes. The other terms are the same as those in **Eq.(3-3)**. The calculated photoneutron production cross sections of copper and lead, for example, are shown in **Figs.3-25,3-26**, and **3-27. Figure 3-28** is given a comparison of the two neutron spectral yield rates for the normal straight section, 19m in length, with 100mA stored current at the residual gas

pressure of 133nPa.

Once the neutron energy spectrum is determined, the ambient dose equivalent, *H*(10)* is given as,

$$H^*(10) = \int H(En) \cdot \Phi(En) \cdot dEn \qquad (3-5)$$

where *H(En)* are the neutron fluence to ambient dose equivalent conversion coefficients by Ferrari et al.,[3-35]. $\Phi(En)$ is the spectral fluence. As shown in **Fig.3-29**, almost all of the generated photo-neutrons are emitted at the injection point of the photon stop. Then, assuming an isotropic neutron point, we calculated the ambient dose equivalent rates at 1 m away from the center of the photon stop, yielding 1.5 μ Sv/h and 1.8 μ Sv/h for the neutron spectrum based on the Dietrich and Berman's cross section and on the cross section by MCPHOTO and PICA, respectively. Neglect of neutron production by the quasi-deuteron and photo-pion reactions by the photons above 40MeV is seen to result in only less than 17 % underestimate of the ambient dose equivalent. In the calculation of the maximum dose equivalent along the principal diameter of the ICRU sphere[3-37], 1.6 μ Sv/h and 2.0 μ Sv/h were also obtained for the neutron spectrum based on the Dietrich and Berman's cross section and that based on the cross section by MCPHOTO and PICA, respectively.

3.3.2 Measurement of photoneutrons due to gas bremsstrahlung

(1)Experiment.

The targets and the PWO detector were installed alternately on the photon beam axis upstream of the monochromator at the undulator beamline of BL11XU, as illustrated in **Fig.3-30**. The targets were employed for lead, 20 cm in height, 20 cm in width, and 10 cm in thickness ($17.8X_0$, X_0: radiation length), and copper, 15 cm in height, 15 cm in width, and 10 cm in thickness ($6.94X_0$). The X-Y slit made of oxygen-free copper, 50 cm in length, and tantalum, 2 cm, was set to the maximum aperture size of 8 mm × 8 mm (277 μradian × 277 μradian) during the experiments. The vacuum pressures are monitored during the stored electron beam operation 1.5 m

from each side of the center of the straight section, as shown in **Fig.3-13**. The measurements were performed during the stored beam current of 72 to 98 mA, and vacuum pressures of 25.2 to 30.4 nPa and 35.4 to 40.8 nPa. The variations of the current and vacuum pressures during measurement were less than 2 % and 1 %, respectively

The helium-3 counters with moderators of various thickness are shown in **Fig.3-31**, and were set outside the optics hutch. The helium-3 counters with high sensitivities consist of helium-3 of 8 atmospheric pressure and a volume of 1013 cm^3. Four kinds of polyethylene moderators were employed and the responses were calculated by MCNP4a[3-38] with DLC105C[3-39] library for thermal neutron energy to 20 MeV and ANISN[3-40] with HILO86R library[3-41] for neutron energy of 20 MeV to 400 MeV. The calibrations were performed using a neutron source of californium-252 with well-known emission rate, and inverse square law of distance to estimate the effect of the scattered neutrons. The responses are shown in **Fig.3-32**. The arrangements of the counters are also indicated in **Fig.3-30**. The distances from the center of the targets to the counters are 330.6 cm and 340.2 cm for upstream and downstream sides, respectively. The counters were set at 60 cm in height from the experimental floor.

(2) Calculation

Using the cross section library of photoneutron production of MCPHOTO and PICA, photoneutron production yields and photoneutron spectra within the targets are shown in **Fig.3-33** and **Fig.3-34**, respectively. The photoneutron yields were normalized with the gas bremsstrahlung power of 25.8 nW at beam current of 1 mA and residual gas pressure of 10 nPa. The yield of neutron production is not saturated within the copper target because of insufficient thickness. Otherwise, the lead target has sufficient thickness for photoneutron production. In the calculations, the yields of photoneutron production are 59 % and 96 % of the saturated yields for the copper

target and lead target, respectively. The depths where half of the photoneutrons are produced within the targets are 6.5 cm and 2.1 cm for copper and lead targets, respectively. The photoneutron transport calculation from the target to the estimated points and conversion to the effective dose is performed by using MCNP4b with LANLHE library[3-42], and the photoneutron spectra with the photoneutron yields, as shown in **Fig.3-33,3-34**. The cylindrical volume sources with isotropic emissions of photoneutrons were assumed in the calculations. The assumed cylinders have a radius of 1 cm and 10 cm in length for the copper target, and 1 cm in radius and 4 cm in length for the lead target because of the consideration of the photoneutron production distributions. The calculated results are shown in **Fig.3-35** and **3-36**, and the spectra are employed to the initial guess spectra for the unfolding calculations.

(3) Results and discussion

The measurement data of helium-3 counters with polyethylene moderators, 2.6 cm and 8.6 cm in thickness, are shown in **Fig.3-37** while the closed main beam shutter is and moved to open up. when the main beam shutter is closed, the counting rates were the same as those of the background due to cosmic rays under closing the accelerator[3-43]. As shown in this figure, opening of the main beam shutter was accompanied with a rise in the counting rates, and there was sufficient difference between the background and the increased counting rates due to photoneutrons. The counting rates due to photoneutron are summarized in **Table 3-5**, including the backgrounds. The neutron spectra were unfolded with the SAND II code[3-44], shown in **Fig.3-38**. The effective doses evaluated using the conversion factor of the ICRP data[3-45] in the anterior-posterior geometry were summarized in **Table 3-6**, including the calculated data and the reference data[3-17] based on the dose equivalent of ICRP21[3-46]. The spectra and effective doses were measured with the maximum aperture size of 277 μ radian x 277 μ radian so that the total dose of photoneutrons due to total gas bremsstrahlung was 1.4 times that of measured data. (See Table 4-3 in chapter 4. The

ratio of the intensity of gas bremsstrahlung within the aperture size of 277 μ radian x 277 μ radian to the total is 1:1.4.). The reference data were calculated by using the figurative data[3-17] and the calculated photoneutron yields of targets with considering the gas bremsstrahlung power.

As indicated in **Table 3-6**, the measurement data agree with the calculated data within 22 %, except for the data of the lead target at position No.2. The data of the lead target at position No.2 is about 70 % higher than that of the measurement. The reasons for the differences should be due to the assumption of isotropic emission and cylindrical volume sources because of the anisotropic emission in higher energy neutrons and strong depth dependence of the emission distribution within the target. In comparisons with the reference data, the data agree with the measured data within a factor of 2. The main reason for the differences is without considering the scattered neutrons in reference data, even if there were different doses. Because it is clarified that the differences are less than 10 %[3-43] between the dose equivalent based on the ICRP21[3-46], ambient dose equivalent based on the ICRP51[3-47], and effective dose based on the ICRP74[3-45] range from thermal to several MeV neutron energies. As shown in **Fig.3-38**, there are many scattered neutrons outside the hutch that contribute to the dose estimations.

The APS data[3-15] are 3.7 rem/h for gas bremsstrahlung of 1 W at 80 cm distance from the lead thick target, 3.0 rem/h for the thick target of copper so that the neutron doses are 2.4 x 10^{-2} Sv/h/W at 1 m distance for lead target and 1.9 x 10^{-2} Sv/h/W for the copper target. In the present data, the effective dose rates of photoneutrons are 4.3 x 10^{-2} Sv/h/W at 1 m distance for the lead target, and 1.9 x 10^{-2} Sv/h/W for the copper target. However, the neutron yield of the copper target in this study is about 0.6 times that of the thick target so that the APS data are about 0.6 times that of our data for both targets.

Table 3-5 Counting rate of helium-3 counters with polyethylene moderators due to the interaction of gas bremsstrahlung of stored current of 1 mA and residual gas pressure of 10^{-8} Pa on a normal straight section with lead and copper targets at the positions No.1 and No.2 outside the shield hutch.

Target	Counter	Position No.1 (cps/mA/10^{-8}Pa)	Position No.2 (cps/mA/10^{-8}Pa)
Pb	Bare	$0.0024_2 \pm 3.0_3 \times 10^{-5}$	$0.0017_9 \pm 7.0_4 \times 10^{-5}$
	Poly.(2.6cm)	$0.0073_8 \pm 1.1_6 \times 10^{-4}$	$0.0043_5 \pm 7.0_9 \times 10^{-5}$
	Poly.(4.6cm)	$0.0086_3 \pm 1.2_1 \times 10^{-4}$	$0.0048_4 \pm 1.0_1 \times 10^{-4}$
	Poly.(8.6cm)	$0.0049_8 \pm 5.0_1 \times 10^{-5}$	$0.0025_3 \pm 7.8_0 \times 10^{-5}$
	Poly.(20cm)	-	$0.00015_7 \pm 1.4_8 \times 10^{-5}$
Cu	Bare	$0.00086_0 \pm 5.5_6 \times 10^{-5}$	$0.0012_6 \pm 5.2_3 \times 10^{-5}$
	Poly.(2.6cm)	$0.0036_0 \pm 5.3_8 \times 10^{-5}$	$0.0033_2 \pm 7.2_5 \times 10^{-5}$
	Poly.(4.6cm)	$0.0039_8 \pm 7.5_9 \times 10^{-5}$	$0.0037_9 \pm 7.5_6 \times 10^{-5}$
	Poly.(8.6cm)	$0.0022_8 \pm 5.8_0 \times 10^{-5}$	$0.0021_0 \pm 6.0_1 \times 10^{-5}$
	Poly.(20cm)	-	$0.00015_2 \pm 1.4_9 \times 10^{-5}$
MBS Closed		(cps)	(cps)
(B.G.)	Bare	$0.24_9 \pm 6.2_4 \times 10^{-3}$	$0.29_3 \pm 1.0_2 \times 10^{-2}$
	Poly.(2.6cm)	$0.52_4 \pm 1.2_7 \times 10^{-2}$	$0.51_2 \pm 1.2_6 \times 10^{-2}$
	Poly.(4.6cm)	$0.55_4 \pm 1.3_0 \times 10^{-2}$	$0.56_7 \pm 1.3_1 \times 10^{-2}$
	Poly.(8.6cm)	$0.30_3 \pm 1.0_3 \times 10^{-2}$	$0.33_5 \pm 1.0_7 \times 10^{-2}$
	Poly.(20cm)	-	$0.072_5 \pm 4.2_6 \times 10^{-3}$

Table 3-6 Measurement results and calculated results of leakage photoneutron dose due to the interaction of the gas bremsstrahlung with a lead and copper target. The reference data were also indicated.

Target (position No.)	Measurements (pSv/h/mA/10^{-8}Pa)	Calculation (pSv/h/mA/10^{-8}Pa)	Reference (pSv/h/mA/10^{-8}Pa)
Pb (1)	$67._9$ $(95._1)^{(*)}$	$110^{(\dagger)}$	$63^{(\ddagger)}$
Pb (2)	$33._1$ $(46._3)^{(*)}$	$79._2{}^{(\dagger)}$	$60^{(\ddagger)}$
Cu (1)	$30._0$ $(42._0)^{(*)}$	$32._8{}^{(\dagger)}$	$21^{(\ddagger)}$
Cu (2)	$28._6$ $(40._0)^{(*)}$	$32._3{}^{(\dagger)}$	$20^{(\ddagger)}$

(*) The measurements were performed with an aperture size of 277 μ radian x 277 μ radian so that the photoneutron dose and intensity of gas bremsstrahlung must be multiplied by 1.4 to compare the reference data, and the parenthetic data are 1.4 times of measured data.

(†) The data were obtained with photoneutron production calculation and transport calculation with isotropic emission assumption.

(‡) The doses are calculated with considering the distances and the relative neutron production yields.

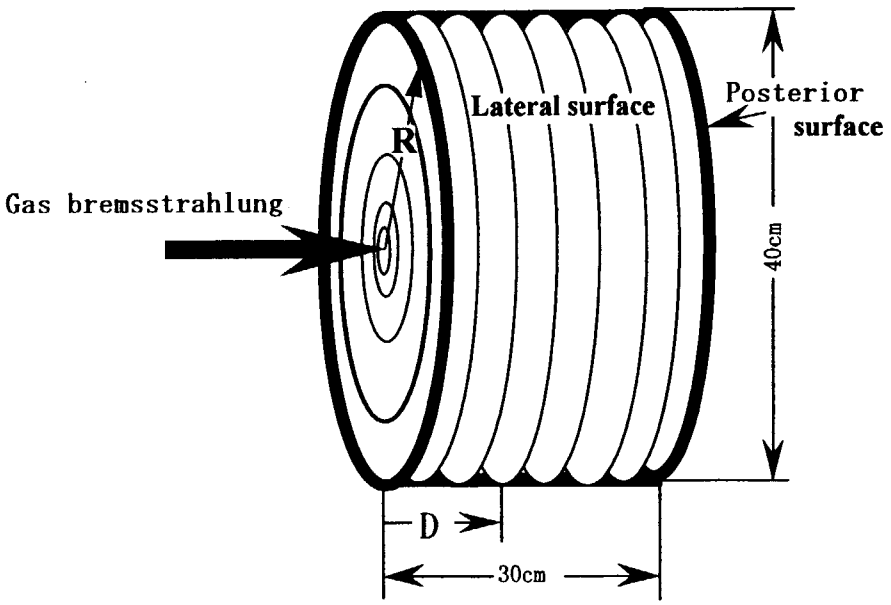

Fig.3-24 Calculational configuration of a photon stop. The photon stop made of lead was divided into several sectors with a radius, R and the depth from the surface, D.

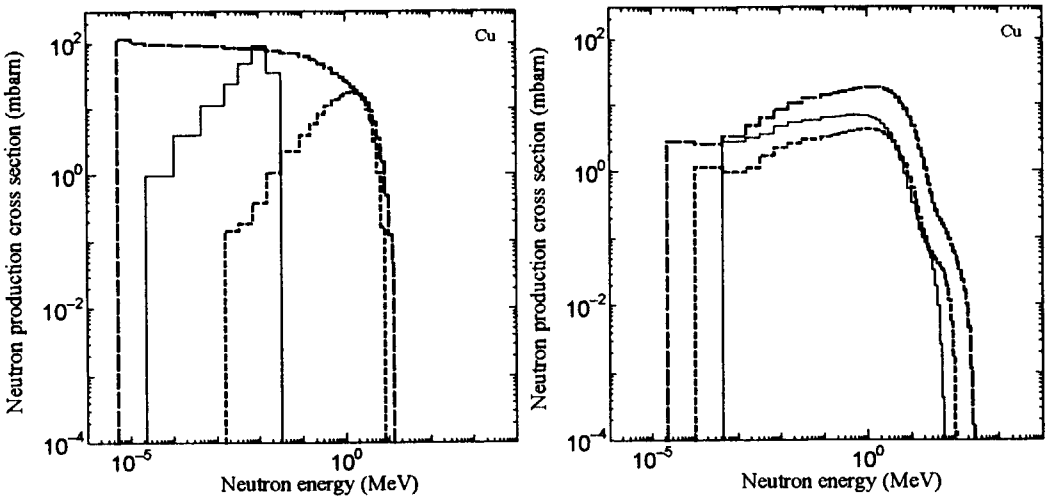

Fig.3-25 Photoneutron production cross section due to the photo-nuclear reaction with natural copper, Cu(γ , xn). The solid line, dot line, and dashed line in the figure on the left indicate the production cross section due to the incident γ energies of 8.0, 18.0, and 22.5 MeV, respectively. In the figure on the right hand side, the incident γ energies of 65.0, 120.0, and 300.0 MeV are also indicated.

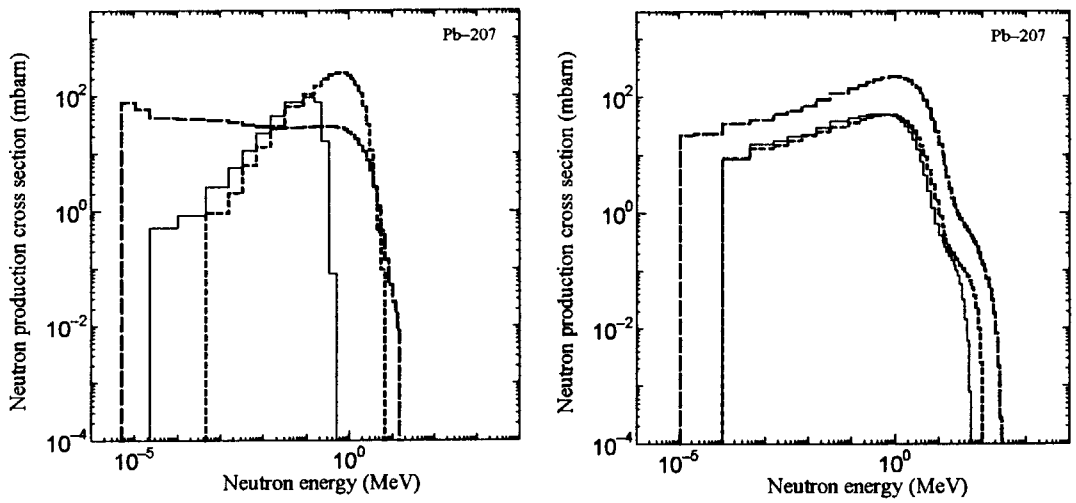

Fig.3-26 Photoneutron production cross section due to the photo-nuclear reaction with lead-207, ^{207}Pb(γ , xn). The solid line, dot line, and dashed line in the left side figure indicate the production cross section due to the incident γ energies of 7.5, 14.0, and 22.5 MeV, respectively. In the figure of right hand side the incident γ energies of 65.0, 120.0, and 300.0 MeV are also indicated.

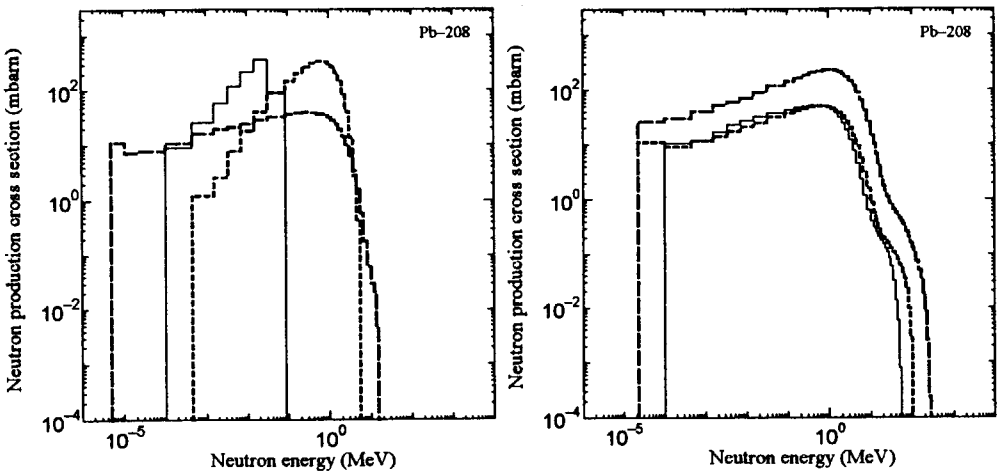

Fig.3-27 Photoneutron production cross section due to the photo-nuclear reaction with lead-208, $^{208}Pb(\gamma, xn)$. The solid line, dot line, and dashed line in the left side figure indicate the production cross section due to the incident γ energies of 7.5, 14.0, and 22.5 MeV, respectively. In the figure of right hand side the incident γ energies of 65.0, 120.0, and 300.0 MeV are also indicated.

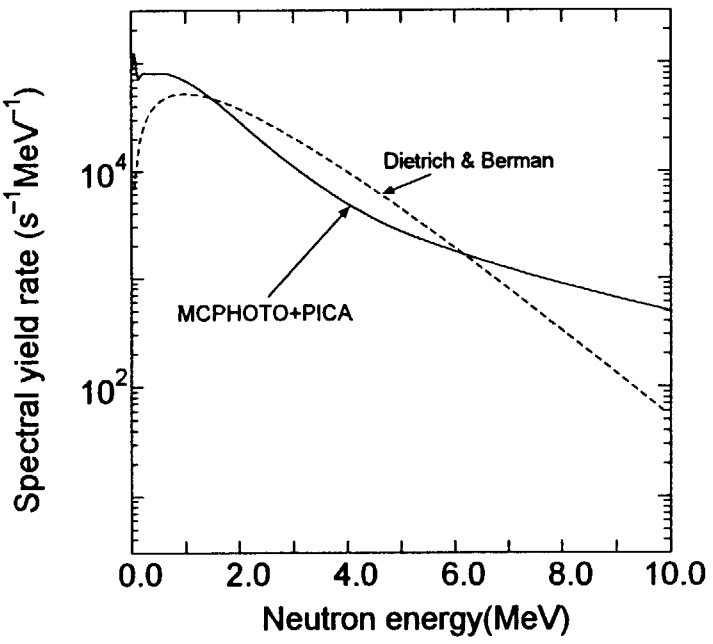

Fig.3-28 Calculated photo-neutron spectral yield rate within the lead photon stop by using track-length distribution multiplied by the Lorenzian fitted neutron production cross section of Dietrich and Berman and photo-neutron production cross section generated with MCPHOTO and PICA for the conditions of a normal straight section 19m in length and 100mA stored current.

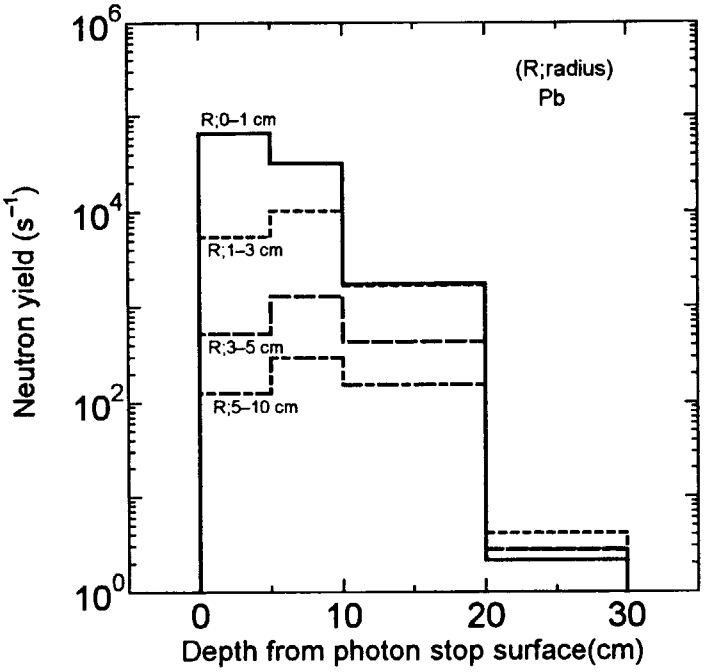

Fig.3-29 Neutron yield rate from different sections within the lead photon stop generated by the gas bremsstrahlung for the conditions of a normal straight section of 19m in length and 100mA stored current. R is the radial length of the photon stop.

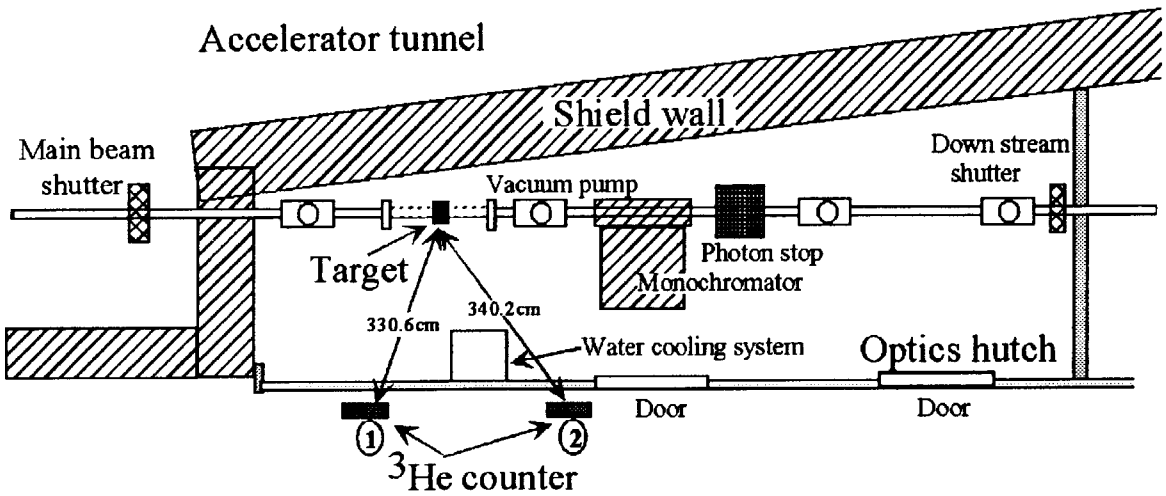

Fig. 3-30 Illustration of experimental setup for photoneutron measurement in a SPring-8 insertion device beamline. The helium-3 counters with polyethylene moderator were set up at the positions 1 and 2, outside the optics hutch. The distances from the target to the counters are 330.6 and 340.2 cm for counter No.1 and counter No.2, respectively.

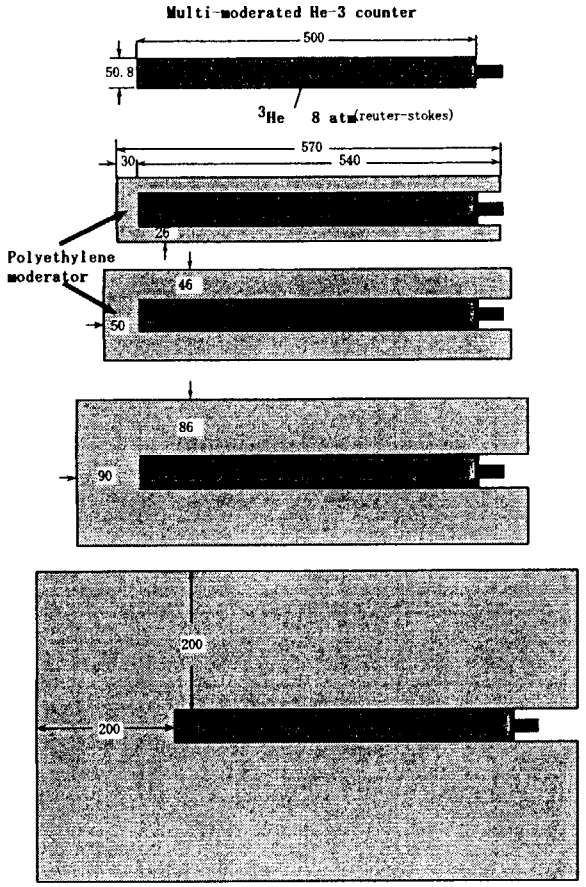

Fig.3-31 Cut away view of the high sensitive Bonner type helium-3 counter with polyethylene moderators.

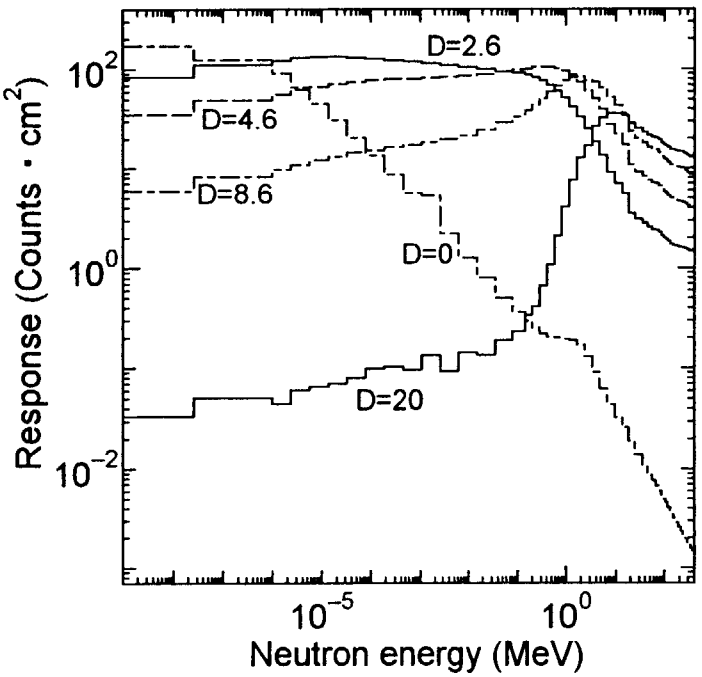

Fig.3-32 Response functions for high sensitive Bonner type helium-3 counters with polyethylene moderators. D indicates the thickness of the moderator in cm.

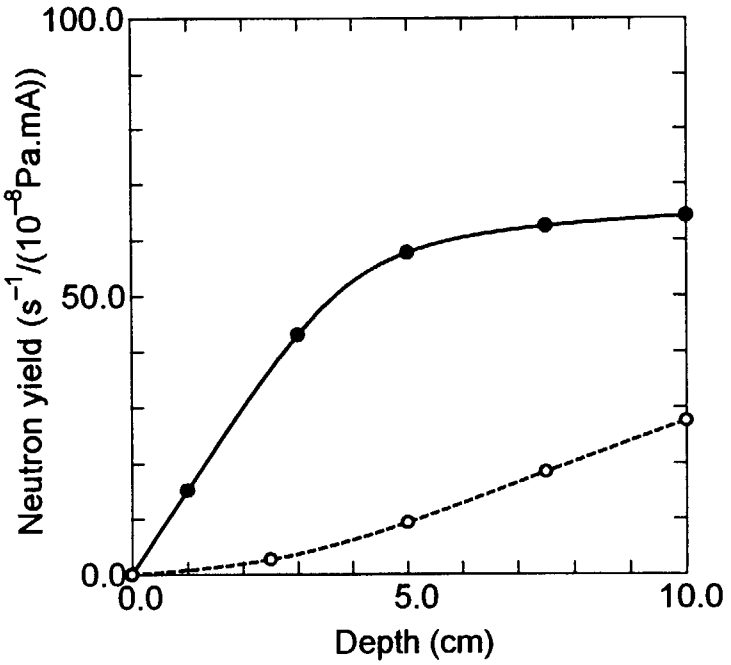

Fig.3-33 Cumulative photoneutron yield within thick targets due to gas bremsstrahlung produced by the interaction of 8 GeV stored electrons with residual gas molecules in a 16.54 m straight section. Full circle and solid line indicates the cumulative photoneutron yield within a lead target, open circle and dot line indicates the yields within a copper target.

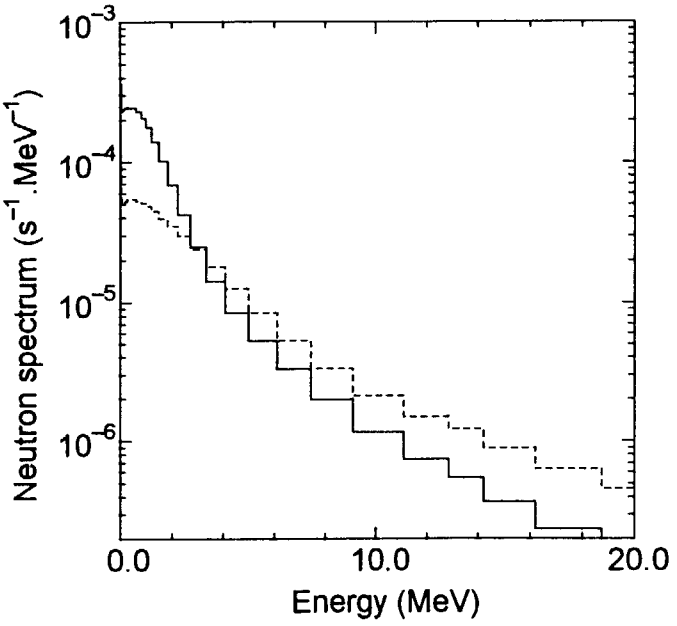

Fig.3-34 Photoneutron spectrum produced by the interaction of the gas bremsstrahlung and thick targets due to gas bremsstrahlung on the normal straight section at a stored current of 1 mA and vacuum pressure of 10 nPa. Solid line indicates the photoneutron spectrum produced by a lead target and dashed line indicates for a copper target.

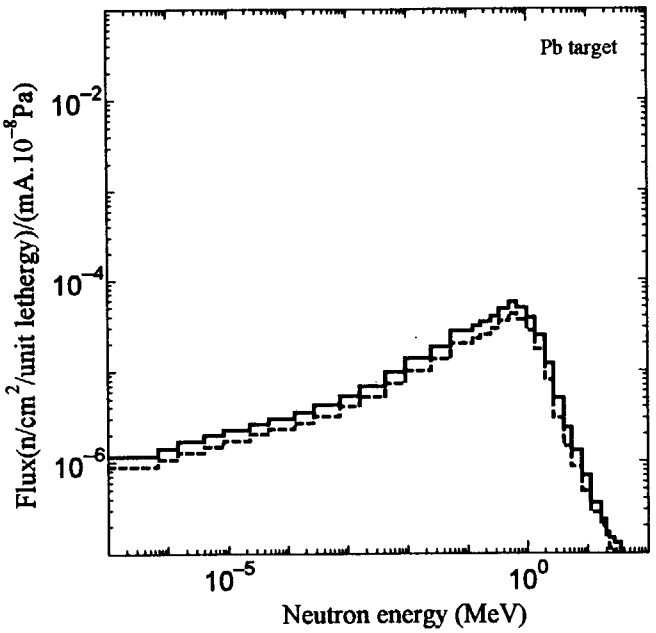

Fig.3-35 Calculated photoneutron spectra due to the interaction of a lead target with the gas bremsstrahlung. Solid line indicates the spectrum at position No.1 outside the beamline hutch, and dashed line is for the spectrum at position No.2.

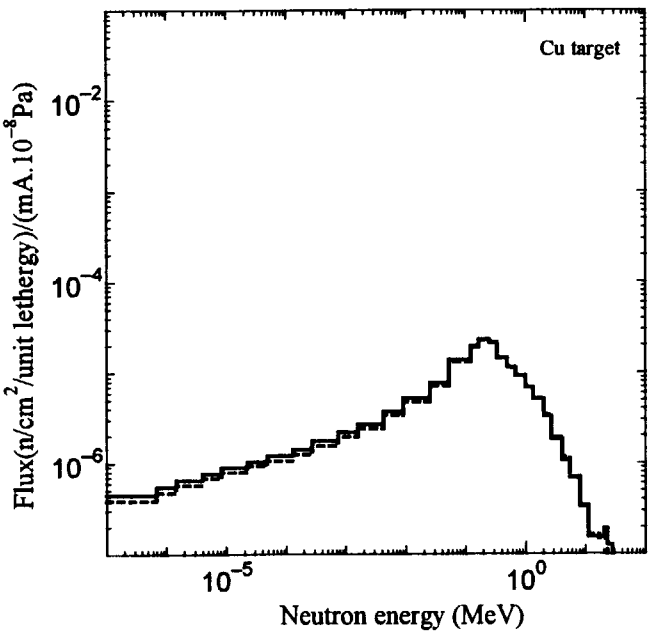

Fig.3-36 Calculated photoneutron spectra due to the interaction of a copper target with the gas bremsstrahlung. Solid line indicates the spectrum at position No.1 outside the beamline hutch, and dashed line is for the spectrum at position No.2.

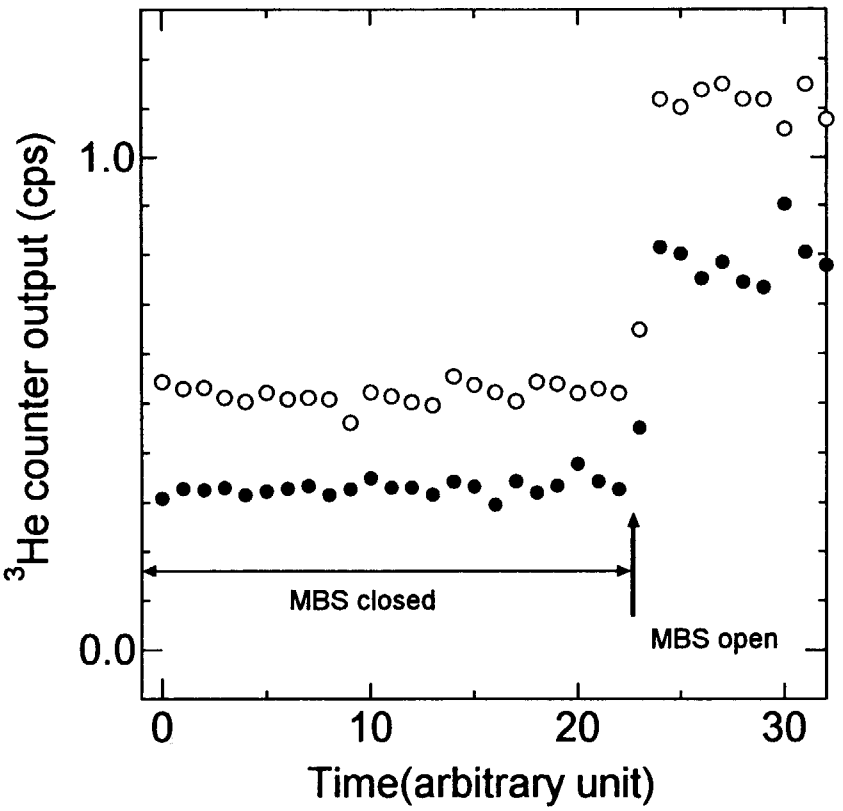

Fig.3-37 The counting rates of helium-3 counters with polyethylene moderators which change every 1000 seconds. The main beam shutter was opened during the measurements. Open circles indicate the output of helium-3 counter with the moderator of 2.6 cm in thickness and full circles are for 8.6 cm in thickness.

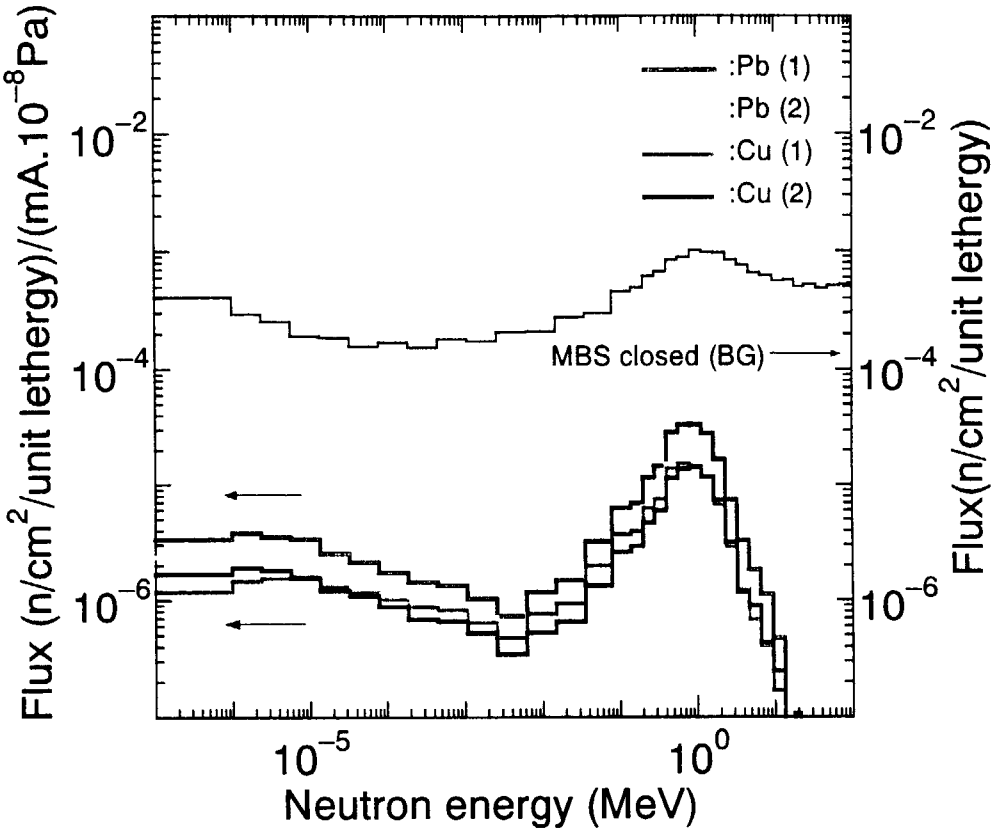

Fig.3-38 Leakage photoneutron spectra at the position No.1 and No2 due to gas bremsstrahlung produced by the interaction of a 8 GeV stored electrons of 1 mA current with the residual gas molecules of 10 nPa vacuum pressure within the normal straight section of 16.54 m. The power of the gas bremsstrahlung is 25.8 nW/mA/10^{-8} Pa. The solid line indicates the background neutron spectrum due to cosmic rays with right absissa. The red and yellow lines indicate the spectra at position No.1 and No.2 due to the interaction of gas bremsstrahlung with a lead target, respectively. The green and blue lines indicate the spectra at position No1 and No2 with a copper target, respectively.

This is a blank page.

3.4 Laser electron photon beamline

. Using ultra-violet laser with a wavelength of 200nm, a laser electron photon beam will be produced by Compton back scattering with a maximum energy of 3.5 GeV. The laser light is reflected by a mirror, and then injected into the interaction region from 36 m down stream of the center of the interaction region, 7.8 m long, as illustrated in **Fig.3-39**. These photons, ranging from 1.5 GeV to 3.5 GeV, are emitted within 0.1 mradian. The intensity of photons will be up to 10^7 s^{-1} using an ultra-violet laser with the power of 5 W and the intensity is about three orders higher in magnitude than that of gas bremsstrahlung. The laser electron photon beam of SPring-8 is incommensurably high intensity with extremely high energy and directivity. In the first stage, an Argon laser of 5 watts at a 351nm wavelength has been installed. The corresponding laser electron photon beam has a maximum energy of 2.4 GeV and intensity of 1.0×10^7 s^{-1} when the stored electron beam current is 100 mA. The calculated results of the energy spectra of the laser electron photon beam and measurement results using PWO are shown in **Fig.3-40**, together with gas bremsstrahlung generated in the interaction region.

Because of extremely intense photons with high energy and narrow space, the beamline must be designed under severe conditions. The analysis methods, which were developed during the measurements of gas bremsstrahlung and associated photoneutrons can be utilized with sufficient accuracy.

Two separate hutches were designed for the laser electron photon beamline; one is a laser hutch to enclose the laser and optical elements, and the other is an experimental hutch to enclose the experimental instruments. These are connected by a beam transport pipe with a diameter of 150 mm. The beam transport pipe is covered with lead, 2 mm thick. The sweep magnet with lead collimator and lead shield of electron-positron are installed along the axis of the beam transport line upstream of the beam dump of the laser hutch. The sweep magnet designed to prevent converted electrons and positrons in the photon beamline from hitting the beam transport pipe directly. The beam dumps are installed in both hutches to perform the

experiments mutually. The target is set in front of the beam dump of the laser hutch or analyzer magnet of experimental hutch. Big counters such as a drift chamber or a 2π gamma counter are installed in the experimental hutch.

(1) Dose outside the beam transport pipe

A sweep magnet with collimator and electron-positron shield is illustrated in **Fig.3-41**, and installed in the laser hutch as shown in **Fig.3-39**. The laser electron photon beam including the gas bremsstrahlung is to be transmitted into the beam dump of the laser hutch or experimental hutch after passing through the collimator and electron-positron shield. Electrons and positrons, which are generated by interaction in the mirror or thin plate of a blank flange with high energy photons, are swept by a 5 kGass sweep magnet. The electrons and positrons refracted from the beam axis are stopped by the lead shield. The displacement of the electrons or positrons with 3.5 GeV energy in a 1m path of the sweep magnet is about 23mm. Therefore, the high energy electrons or positrons, which are generated upstream of the sweep magnet, do not hit the beam transport pipe.

The leakage dose distribution outside the beam transport pipe is calculated by Monte Carlo code EGS4. In the calculation, the beam profile and angular divergence distribution of laser electron photons are assumed to be the same as the stored electron beam, and these are σ = 394 μm and σ = 17.6 μrad of Gaussian distributions in the horizontal axis and 27.1 μm and 2.56 μrad in the vertical axis. The materials of the interaction with high energy photons assume an inclined silicon crystal of 1 cm in thickness for the mirror and the aluminum, 0.05 cm in thickness, for the blank flange. These are set at 36 m and 39.5 m from the center of the interaction region.

The results of the calculations are shown in **Fig.3-42**, together with the leakage dose distributions with no sweeping effect. As shown in this figure, the effect of the sweep magnet is very clear and the leakage dose outside the beam transport pipe can be reduced successfully.

(2) Photoneutron dose outside the laser hutch

The leakage dose outside the hutch due to photoneutrons is estimated for two cases. One is the interaction of the laser electron photon beam and gas bremsstrahlung with a lead target that is 3 mm in thickness (about 0.5 radiation length), and the other is the interaction with the beam dump of lead in the laser hutch. The detailed structure of the beam dump is shown in **Fig. 3-43**. The beam dump consists of a lead cube, and its enclosures of polyethylene and heavy concrete for photo-neutron shield.

Neutron yields and spectra were calculated by multiplying the EGS4 calculated track-length distribution with photoneutron production cross-sections generated with MCPHOTO[3-34] and PICA[3-35]. The energy spectra of photoneutrons due to the interaction of the laser electron photon beams with the lead target are shown in **Fig.3-44**, together with the spectrum due to gas bremsstrahlung. Once the neutron energy spectrum is determined, the maximum dose equivalent and ambient dose equivalent are calculated using the conversion coefficients[3-36].

Table 3-7 summarizes the neutron dose rate at 1 m distance without shielding and neutron emission rate for the lead target and the beam dump of lead. In the case of a lead target, the dose rate and neutron emission rate due to the laser electron photons with a maximum energy of 2.5 GeV are higher than that of 3.5 GeV, as shown in **Fig.3-44** and **Table 3-7**. The dose due to gas bremsstrahlung is negligible in comparison with that of laser electron photons. On the other hand, the dose rate and neutron emission rate due to the laser electron photons with a maximum energy of 3.5 GeV are higher than that of 2.5 GeV, in the case of a beam dump. Both the doses are so high that the neutron shielding of the beam dump must be considered at the restricted narrow space. The doses due to the laser electron photons reach about 30 times that of gas bremsstrahlung in the case of a lead target, and 150 times that in the case of a beam dump.

The neutron transport calculations were performed with MCNP4b[3-38] assuming an isotropic emission of the neutrons. **Figure 3-45** shows the leakage neutron dose

distributions due to the laser electron photons with a maximum energy of 3.5 GeV outside the hutch and on the roof. In this figure, all the points are expressed by using Cartesian coordinates where the origin is the point of the beam injection into the dump. The roof of the hutch is 1.9 m in height from the beam axis.

As shown in **Fig.3-45**, the leakage dose is seriously high in conditions when the beam dump is without shielding upstream and topside. It is clear that the leakage dose due to photoneutrons will be reduced successfully by using polyethylene shields. From the comparison of the neutron leakage dose due to the interaction of the lead target with that of the beam dump, it is identified that the neutrons from the beam dump are to be dominant even for the dump with a polyethylene shield.

Table 3-7 Dose rate at 1 m distance without shielding and neutron emission rate due to laser electron photons and gas bremsstrahlung. Two types of doses, (1) maximum dose equivalent along the principal diameter of the ICRU sphere and (2) ambient dose equivalent, are summarized. The intensities of the laser electron photons are normalized at 10^7 photon/s. The intensity of gas bremsstrahlung is normalized for the conditions of an air target of 7.8 m, residual gas pressure of 133nPa(10^{-9} Torr) and stored current of 100 mA.

			Laser electron photon		Gas bremsstrahlung
	Max. Energy		2.5 GeV	3.5 GeV	
Pb target (0.5 X_0)	(1)	Dose rate at 1 m (μSv/h)	0.41	0.37	0.012
	(2)	Dose rate at 1 m (μSv/h)	0.38	0.35	0.011
		Neutron emission rate(s^{-1})	3.0×10^4	2.7×10^4	9.6×10^2
Beam dump	(1)	Dose rate at 1 m (μSv/h)	80.	110.	0.74
	(2)	Dose rate at 1 m (μSv/h)	92.	120.	0.82
		Neutron emission rate(s^{-1})	7.6×10^6	9.6×10^6	6.8×10^4

X_0 is Radiation length

This is a blank page.

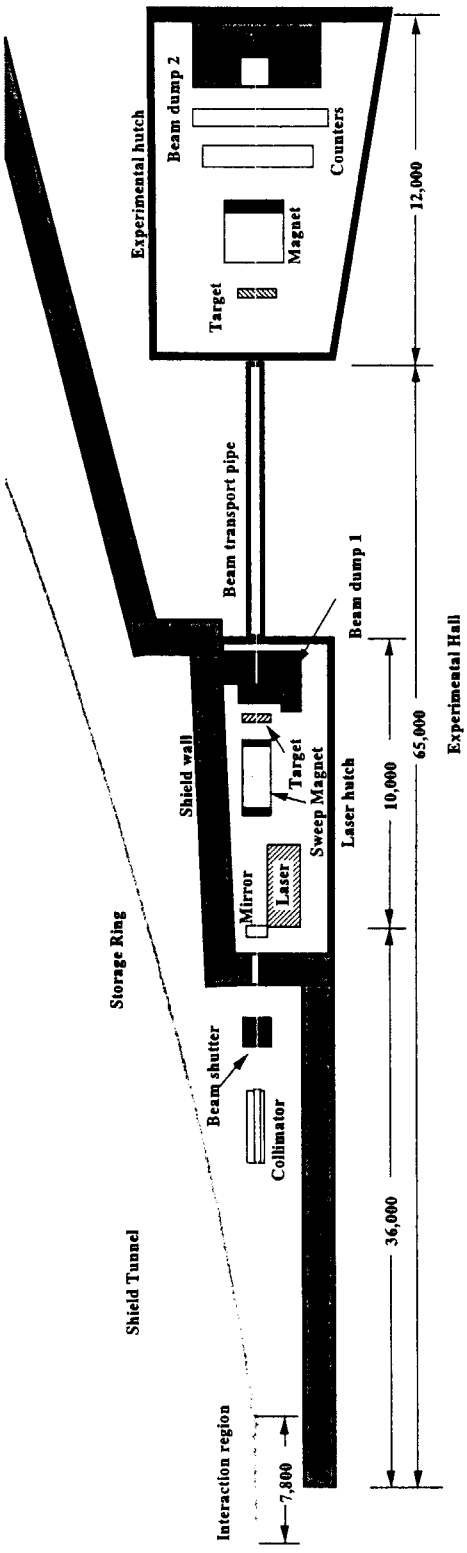

Fig. 3-39 Illustration of the laser electron photon beamline of SPring-8. The beamline has two hutches, one is the laser hutch and the other is an experimental hutch. Experiments will be mutually performed in a laser hutch and experimental hutch by removing the beam dump of the laser hutch.

This is a blank page.

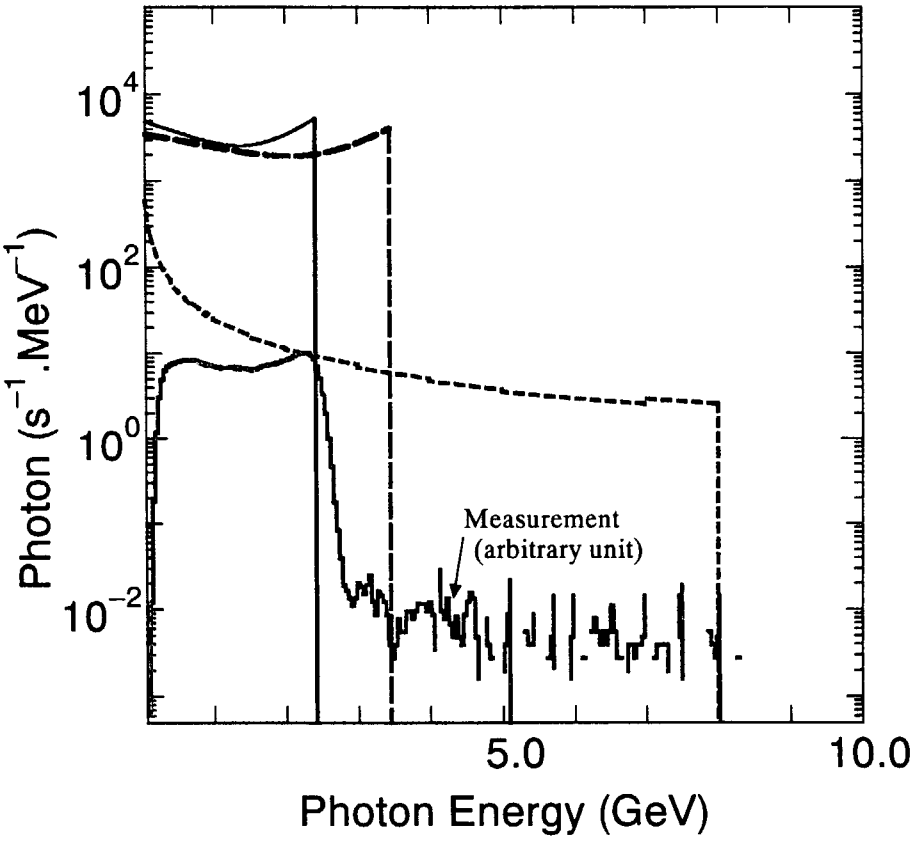

Fig.3-40 Energy spectra of laser electron photons. Solid line shows the laser electron photon spectrum using an Argon laser (wave length, 350 nm); dashed line is the laser electron photon spectrum using an ultra-violet laser system (wave length, 200nm); dot line is the gas bremsstrahlung spectrum generated by the interaction between stored electrons and residual gas molecules, of which the pressure is assumed to be 133nPa and stored current is 100mA. The red line indicates the measurement data of laser electron photons including gas bremsstrahlung in an arbitrary unit using a PWO detector and Argon laser without focusing.

This is a blank page.

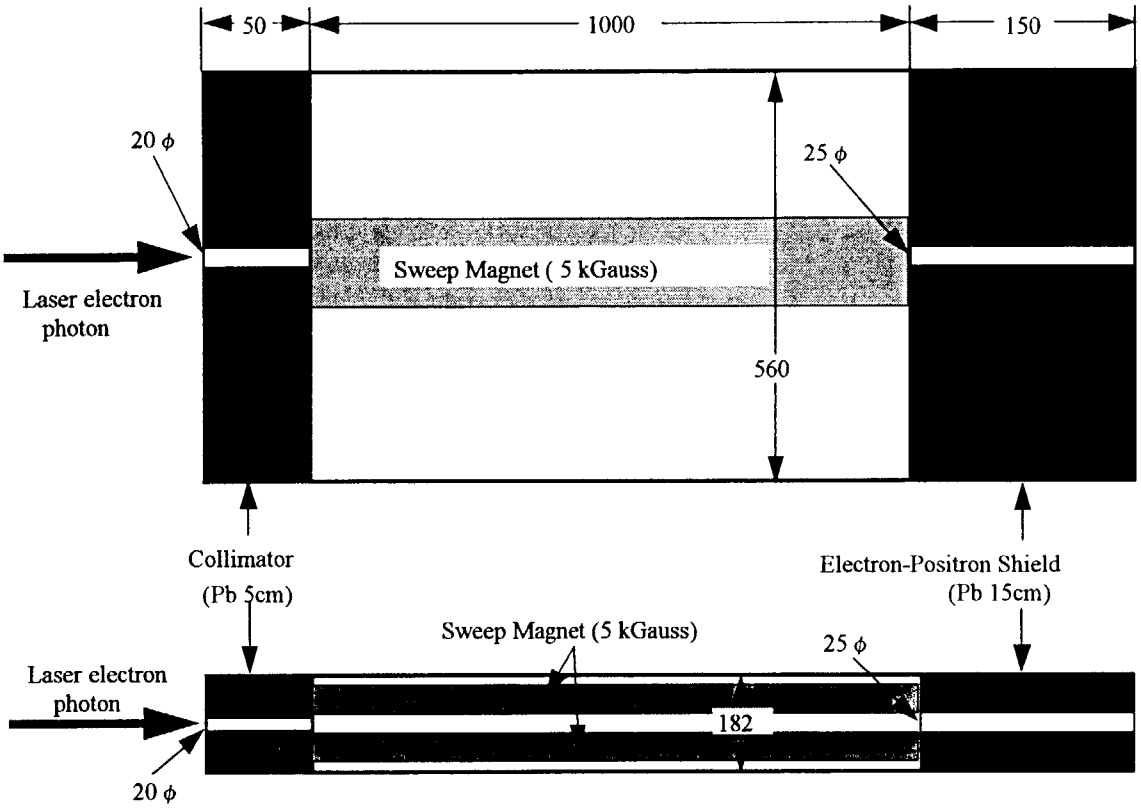

Fig.3-41 Illustration of the sweep magnet with the collimator and electron-positron shield. The magnetic field strength of the sweep magnet on the beam axis is 5 kGauss. A collimator that is 5 cm thick and made of lead has an aperture of 20 mm in diameter. The electron-positron shield that is 15 cm thick and made of lead has an aperture of 25 mm in diameter.

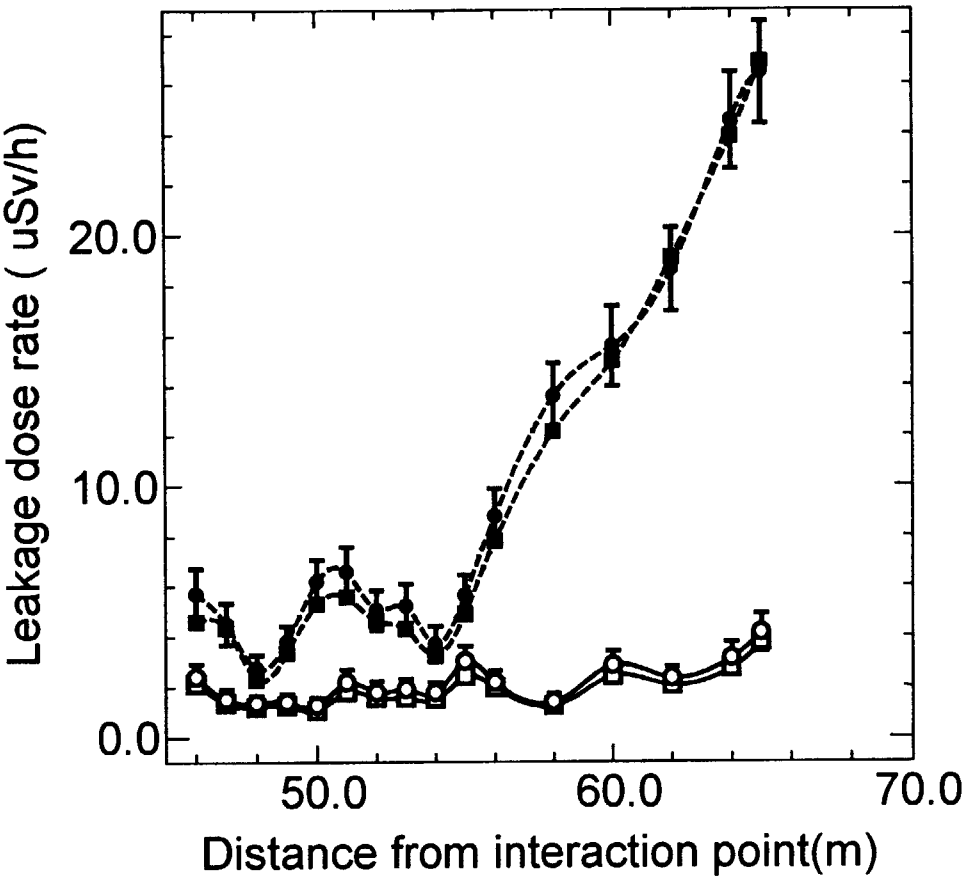

Fig.3-42 Leakage dose rate distribution outside the beam transport pipe. Open circles with solid line indicate the dose rate due to laser electron photons with a maximum energy of 2.5 GeV; open squares with solid line are the sample with maximum energy of 3.5 GeV. Full circles with dot line show the leakage dose due to the laser electron photons with a maximum energy of 2.5 GeV and without the effect of the sweep magnet; full squares with dot line are with the maximum energy of 3.5 GeV and without the effect of the sweep magnet.

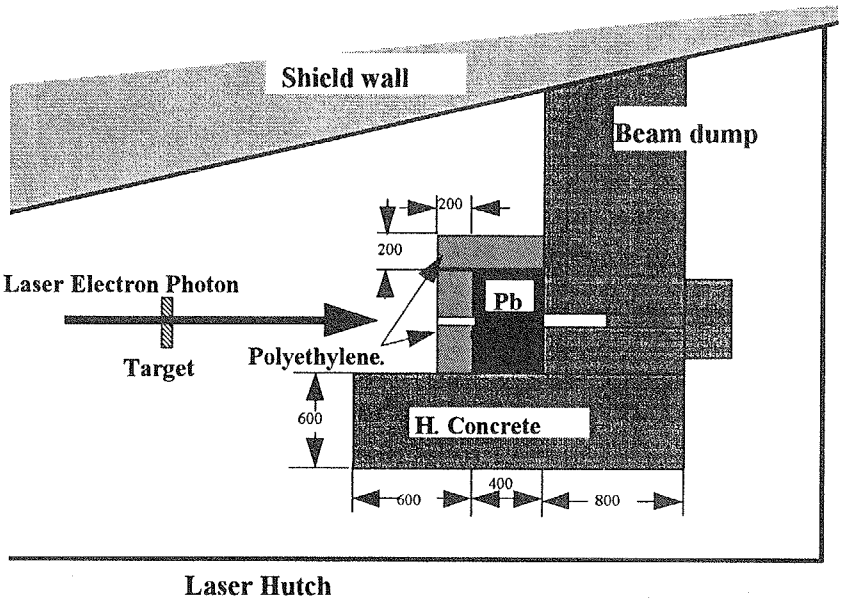

Fig. 3-43 Cross-sectional view and dimensions of the beam dump of the laser hutch. The top of the lead cube is also covered by polyethylene, 20 cm thick.

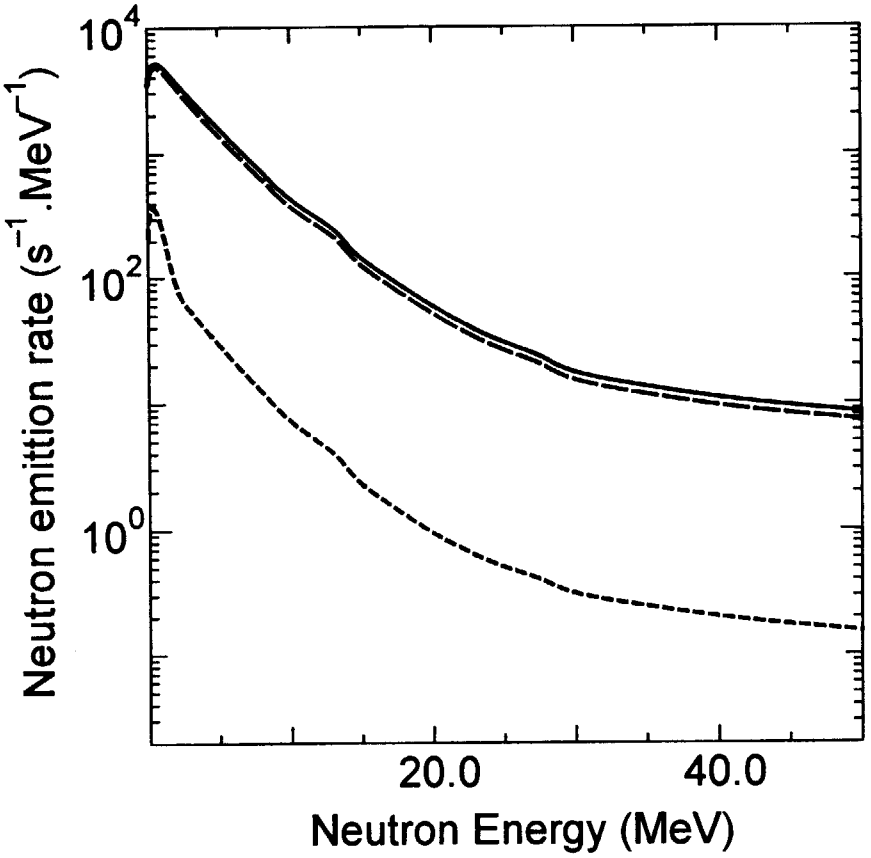

Fig. 3-44 Calculated photo-neutron spectral emission rate within the lead target of 3 mm thick using track-length distribution multiplied by a photoneutron production cross section generated with MCPHOTO and PICA. The solid line indicates the spectrum due to laser electron photons with a maximum energy of 2.5 GeV ; the dashed line is that with a maximum energy of 3.5 GeV and the dotted line is that due to gas bremsstrahlung.

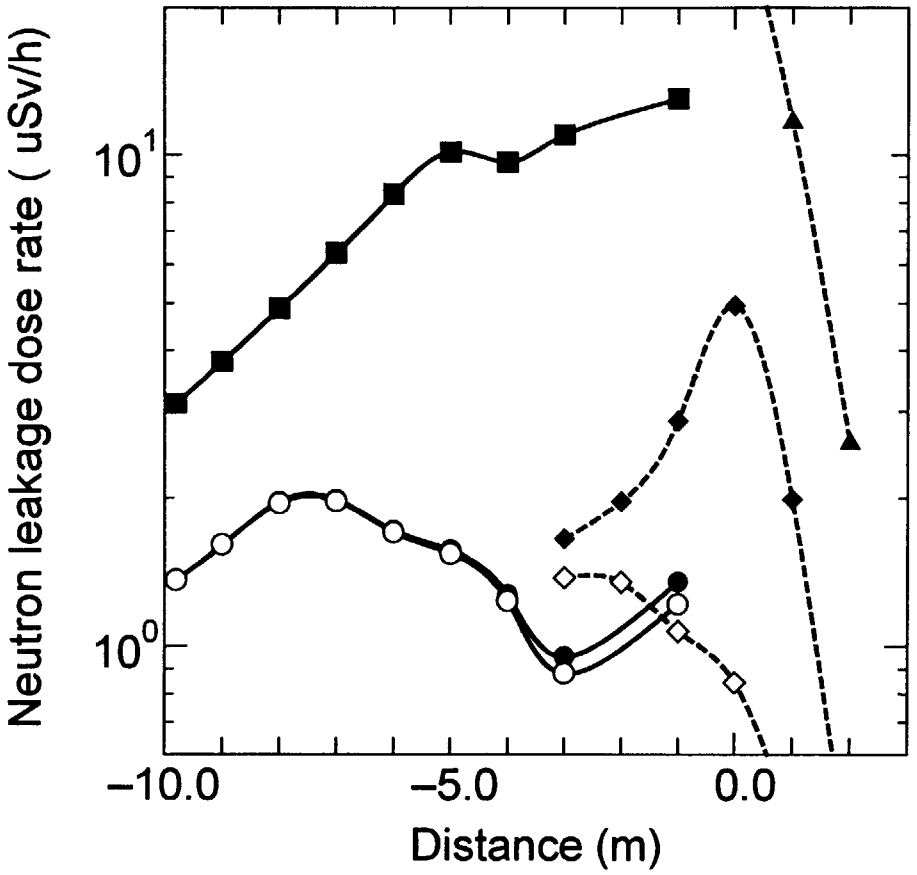

Fig. 3-45 Neutron leakage dose distributions due to the laser electron photons with maximum energy of 3.5 GeV. The horizontal axis indicates the distance from the vertical plane at the origin. The solid line with full squares indicates the dose rate outside the hutch without the polyethylene shield upstream of and the top of the beam dump; the solid line with open circles is the dose outside the hutch with a polyethylene shield that is 20 cm thick; the solid line with full circles is the dose outside the hutch with ordinary concrete instead of the upstream polyethylene. The dotted line with full triangles indicates the dose on the roof of the hutch without the shield upstream and on the top; the dotted line with open diamonds is the dose on the roof with polyethylene shields; the dotted line with full diamonds is the dose on the roof with ordinary concrete instead of the upstream polyethylene.

3.5 Conclusions

The simulations of gas bremsstrahlung production were performed as functions of the residual gas pressure, the number of the stored electron interaction with residual gas molecules, and lower cut off energy for electron transport, AE, to get sufficient accuracy of photon intensity and angular distribution. As the results, the path length of stored electrons is required to be less than 10^{-2} g/cm^2 for the simulation of gas bremsstrahlung production in the SPring-8 straight section instead of the recommendation of Ferrari et al. to set a pressure of 10.13 kPa(0.1 atm) and AE of 10 MeV. Moreover, it is not required to consider the restriction of the single interaction of stored electrons with residual gas molecules.

Gas bremsstrahlung was measured in the typical insertion device beamlines of SPring-8 with different stored electron beam sizes and divergences (high and low betatron function beamlines) using the PWO ($PbWO_4$) scintillation array detector and the measurements were compared with the Monte Carlo simulations. Because of its distinguishing features such as fast response and good energy resolution, the PWO detector, is found to be an excellent detector for the accurate measurement of gas bremsstrahlung. The detector size can be reduced to one third by using PWO detector instead of lead glass, and the energy resolution, $(3.0\pm0.3)\%/\sqrt{E}$, is found to be three times as good as that of lead glass. The gas bremsstrahlung power from a straight section 16.54 m in length for the standard in-vacuum type undulator beamline at SPring-8 was estimated to be 25.8±0.8 nW/10^{-8}Pa/mA (161 ± 5 GeV/s/10^{-8}Pa/mA). The effective atomic number was also estimated to be 8.1 ± 0.3 on the assumption of monatomic molecules. The beam profile of gas bremsstrahlung was measured using the X-Y slit, showing strong dependence on stored electron beam divergence. The Monte Carlo calculations using EGS4 were performed considering beam size and divergence, and reproduced measurements with good agreement. The average horizontal beam divergence was measured to be 46.5 μradian and 95.9 μradian for the straight sections of the high and low betatron function beamlines, respectively, showing good agreement with the stored beam analysis. Based on the measurements, the effective doses due to gas bremsstrahlung were obtained in anterior-posterior irradiation geometry considering the beam size and divergence, and the scoring area dependence was also investigated. As a result, the effective dose with the

stored beam of high betatron function at a distance of 40 m from the center of the straight section was estimated to be 15.8 nSv/ s/10^{-8}Pa/mA for a scoring area with a radius of 0.023 cm, 9.22 nSv/ s/10^{-8}Pa/mA for the low betatron function, and 25.9 nSv/ s/10^{-8}Pa/mA neglecting the stored beam size and divergence. The effective doses in isotropic irradiation geometry are estimated to be about 1.8 times as high as that in anterior-posterior irradiation geometry. The maximum dose equivalents are obtained to be about 3.4 times as high as the equivalent doses in anterior-posterior irradiation geometry.

The photo-neutrons induced by gas bremsstrahlung were obtained using the two different photo-neutron production cross sections, the difference of which comes from whether or not neglecting the neutron production by photons above 40MeV. The difference of the cross sections results in a difference of about 17 % in neutron dose equivalent. The photoneutron spectra outside the hutch of the SPring-8 beamline due to the interactions of lead and copper targets with gas bremsstrahlung were measured using a highly sensitive helium-3 counter with polyethylene moderators, and the effective dose rates were obtained on the basis of the measured data. As the results, the calculations on the assumption of isotropic emissions could be compared with the measurement data, showing good agreement within 20 % error on the upstream side of the target. On the other hand, a difference of about 70 % is recognized on the downstream side of the lead target. In comparison with previous data, we obtained agreements within a factor of 2 for calculated data without considering the scattering neutrons, and within a factor of 1.7 for measurement data using an Anderson Brawn type REM meter.

The shielding design calculations were performed for the laser electron photon beamline of SPring-8 using the analysis methods of gas bremsstrahlung and associated photoneutrons. It was certified that the beam transport pipe could be installed between the laser hutch and experimental hutch using a sweep magnet with a lead collimator and a lead shield for the electron-positron pair creation. The effect of the sweep magnet was clarified to reduce substantially the leakage dose outside the beam transport pipe. The photoneutron production due to the interaction with a lead target of 0.5 radiation length and the beam dump of the laser hutch were calculated. The dose due to the laser electron photons was certified to be seriously high, which requires the beam dump

with polyethylene shield. It is clarified that most of the leakage neutron dose is attributed to interaction between the laser electron photons and the beam dump, even if the dump is shielded with polyethylene that is 20 cm in thickness.

4. Summary and conclusions

The main purposes of the present study have been (1) to establish a method of shielding design for the beamline of synchrotron radiation on and after third generation synchrotron radiation facilities including the development of shielding design code and the verification of its validity, (2) to apply this method to shielding calculation of 8 GeV class synchrotron radiation beamlines, and (3) to investigate the characteristics of the radiation fields around the beamlines of the third generation synchrotron radiation facility.

The main results presented in each Chapter can be summarized as follows.

Chapter 1 was devoted to a brief presentation of the history of synchrotron radiation facilities and the present status of this study, including the constitution and outline of this study.

In Chapter 2, the newly developed shielding design code for synchrotron radiation beamline, STAC8, was described in comparison with the PHOTON II code. The PHOTON II code was actually applied to the design calculation for the beamlines. However in some cases it seriously underestimated doses outside the shield wall of the hutches. The PHOTON II code has been validly created for calculations of attenuation by filters, the isotropic scattering process by the optical elements and the shielding with the walls of the hutches ignoring the build-up effect of the synchrotron radiation emitted from a wiggler and a bending magnet. The polarization effect is actually dominant in synchrotron radiation and the code does not simulate the scattering process. Furthermore, with considerably high energy X-rays as generated in the third generation synchrotron radiation facilities, the dose outside the shield wall strongly depends on the scattering angle. A new shielding design code STAC8 has been developed in order to fill up the deficiencies in the PHOTON II code and to be applicable to the consistent calculations of radiation emitted from insertion devices including undulators, the effect of linear polarization of photons on the scattering process, and the angular dependence of coherent and incoherent scattering. For dose estimation, the code can calculate each ambient dose equivalent, effective dose, and absorbed dose due to scattering photons considering build-up effect and slant length of the shield wall of the hutch. The doses by the scattered photons can be calculated with and without

introducing the self-shielding of the scatterer.

In the validity verification of the code, the STAC8 calculations were compared with EGS4 simulation, and the measurements of dose distributions inside the hutch of the insertion device beamline, showed fairly good agreement. Especially, the dose distributions strongly depend on the scattering angle and azimuthal angle, while PHOTON II does not.

To apply to practical beamlines, the dose distributions outside the hutch of the typical beamlines of SPring-8 were carried out considering the polarization and then compared with the measurement data of the bending magnet beamline. As the results, the calculated leakage dose distribution by using STAC8 is well coincident with those of the measurements, while the PHOTON II calculations were underestimated remarkably. This means that with STAC8 the shielding design calculations can be carried out easily and quickly with satisfactory accuracy.

In the applied usage of STAC8 for investigations of groundshine, it was found that the ground shine is a dominant source to determine the structure at the joint between the hutch wall and the concrete floor, and that adding lead plate shielding along the foot outside of the hutch wall is the most effective structure.

Chapter 3 was devoted to the behaviors of gas bremsstrahlung and associated photoneutron within the beamline of the third generation synchrotron radiation facility. In the gas bremsstrahlung estimations, we made it appear that the simulations based on the conditions of the previous recommendation bring inaccurate results for angular distributions of photon emission in the SPring-8 beamlines, and a new recommendation was proposed to set the electron path length in the straight section of storage ring to be less than 10^{-2} g/cm^2.

The measurement results of the gas bremsstrahlung at the SPring-8 insertion device beamlines with different beam sizes and divergences of stored electron were presented as a function of the aperture size of the photon beam by using a new type scintillation detector, PWO. In the measurements, it was found that the beam profile of the gas bremsstrahlung and its creeping into the beamline strongly depend on the stored beam divergence, and that the performance of the PWO is excellent in fast

response and good energy resolution for the accurate measurement. The energy resolution of PWO was found to be three times as good as that of lead glass by using the gas bremsstrahlung.

The Monte Carlo simulations of gas bremsstrahlung were performed with considering the beam size and divergence, and showed good agreement. As a result, the effective dose and absorbed dose depending on the stored beam divergence could be estimated precisely. Moreover the dependency of scoring area for the effective dose was also investigated.

The photoneutron production cross section data were improved, ranging from giant resonance to quasi-deuteron and pion production process, and the photoneutron yields and doses due to the interaction of the photon stop with gas bremsstrahlung were estimated by using the two different photoneutron production cross sections, one is the improved cross sections and the other is the Dietrich and Berman's data, ranging from the reaction thresholds to 40 MeV. The difference of the cross sections results in a difference of about 17 % in neutron dose equivalent. The measurement results of the photoneutron spectrum due to gas bremsstrahlung outside the hutch of the beamline of SPring-8 were presented. Using a highly sensitive helium-3 counter with polyethylene moderators, and lead and copper targets the measurements were performed, showing good agreement with the photoneutron production and transport calculations. Although the previous dose data is not considered to be the scattered neutrons, the present dose data agreed within a factor of 2.

For the practical exercises, the analytical methods of gas bremsstrahlung and associated photoneutrons were applied to the shielding design calculations of a laser electron photon beamline. The laser electron photon beamline provides such incommensurably high intensity with an extremely high energy beam that the shields must be in severe condition. Furthermore, the beamline was required to be shielded sufficiently at the restricted narrow space. Using the local shield that has special structure, that is a combination of a sweep magnet and collimators, we found the solution and presented the effect of the local shield to reduce the leakage dose successfully. In addition, with a good choice of shield materials, it was clarified that the photoneutrons produced by laser electron photons could be shielded effectively.

Throughout the present study, the method of shielding design for synchrotron radiation beamline was developed, and equipped us to estimate the leakage dose distribution easily and quickly with satisfactory accuracy. All the beamlines of SPring-8 including beamlines under design (38 beamlines until now) were analyzed and designed using this method and the effectiveness of this method was certified by safety check of radiation.

In addition, it was pointed out that the doses due to gas bremsstrahlung as well as the beam profile depend on the divergence of stored electron beam, and photoneutron spectra outside the hutch of a beamline due to gas bremsstrahlung of the third generation facility were clarified. Furthermore, for unique beamline such as the beamline of laser electron photons, the effective design of shielding was provided by using the analytical methods of gas bremsstrahlung and associated photoneutrons.

In the present study, some future problems are pointed out, one of which is to establish the conceptual framework of radiation protection for beam radiation. However doses due to direct gas bremsstrahlung depend strongly on the size of the scoring area, the investigations, which make the unified guideline of radiation protection to the beam irradiation are quite insufficient. Another problem is the lack of experimental data of photoneutron production cross sections in high energy regions. Benchmark experiments for photoneutron production including the angular distribution are strongly expected.

Acknowledgments

First and foremost, the author acknowledges his deep gratitude to Dr. Nobuo Sasamoto of Japan Atomic Energy Research Institute and Professor. Masaharu Nakazawa of the University of Tokyo for their helpful discussions and continuing encouragement. The author also wishes to express his deep obligation to Professor Yoshiyuki Amemiya, Professor Yoshiaki Oka and Associate Professor Hiroyuki Takahashi of the University of Tokyo, and Professor Hideo Hirayama of High Energy Accelerator Research Organization for their valuable suggestions and encouragement.

The author is grateful to the members of the beamline of the laser electron photon, Professor Hajime Shimizu of Osaka University and the staff of the laboratory for their valuable discussions. Gratitude is also expressed to Professor Kenichi Hasegawa of Hosei University and the members of the construction group of SPring-8 for useful suggestions and their help.

References

(1-1) T Sasaki , " Synchrotron radiation in Bioscience", Oxford Univ. Press (1994)

(1-2) K.Kora et al., "Application Technology of Synchrotron radiation", Science forum, Tokyo (1989) (in Japanese)

(1-3) H.Winick, "Synchrotron Radiation Sources –A primer", World Scientific MA USA ISBN 9810218567 (1994)

(1-4) T.Miyahara et al., "SOR-RING, an electron storage ring dedicated to spectroscopy", Particle Accelerators 7 (1976)

(1-5) J.A.Clarke and M.W.Poole," Upgrading the Daresbury SRS with additional insertion device and its implications for storage ring layout", European particle accelerator conf. Spain (1996)

(1-6) K.Kora and T.Matsushita,Photon Factory Activity Report 1982/83 KEK (1984)

(1-7) P.M.Stefan et al., "Small gap insertion device developmemt in the X13 straight of NSLS X-ray ring", Particle accelerator conf. 95 Dallas (1995)

(1-8) European Synchrotron Radiation Facility, " The red Book Draft B". Grenoble France (1987)

(1-9) Argonne National Lab. "7 GeV Advanced Photon Source Conceptual Design Report", ANL-87-15 Argonne USA (1987)

(1-10) JAERI-RIKEN SPring-8 Project Team "SPring-8 Project Part 1 Facility Design". 1991(Revised). Tokyo Japan (1991)

(1-11) A.Bienenstock et al., Review Sci. Instr. 60 (7) 1393-1398 (1989)

(1-12) W.Brefeld, SSRL Report 92/02 p115 (1992)

(1-13) N.Yagi et al., J. Synchrotron Radiation 3 305-312 (1996)

(1-14) A.Rindi," Gas bremsstrahlung from electron storage rings", Health Physics 42 (1982)

(1-15) S.Ban, H. Hirayama and S.Miura," Estimation of absorbed dose due to gas bremsstrahlung from electron storage rings", Health Physics 57 (1989)

(1-16) G.Tromba, and P.Rindi,"Gas bremsstrahlung from electron storage rings- a Monte Carlo evaluation and some useful formulae", Nucle.Instr. Methods A292 (1990)

(1-17) A.Ferrari, M.Pelliccioni and P.R.Sala," Estimation of fluence rate and absorbed dose rate due to gas bremsstrahlung from electron storage rings", Nucle. Instr. Methods B83 (1993)

(1-18) T.M.Jenkins," Neutron and photon measurements through concrete from a 15 GeV electron beam on a target.- Comparison with models and calculations", Nucle. Instr. Methods 159 (1979)

(1-19) H.Dinter and K.Tesch," Dose and shielding electron beam", Nucle. Instr. Methods 143 (1977)

(1-20) W.P.Swanson," Radiological safety aspects of the operation of electron linear accelerators", IAEA Technical Reports Series No.188 Vienna (1979)

(1-21) Y.Asano and N.Sasamoto "Radiation shielding and safety analysis for SPring-8", JAERI-Tech 98-009, (in Japanese) (1998)

(1-22) Y.Asano and N.Sasamoto," Benchmark experiment for radiation shielding around the beam dump of the SPring-8 injector", Japanese J. of Nucle. Science and Tech. Supple 1 (2000)

(1-23) N.Sasamoto and Y.Asano," Shielding design study for SPring-8", Proc. of the specialist's meeting on shielding aspects of accelerators target and irradiation facilities, OECD-NEA Arlinton (1994)

(1-24) D.Chapman, " PHOTON, A user's manual" BNL 40822 (1988)

(1-25) E.Braeuer and W.Thomlinson, " Experimental verification of the PHOTON-A program for use in X-ray shielding calculations", Nucle. Instr. Methods A266 (1988)

(1-26) P.Berkvens, ESRF annual reports 1993 Grenoble France (1994)

(1-27) P.K.Job,D.R. Haeffner and D.Shu, " Bremsstrahlung scattering calculations for the beam stops and collimators in the APS insertion device beamlines", ANL/APS/TB-20 (1994)

(1-28) N.E.Ipe and A.Fasso, "Gas bremsstrahlung considerations in the shielding design of the Advanced Photon Source synchrotron radiation", Nucle. Instr. Methods A351 (1994)

(1-29) W.R.Nelson, H.Hirayama and D.W.O Rogers, " The EGS4 code system" SLAC-265 (1985)

(1-30) A.Fasso et al., FLUKA 92", proc.of Workshop on Simulating Radiation Environments 11-15 Jan. 1993 Santa Fe New Mexico (1993)

(1-31) S.Ban, H.Hirayama, and S.Miura," Measurement of absorbed dose in water irradiated by 2.5 GeV bremsstrahlung", Health Physics 53 (1987)

(1-32) M.Pisharody, P.K.Job, S.Magill, J.Proudfoot, and R.Stanek, Nucl. Instr. Meth. A401 (1997) 442

(1-33) J.C.Liu, W.R.Nelson, and K.R.Kase;"Gas bremsstrahlung and associated photon-neutron shielding calculations for electron storage rings", Health Physics Vol.68 205-213 (1995)

(1-34) M.Pisharody, E.Semones, and P.K.Job, "Dose measurements of gas bremsstrahlung-produced neutrons from thick targets", Nucle. Instr. Methods A 430 542-558 (1999)

(1-35) J.M.J.Madey, J.Appl. Physics 42 (1971)

(1-36) T.Tomimasu," Synchrotron radiation techniques", Kogyo-chosakai, Tokyo
ISBN 476931085403055 (1990) (in Japanese)

(1-37) M.Fujiwara et al., *ACTA PHYSICA POLONICA B 29* (1998)

(1-38) H.Winick, "Synchrotron radiation sources-Preset capabilities and future directions" J. of Synchrotron Radiation 5 (1998)

(1-39) Y.Asano and N.Sasamoto, " Development of shielding design calculation for synchrotron radiation beamline", Radi. Physics and Chem. 44 No1/2 (1994)

(1-40) Y.Asano et al., "Radiation Exposure due to synchrotron radiation with linear polarization", PF Activity Report 93 Vol 11 KEK (1994)

(1-41) Y.Asano,"Estimation of synchrotron radiation dose outside the hutch of SPring-8 beamline", Proc. of 10th International Congress on Radiation Protection Association, Hiroshima Japan (2000)

(1-42) Y.Asano," Shielding design Calculation of SPring-8 beamline using STAC8", J. Synchrotron Radiation Vol.5 (1998)

(1-43) Y.Asano and N.Sasamoto," Characteristics of shielding design calculation for synchrotron radiation beamline of SPring-8", Radiation Protection Dosimetry Vol.82 (1999)

(1-44) Y.Asano et al., "Measurement of gas bremsstrahlung at the SPring-8 insertion device beamline using PWO scintillator", Nucle. Instr. Methods A451 No.3 (2000)

(1-45) Y.Asano," Simulation of angular distribution of gas bremsstrahlung depending on the residual gas pressures of a storage ring", submitted to The 2nd International Workshop on EGS, Tukuba KEK(2000)

(1-46) Y.Asano, T.Nakano,T.Hotta, and Y.Ohashi," Shielding design calculations for a laser electron

photon beamline of SPring-8", Japanese J. Nucle. Science and Technology Supple.1 (2000)

(1-47) J.H.Hubbell and I.Øverbo, "Relativistic atomic form factors and photon coherent scattering cross sections", J.Phy. & Chem. Ref.Data 8.1 (1979)

(1-48) Y.Harima et.al., "Validity of the geometric-progression formula in approximating gamma ray buildup factors", Nucle. Sci. & Eng. 94 (1986)

(1-49) Y.Yamakawa et al., "The Construction of the Superconducting Vertical Wiggler and its Operation in the Photon Factory", Nucle. Instrum. & Meth. A246 32-36 (1986)

(1-50) S.S.Dietrich,. and B.L.Berman,."Atlas of photoneutron cross sections obtained with monoenergetic photons", Atomic Data and Nuclear Data Tables **38** 199-338 (1988)

(1-51) N.Kishida, " Methods used in photonuclear data evaluation at JNDC". Int. Symposium on Nuclear Data Evaluation Methodology 12-16 Oct. BNL 598 (1992)

(1-52) T.A.Gabriel, M.P.Guthrie, and O.W.Hermann, "PICA, Monte Carlo Medium-Energy Photon-Induced Intranuclear Cascade Analysis Code System", ORNL CCC-160 (1972)

(1-53) S.Berg et al., AFWL-TR-67-41 CCC-112 (1969)

(2-1) European Synchrotron Radiation Facility, "The red Book Draft B", Grenoble France (1987)

(2-2) Argonne National Lab., "7 GeV Advanced Photon Source Conceptual Design Report", ANL-87-15 Argonne USA (1987)

(2-3) JAERI-RIKEN SPring-8 Project Team, "SPring-8 Project Part 1 Facility Design", 1991(Revised). Tokyo Japan (1991)

(2-4) D.Chapman, "PHOTON ;A user's manual", BNL 40822.(1988)

(2-5) E.Braeuer, Private Communication (1992)

(2-6) P.Berkvens, ESRF annual report 1993 (Grenoble) France (1994)

(2-7) Y.Asano and N. Sasamoto, "Development of shielding design code for synchrotron radiation beamlines", Radiat. Phys.Chem. Vol.44 (1994)

(2-8) W.R.Nelson, H.Hirayama and D.W.O Rogers, " The EGS4 code system", SLAC-265 (1985)

(2-9) Y.Asano et.al., "Radiation exposure due to synchrotron radiation with linear polaridzation", National Lab. for High Energy Physics Photon Factory Activity Report (1993)

(2-10) National Lab. for High Energy Physics, Photon Factory Activity Report #9 KEK 18 (1991)

(2-11) Y.Yamakawa et al., "The Construction of the Superconducting Vertical Wiggler and its Operation In the Photon Factory", Nucle. Instr. Methods. A246 32-36 (1986)

(2-12) Y.Asano," Shielding design Calculation of SPring-8 beamline using STAC8", J. Synchrotron Radiation Vol.5 (1998)

(2-13) Y.Asano, " Estimation of Synchrotron Radiation Dose Outside The Hutch of SPring-8 Beamline", Proc. of 10th International Con. of The Int. Radi. Pro. Association. Hiroshima (2000)

(2-14) Y.Asano and N.Sasamoto, "Characteristics of shielding design calculation for the SPring-8 synchrotron radiation beamlines", Radiat. Prot.Dosim. 82(3) 167-174 (1999)

(2-15) R.P.Walker and B.Diviacco, "URGENT-A computer progrum for calculation undulator radiation", Rev.Sci. Instrum. Vol .63 392 (1992).

(2-16) K.Kora et al., "Application Technology of Synchrotron Radiation", Science forum, Tokyo (1989)

(in Japanese)

(2-17) J.H.Hubbell et al.," Photon mass attenuation and energy absorption coefficients from 1keV to 20MeV", Int. J.Appl. Radiat. Isot. Vol 33 p1269 (1982)

(2-18) S.M.Seltzer," Calculation of photon mass energy transfer and mass energy absorption coefficients", Radition Research Vol. 136 p147 (1993)

(2-19) F.Biggs, and R.Lighthill, SC-RR 71 45073 (1971)

(2-20) F.Biggs, and R.Lighthill, SC-RR 72 0685 (1972)

(2-21) A.L.Hansen," The calculation of scattering cross sections for polarized X-rays", Nucle. Instr. Methods A243 583 (1986)

(2-22) J.H.Hubbell and I. Øverbo,"Relativistic atomic form factors and photon coherent scattering cross sections", J.Phy. & Chem. Ref.Data 8.1 (1979)

(2-23) I.Øverbo," Large-q form factors for light atoms", Phys.Scripta Vol.17 547 (1978)

(2-24) D.T.Cromer and J.B.Mann," X-ray scattering factors computed from numerical Hartree-Fock wave functions", Acta Cryst. Vol A24 321 (1968)

(2-25) J.H.Hubbell et al., NBS-NSRD Data Base System XGAM (1985)

(2-26) V.H.Smith Jr, A.J.Thakkar and D.C.Chapman," A new analytic approximation to atomic incoherent X-ray scattering intensities", Acta cryst. Vol.A31 391 (1975)

(2-27) J.H.Hubbell et al., "Atomic form factors, incoherent scattering functions and photon scatterinhg cross sections", J.Phys.Chem. Ref. Data 4.3 (1975)

(2-28) S.Tanaka and T.Suzuki, Radioisotopes Vol.38 2 (1989) (in Japanese)

(2-29) Y.Harima et.al., "Validity of the geometric-progression formula In approximating gamma ray buildup factors", Nucl.Sci & Eng. 94 (1986)

(2-30) ICRP Committee, "Data for use in protection against external radiation", A. ICRP Pub 17 ,No.2/3 (1987)

(2-31) H.Nakashima et.al., " Characteristics of a vacuum type microcalorimeter for synchrotron radiation measurements", Nucle. Instr. Methods A365 553-558 (1995)

(2-32) Y.Sakamoto and S. Tanaka, "QAD-CGGP2 and G33-GP2; Revised version of QAD-CGGP and G33-GP", JAERI-M90-110 (JAERI, Japan) (1990)

(2-33) J.A.Halbleib, R.P. Kensek, T.A.Mehlhorn, G.D.Valdez, S.M.Seltzer, and M.J.Berger, "ITS 3.0: Integrated TIGER Series of Coupled Electron/Photon Monte Carlo Transport Codes",. SAND91-1634 UC-405 (1992)

(2-34) H.Kitamura, *Insertion Device Handbook '96.* (JASRI, Hyogo Japan) (1996)

(2-35) H.Konishi, W.Utumi, and M.Takahashi, "JAERI BL14B1", SPring-8 Annual Report 1997. 114-117 (Hyogo Japan) (1998)

(2-36) B.L.Henke, P.Lee, T.J.Tanaka, R.L.Shimabukuro, and B.K.Fujikawa, "Low-energy X-ray interaction coefficients: Photoabsorption, scattering and Reflection", Atomic Data and Nucl.Data Tables. 27 1-144 (1982)

(3-1) European Synchrotron Radiation Facility, "The red Book Draft B". Grenoble France (1987)

(3-2) Argonne National Lab., "7 GeV Advanced Photon Source Conceptual Design Report",

ANL-87-15 Argonne USA (1987)

(3-3) JAERI-RIKEN SPring-8 Project Team ,"SPring-8 Project Part 1 Facility Design", 1991(Revised). Tokyo Japan (1991)

(3-4) H.C.Dehne, M.A.Preger, S.Tazzari, and G.Vignola, Nucle. Instr. Methods 116 p345 (1974)

(3-5) A.Rindi, "Gas bremsstrahlung from an electron storage ring", Health Phys. 42 p187-193 (1982)

(3-6) H.Kobayakawa, K. Huke, M.Izawa, Y.Kamiya, M.Kihara, M.Kobayashi, and S.Sakanaka, Nucle. Instr. Methods A248 p565-568 (1986)

(3-7) S.Sakanaka, M.Izawa, H.Kobayakawa, M.Kobayashi, Nucle. Instr. Methods A256 p.184-188 (1987)

(3-8) H.Hirayama, S.Ban, S. Miura, Nuclear Science & Eng. 96 p.66-72 (1987)

(3-9) S.Ban, H.Hirayama, S. Miura, Health Physics 53 p.67-72 (1987)

(3-10) J.C.Frank, "*BREMSSTRAHLUNG DU FAISCEAU STOCKE SUR LES MOLECULES RESIDUELLES DE LA CHAMBRE AVIDE DE SUDER ACO*", LURE EP 88-01 (1988)

(3-11) G.Tromba & A.Rindi, Nucle. Instr. Methods A292 p.700 (1990)

(3-12) S.Ban, H.Hirayama, & S.Miura Health Physics 57 p.407 (1989)

(3-13) A.Ferrari, M.Pelliccioni and P.R.Sala, Nucle. Instr. Methods. B83 (1993) 518

(3-14) M.Pisharody, P.K.Job, S.Magill, J.Proudfoot, and R.Stanek, Nucle. Instr. Methods. A401 (1997) 442.

(3-15) M.Pisharody, E.Semones, and P.K.Job, "Dose measurements of gas bremsstrahlung-produced neutrons from thick targets", Nucle. Instr. Methods A 430 542-558 (1999)

(3-16) W.R.Nelson, H.Hirayama, and D.W.O.Rogers," The EGS4 code system", Stanford,CA Stanford Accelerator Center; SLAC-265 (1985)

(3-17) J.C.Liu, W.R.Nelson, and K.R.Kase, "Gas bremsstrahlung and associated photon-neutron shielding calculations for electron storage rings", Health Physics Vol.68 205-213 (1995)

(3-18) T.Nakano, Proc. of nuclear physics frontiers with electro-weak probes, Osaka, Japan (1996)

(3-19) M.Fujiwara et al., ACTA PHYSICA POLONICA *B 29* (1998)

(3-20) S.Date et al., Proc. Particle Accelerator Conf. New York (1999) 2349.

(3-21) M.Kobayashi, M.Ishii, Y.Usuki, and H.Yahashi, Nucle. Instr. Methods. A373 (1996) 333.

(3-22) A.F.Bielajew et al., National Research Council of Canada, Internal Report PIRS-0203 (1989)

(3-23) N.E.Ipe and A.Fasso, "Gas bremsstrahlung considerations in the shielding design of the Advanced Photon Source synchrotron radiation", Nucle. Instr. Methods **A351** 534-544 (1994)

(3-24) J. Andruszkow et al., "Calibration Procedure of the calorimeters of the ZEUS Luminosity Monitor, Deutches Electronen-Synchrotron (DESY)", HERA ZEUS-94-071, Hamburg, Germany, 1994

(3-25) H.Shimizu et al., " Performance of a PbWO4 Crystal calorimater for 0.2-1.0 GeV Electrons", Nucle. Instr. Methods. A 447 No.3 p463 (2000)

(3-26) H.Tanaka, private communications, 1999

(3-27) Y.Asano and N.Sasamoto., Radiation Protection Dosimetry. 82 (1999) 167.

(3-28) International Comission on radiation Units and Measurements. Radiation Quantities and Units, ICRU report 33 (1980)

(3-29) A.Ferrari, M.Pellicioni, and M.Pillon, Radiation Protection Dosimetry. 67 (1996) 245.

(3-30) B.Rossi, High Energy Particles, Prentice-Hall press. Englewood N.I 1952

(3-31) D.W.O Rogers, Health Phys. 46 (1984) 891.

(3-32) S.S.Dietrich, and B.L.Berman, "Atlas of photoneutron cross sections obtained with monoenergetic photons", Atomic Data and Nuclear Data Tables **38** 199-338 (1988)

(3-33) W.P.Swanson, "Radiological Safety Aspects of the Operation of Electron Linear Accelerators". IAEA Technical Report No.188 IAEA Vienna (1979)

(3-34) N.Kishida, "Methods used in photonuclear data evaluation at JNDC", Int. Symposium on Nuclear Data Evaluation methodology 12-16 Oct. BNL 598 (1992)

(3-35) T.A.Gabriel, M.P.Guthrie, and O.W.Hermann, "PICA, Monte Carlo Medium-Energy Photon-Induced Intranuclear Cascade Analysis Code System", ORNL CCC-160 (1972)

(3-36) A.Ferrari, and M.Pelliccioni, "Fluence to Dose Equivalent Conversion Data and Effective Quality Factors for High Energy Neutrons", Radiat. Prot. Dosim. 76(4) 215-224 (1998)

(3-37) International Commission on Radiation Unit and Measurements, "Quantities and Units in Radiation Protection Dosimetry", ICRU Report 51 (Bethesda, MD: ICRU Publications) (1993)

(3-38) J.F.Briesmeister CCC-200 ORNL (1993)

(3-39) R.Kinsey, BNL-NCS-50496 (1979)

(3-40) W.W.Engle, K-1693 (1967)

(3-41) Kotegawa et al., JAERI-M 93-020 (1993) in Japanese

(3-42) M.B.Chadwick et al., " Cross Section Evaluations to 150MeV for accelerator-driven systems and implementation in MCNPX", Los Alamos National Laboratory LA-UR-98-1825 (1998)

(3-43) Y.Asano, "A study on various neutron standard fields for the workplace", JAERI-Research 99-045 (1999) (in Japanese)

(3-44) S.Berg et al., AFWL-TR-67-41 CCC-112 (1969)

(3-45) ICRP Pub.74;" Conversion Coefficients for use in radiological Protection against External Radiation", ISSN 0146-6453 (1996)

(3-46) ICRP Pub.21," Data for Protection against Ionizing Radiation from External Sources" (1973)

(3-47) ICRP Pub.51 " Data for Use in Protection Against External Radiation", Annals of the ICRP 17 (1987)

(A-1) N.Sasamoto and Y.Asano, "Shielding Design Study for the SPring-8", Proceedings of Shielding Aspects of accelerators, targets and irradiation facilities, OECD Documents p.235-245 Arlinton, Texas OECD/NEA (1994)

(A-2) Y.Asano and N.Sasamoto, "Radiation Shielding and Safety Analysis for SPring-8", JAERI-Tech 98-009 (1998) in Japanese

(A-3) E.Braeuer, "Radiation Shielding for the 6 GeV, ESRF", ESRF/SHIEL/88-04, Grunoble (1988) (revised)

(A-4) W.P.Swanson, "Radiological Safety Aspects of the Operation of Electron Linear Accelerators", IAEA Technical Report No.188 IAEA Vienna (1979)

(A-5) S.Ban, et al., "Estimation of Absorbed Dose Due to Gas Bremsstrahlung from Electron Storage Ring", Health Physics Vol.57, No.3 (1989)

Appendix-1 Outline of the shielding design calculation of SPring-8 beamline

The SPring-8, which is the synchrotron radiation facility with currently the highest stored electron energy of 8GeV together with the feature of very low beam emittance of 5.5 to 7.0 nm.radian[3-1], consists of an electron linear accelerator (linac), a booster synchrotron injector and a storage ring, as illustrated in **Fig.1-1**. The linac is about 140m long and accelerates electrons up to about 1GeV. The booster synchrotron with a circumference of 396m accelerates the electrons injected from the linac up to 8GeV. The electrons are then injected into the storage ring, which is capable of storing circulating currents of 8GeV up to 100mA. The storage ring with a circumference of 1496m has 44 straight sections, 38 of which are available for insertion devices such as undulators or wigglers. Thirty-four sections of them are standard ones that are 19m long and the remaining 4 sections are the long ones that are 40m long. Further, 23 beamlines can be installed from bending magnets.

A1-1 Shielding design criteria

The shielding design for the synchrotron radiation beamline is made to keep the ambient dose equivalent rate at the surface of the hutch in occupied areas less than 6.7 μ Sv/h, which is one third of the legal limit on assumption of 50 working hours in a week. The dose rate must also fulfill the criterion of 2.0 μ Sv/h at the boundary of the controlled areas, the outermost boundary of the experimental hall. Moreover the design criterion at the SPring-8 site boundary is assigned to be 50 μ Sv/h to obtain public acceptance[A-1].

A1-2 Radiation source due to electron beam loss

The radiation sources we considered in the shielding design for the synchrotron radiation beamline are, (1) neutrons, photons and muons due to stored electron beam loss within the storage ring vacuum chamber, (2) gas bremsstrahlung, (3) photoneutrons induced by gas bremsstrahlung, and (4) synchrotron radiation. Radiation sources required to be considered at a component of the beamline are quite different

from those at another component, depending on the role of the component for radiation protection purposes. So, in order to make clear the situation, in **Table A-1** a relationship between the beamline component and radiation sources used for its shielding design calculation is summarized. The sources of gas bremsstrahlung, photoneutrons, and synchrotron radiation were covered in the main study so that only the source due to electron beam loss is discussed in this Appendix-1.

Because the emittance of the storage ring is very low, we can assume a point like the source of neutrons, photons and muons generated through interaction of the stored electrons with vacuum chamber walls or other structural materials surrounding the chamber. A beam loss assumption at the storage ring is assigned for each period of commissioning, tuning, beam injection and stably stored beam[A-2]. The assumption for the period of commissioning is too severe to be employed for shielding design, leading to over-designed shielding. For the periods of tuning, injection and stably stored beam, we employed time averaged beam loss assumptions of 2.35×10^9 e/s and 5.23×10^7 e/s at the injection region of the storage ring and other non-injection regions (ordinary one), respectively. During the period of the stably stored beam mode, however, all of the stored beam is assumed to be lost linearly within 10 hours. The assumed beam loss rate is 1.74×10^6 e/s.

A1-3 Shielding design calculation of a shutter

Shielding calculations for the main beam shutter (MBS) were performed to satisfy the criterion that all radiation workers can enter both the optics and the experimental hutches when the MBS is closed. During all operational modes of the storage ring except commissioning, the MBS must reduce the total dose equivalent rate of neutrons, photons and even muons due to stored electron beam loss, the synchrotron radiation and gas bremsstrahlung on the inside wall of the hutch to below 6.7 μSv/h. Shielding calculations for neutrons and photons due to electron beam loss are made using an empirical formula[A-3] for a forward directional calculation employed at the ESRF and for the muon calculation, Swanson's formula[A-4] was used. Gas bremsstrahlung calculation was made using the tabulated data on the basis of the evaluation with EGS4 by Ban et al[A-5].

In **Figs.A-1 and A-2** the attenuation behaviors of the radiation considered within the MBS located at the injection rejoin and the straight section in the non-injection region are given, respectively. In the beamline at the injection region, neutrons due to electron beam loss are the most dominant source, while gas bremsstrahlung is the most dominant source at the straight section in the non-injection region. As a result, we obtained the required thickness of the tungsten shutter to be 18 cm thick for the beamline located at the straight section, while a shutter consisting of tungusten that is 40 cm, stainless steel that is 40 cm and copper that is 20 cm as an absorber was found to be needed at the injection region because of the major high energy neutrons.

As for the downstream shutter (DSS) made of lead, the radiation we have to consider is the monochromized synchrotron radiation and the scattered photons of high energy components, the shielding calculation for DSS was made using the STAC8 code to obtain a required thickness of 4.9 cm thick for the typical undulator beamline. Only the monochromized synchrotron radiation is considered for the beam stop to be a required thickness of 1.2 cm thick in the case of the maximum photon energy of the fundamentals for use of 36 keV and the energy resolution of $\Delta E/E = 0.5$ %. In the calculation we employed the third harmonics of the monochromized radiation as a source.

Table A-1 Radiation sources used for the shielding design for each beamline component.

Beamline component	Stored electron beam loss (γ, n, μ)	Gas bremsstrahlung and associated photo-neutron	Synchrotron radiation γ (X)
Main beam shutter (MBS)	considered	considered	ignored
Down stream shutter (DSS)	ignored	ignored	considered
Beam stop	ignored	ignored	considered
Optics hutch	considered	considered	considered
Experimental hutch	ignored	ignored	considered
Photon stop	considered	considered	ignored

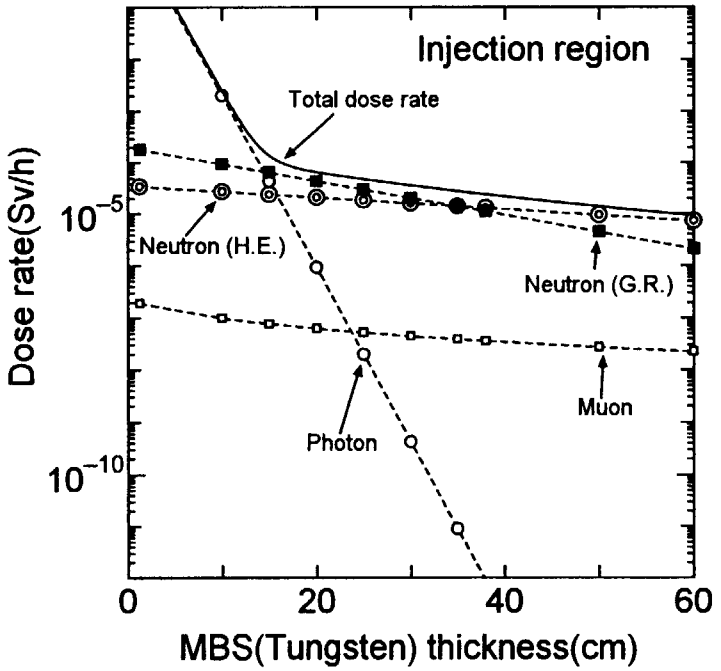

Fig.A-1 Dose attenuation distribution along the MBS axis due to the beam loss of the stored electron beam at the injection region of the storage ring. The solid line indicates the total dose, the open circles: photons due to electron beam loss, the double circles; high energy neutrons, the full squares; giant resonance neutrons, and the open squares are due to muons.

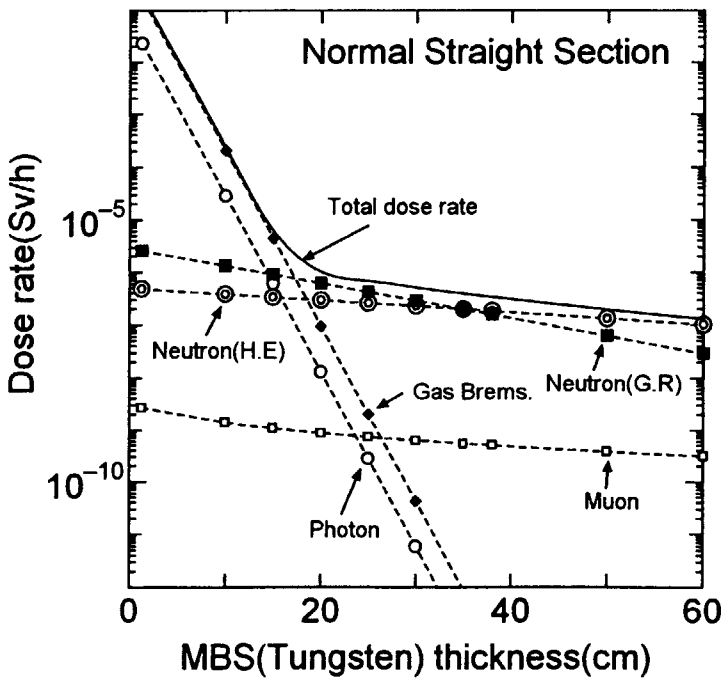

Fig.A-2 Dose distribution due to beam loss of the stored electron at the normal straight section of the non-injection region. Full diamonds indicate the attenuated dose caused by gas bremsstrahlung, and other symbols indicate the same as Fig.A-1

Appendix 2 Simulation of gas bremsstrahlung depending on stored electron energy and residual gas molecules

The intensity and angular distribution of gas bremsstrahlung were carried out at (1) the number of interactions, (2) several AE values ranging from 0.521 to 10 MeV under 1.0 and 0.1 atm, (3) several gas pressure values ranging from 1 to 10^{-3} atm under the lengths of straight section of 1m, 19m, and 40m, (4) several residual gas molecules under 0.1 and 1.0 atm, and (5) several stored electron energies, to investigate the dependence on the energy spectrum and the angular distribution of the emission of the gas bremsstrahlung. The conditions of (1) (2), and (3) were covered in the main study so only (4), and (5) are shown in this Appendix-2. These were calculated allowing only for single interaction. The calculated photon spectra and angular distributions of emission are given in **Figs.A-3, A-5** and **Figs.A-4, A-6** for several residual gas molecules under 0.1 and 1.0 atm, and **Fig.A-7** and **Fig.A-8** for several stored electron energies, respectively.

Figures A-3 and **A-5** show that the intensity of gas bremsstrahlung strongly depends on the residual gas molecules. Therefore the component of the residual gas is very important. **Figures A-7** and **A-8** show that both the energy spectrum and angular distribution strongly depend on the stored electron energy, extreme directivity is especially recognized in stored electron energy of 8 GeV.

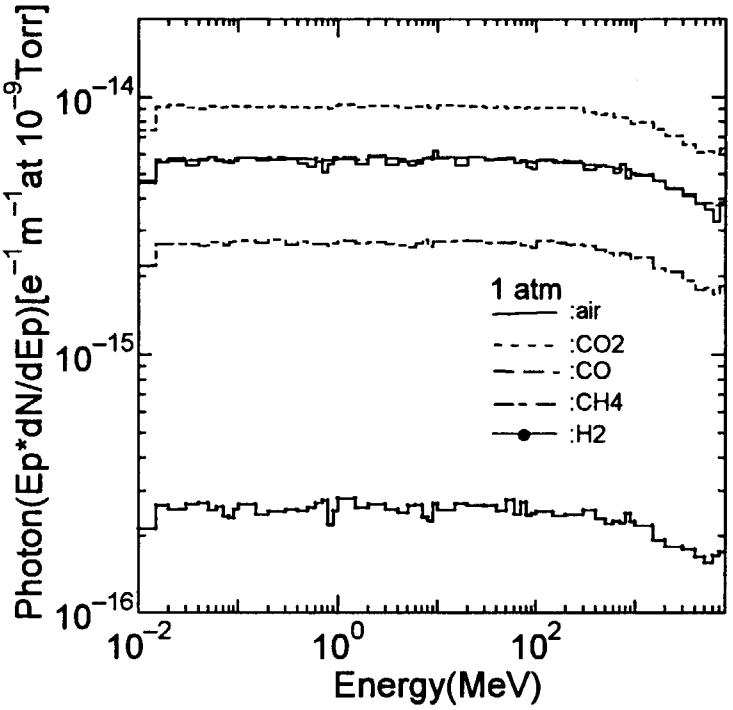

Fig.A-3 Gas bremsstrahlung spectra depending on residual gas material with a path length of 1 m and gas pressure of 1 atm, allowing only single interaction of the electrons.

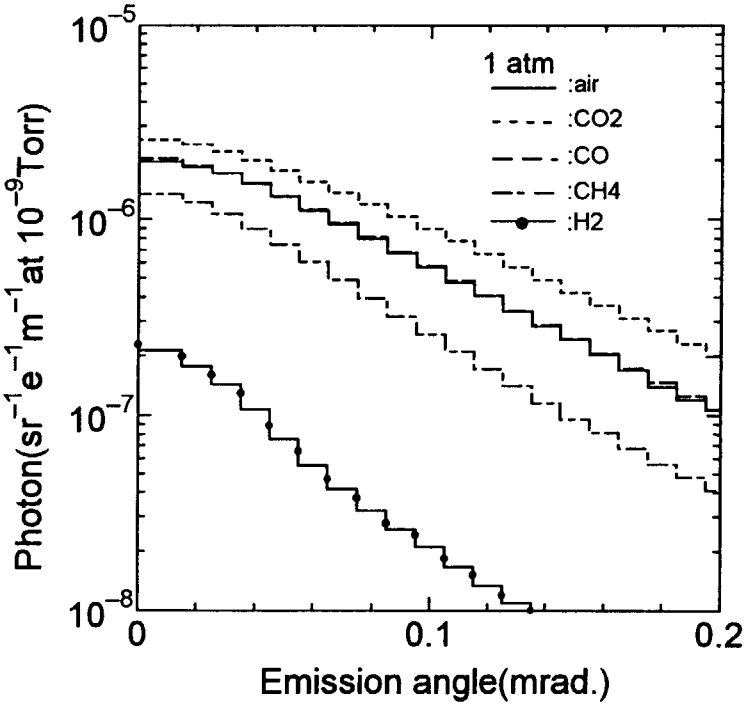

Fig.A-4 Angular distribution of gas brremsstrahlung depending on residual gas material with a path length of 1 m and gas pressure of 1 atm, allowing only single interaction of the electrons.

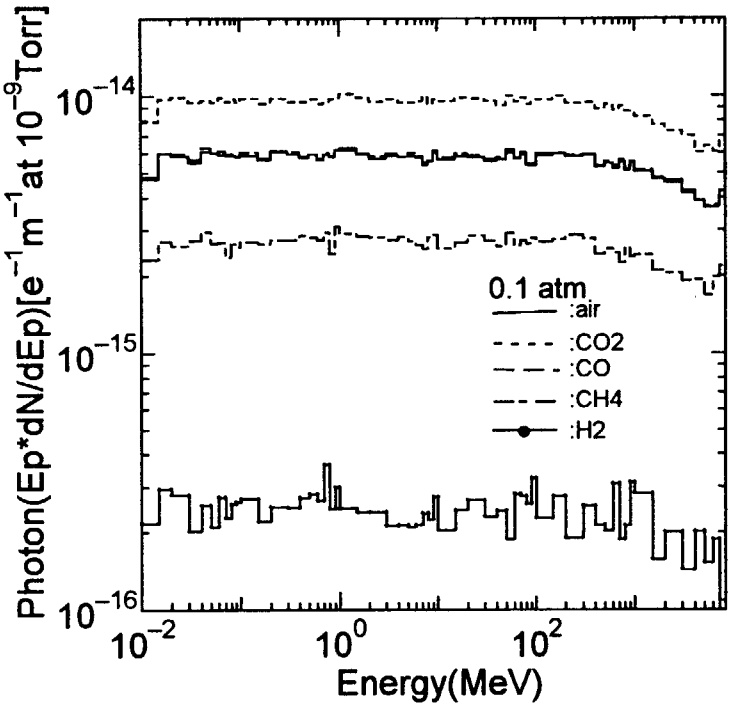

Fig.A-5 Gas bremsstrahlung spectra depending on residual gas material with a path length of 1 m and gas pressure of 0.1 atm, allowing only single interaction of the electrons.

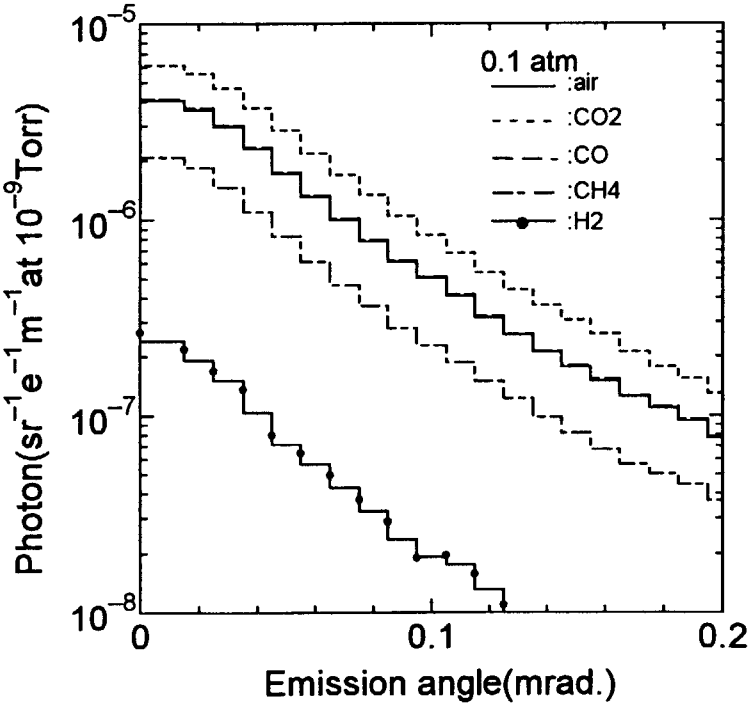

Fig.A-6 Angular distribution of gas bremsstrahlung spectra depending on residual gas material with a path length of 1 m and gas pressure of 0.1 atm, allowing only single interaction of the electrons.

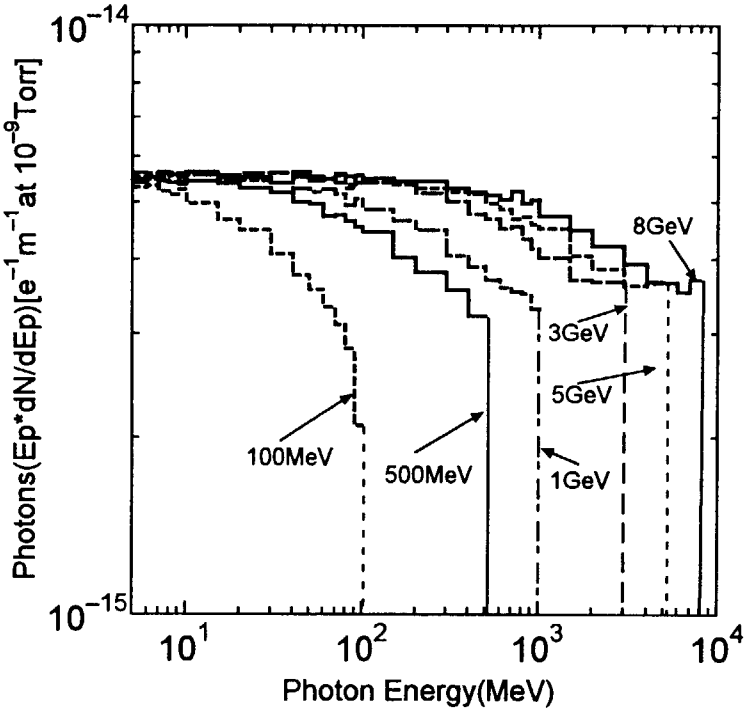

Fig.A-7 Gas bremsstrahlung spectra depending on stored electron energy with a path length of 1 m and gas pressure of 0.1 atm, allowing only single interaction of the electrons.

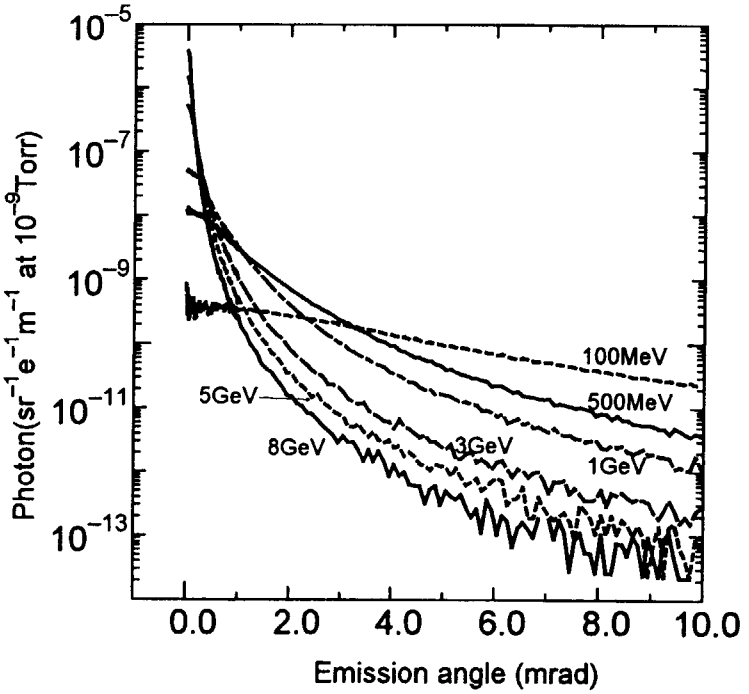

Fig.A-8 Angular distribution depending on stored electron energy with a path length of 1 m and gas pressure of 0.1 atm, allowing only single interaction of the electrons.

国際単位系 (SI) と換算表

表 1　SI 基本単位および補助単位

量	名称	記号
長さ	メートル	m
質量	キログラム	kg
時間	秒	s
電流	アンペア	A
熱力学温度	ケルビン	K
物質量	モル	mol
光度	カンデラ	cd
平面角	ラジアン	rad
立体角	ステラジアン	sr

表 2　SI と併用される単位

名称	記号
分，時，日	min，h，d
度，分，秒	°，′，″
リットル	l，L
トン	t
電子ボルト	eV
原子質量単位	u

1 eV = 1.60218 × 10^{-19} J

1 u = 1.66054 × 10^{-27} kg

表 5　SI 接頭語

倍数	接頭語	記号
10^{18}	エクサ	E
10^{15}	ペタ	P
10^{12}	テラ	T
10^{9}	ギガ	G
10^{6}	メガ	M
10^{3}	キロ	k
10^{2}	ヘクト	h
10^{1}	デカ	da
10^{-1}	デシ	d
10^{-2}	センチ	c
10^{-3}	ミリ	m
10^{-6}	マイクロ	μ
10^{-9}	ナノ	n
10^{-12}	ピコ	p
10^{-15}	フェムト	f
10^{-18}	アト	a

表 3　固有の名称をもつ SI 組立単位

量	名称	記号	他の SI 単位による表現
周波数	ヘルツ	Hz	s^{-1}
力	ニュートン	N	m·kg/s^2
圧力，応力	パスカル	Pa	N/m^2
エネルギー，仕事，熱量	ジュール	J	N·m
工率，放射束	ワット	W	J/s
電気量，電荷	クーロン	C	A·s
電位，電圧，起電力	ボルト	V	W/A
静電容量	ファラド	F	C/V
電気抵抗	オーム	Ω	V/A
コンダクタンス	ジーメンス	S	A/V
磁束	ウェーバ	Wb	V·s
磁束密度	テスラ	T	Wb/m^2
インダクタンス	ヘンリー	H	Wb/A
セルシウス温度	セルシウス度	℃	
光束	ルーメン	lm	cd·sr
照度	ルクス	lx	lm/m^2
放射能	ベクレル	Bq	s^{-1}
吸収線量	グレイ	Gy	J/kg
線量当量	シーベルト	Sv	J/kg

表 4　SI と共に暫定的に維持される単位

名称	記号
オングストローム	Å
バーン	b
バール	bar
ガル	Gal
キュリー	Ci
レントゲン	R
ラド	rad
レム	rem

1 Å = 0.1 nm = 10^{-10} m

1 b = 100 fm^2 = 10^{-28} m^2

1 bar = 0.1 MPa = 10^5 Pa

1 Gal = 1 cm/s^2 = 10^{-2} m/s^2

1 Ci = 3.7 × 10^{10} Bq

1 R = 2.58 × 10^{-4} C/kg

1 rad = 1 cGy = 10^{-2} Gy

1 rem = 1 cSv = 10^{-2} Sv

（注）

1. 表 1－5 は「国際単位系」第 5 版，国際度量衡局 1985 年刊行による。ただし，1 eV および 1 u の値は CODATA の 1986 年推奨値によった。
2. 表 4 には海里，ノット，アール，ヘクタールも含まれているが日常の単位なのでここでは省略した。
3. bar は，JIS では流体の圧力を表わす場合に限り表 2 のカテゴリーに分類されている。
4. EC 閣僚理事会指令では bar，barn および「血圧の単位」mmHg を表 2 のカテゴリーに入れている。

換　算　表

力	N(=10^5 dyn)	kgf	lbf
	1	0.101972	0.224809
	9.80665	1	2.20462
	4.44822	0.453592	1

粘　度　1 Pa·s(N·s/m^2) = 10 P(ポアズ)(g/(cm·s))

動粘度　1 m^2/s = 10^4 St(ストークス)(cm^2/s)

圧力	MPa(=10 bar)	kgf/cm^2	atm	mmHg(Torr)	lbf/in^2(psi)
	1	10.1972	9.86923	7.50062 × 10^3	145.038
	0.0980665	1	0.967841	735.559	14.2233
	0.101325	1.03323	1	760	14.6959
	1.33322 × 10^{-4}	1.35951 × 10^{-3}	1.31579 × 10^{-3}	1	1.93368 × 10^{-2}
	6.89476 × 10^{-3}	7.03070 × 10^{-2}	6.80460 × 10^{-2}	51.7149	1

エネルギー・仕事・熱量	J(=10^7 erg)	kgf·m	kW·h	cal(計量法)	Btu	ft·lbf	eV
	1	0.101972	2.77778 × 10^{-7}	0.238889	9.47813 × 10^{-4}	0.737562	6.24150 × 10^{18}
	9.80665	1	2.72407 × 10^{-6}	2.34270	9.29487 × 10^{-3}	7.23301	6.12082 × 10^{19}
	3.6 × 10^6	3.67098 × 10^5	1	8.59999 × 10^5	3412.13	2.65522 × 10^6	2.24694 × 10^{25}
	4.18605	0.426858	1.16279 × 10^{-6}	1	3.96759 × 10^{-3}	3.08747	2.61272 × 10^{19}
	1055.06	107.586	2.93072 × 10^{-4}	252.042	1	778.172	6.58515 × 10^{21}
	1.35582	0.138255	3.76616 × 10^{-7}	0.323890	1.28506 × 10^{-3}	1	8.46233 × 10^{18}
	1.60218 × 10^{-19}	1.63377 × 10^{-20}	4.45050 × 10^{-26}	3.82743 × 10^{-20}	1.51857 × 10^{-22}	1.18171 × 10^{-19}	1

1 cal = 4.18605 J (計量法)

= 4.184 J (熱化学)

= 4.1855 J (15 °C)

= 4.1868 J (国際蒸気表)

仕事率　1 PS (仏馬力)

= 75 kgf·m/s

= 735.499 W

放射能	Bq	Ci
	1	2.70270 × 10^{-11}
	3.7 × 10^{10}	1

吸収線量	Gy	rad
	1	100
	0.01	1

照射線量	C/kg	R
	1	3876
	2.58 × 10^{-4}	1

線量当量	Sv	rem
	1	100
	0.01	1

（86 年 12 月 26 日現在）

A study on radiation shielding and safety analysis for a synchrotron radiation beamline